Label-Free Detection of Noncoding RNAs

Inauguraldissertation

zur
Erlangung der Würde eines Doktors der Philosophie
vorgelegt der
Philosophisch-Naturwissenschaftlichen Fakultät
der Universität Basel

von

Peter Noij
aus Muttenz, Basel-Landschaft

· Basel, 2012 ·

Genehmigt von der Philosophisch-Naturwissenschaftlichen Fakultät

auf Antrag von

Prof. Dr. Ernst Meyer
Prof. Dr. Martin Hegner

Basel, den 27.03.2012

Prof. Dr. Martin Spiess, Dekan

creative commons

Namensnennung-Keine kommerzielle Nutzung-Keine Bearbeitung 2.5 Schweiz

---

Sie dürfen:

das Werk vervielfältigen, verbreiten und öffentlich zugänglich machen

Zu den folgenden Bedingungen:

Namensnennung. Sie müssen den Namen des Autors/Rechteinhabers in der von ihm festgelegten Weise nennen (wodurch aber nicht der Eindruck entstehen darf, Sie oder die Nutzung des Werkes durch Sie würden entlohnt).

Keine kommerzielle Nutzung. Dieses Werk darf nicht für kommerzielle Zwecke verwendet werden.

Keine Bearbeitung. Dieses Werk darf nicht bearbeitet oder in anderer Weise verändert werden.

- Im Falle einer Verbreitung müssen Sie anderen die Lizenzbedingungen, unter welche dieses Werk fällt, mitteilen. Am Einfachsten ist es, einen Link auf diese Seite einzubinden.
- Jede der vorgenannten Bedingungen kann aufgehoben werden, sofern Sie die Einwilligung des Rechteinhabers dazu erhalten.
- Diese Lizenz lässt die Urheberpersönlichkeitsrechte unberührt.

Die gesetzlichen Schranken des Urheberrechts bleiben hiervon unberührt.

Die Commons Deed ist eine Zusammenfassung des Lizenzvertrags in allgemeinverständlicher Sprache: http://creativecommons.org/licenses/by-nc-nd/2.5/ch/legalcode.de

Haftungsausschluss:
Die Commons Deed ist kein Lizenzvertrag. Sie ist lediglich ein Referenztext, der den zugrundeliegenden Lizenzvertrag übersichtlich und in allgemeinverständlicher Sprache wiedergibt. Die Deed selbst entfaltet keine juristische Wirkung und erscheint im eigentlichen Lizenzvertrag nicht. Creative Commons ist keine Rechtsanwaltsgesellschaft und leistet keine Rechtsberatung. Die Weitergabe und Verlinkung des Commons Deeds führt zu keinem Mandatsverhältnis.

Quelle: http://creativecommons.org/licenses/by-nc-nd/2.5/ch/ Datum: 3.4.2009

Abstract

v7.6e final (!!)

Noncoding RNAs have emerged as highly conserved regulators for gene expression. Their detection is a biomarker for the identification and understanding of fundamental biological processes and diseases. They also play an important role in drug development.

To facilitate the detection of noncoding RNAs we set up a label-free direct binding assay. The assay is based on nanomechanical cantilever arrays for the detection of surface stress induced by immobilized biomolecules and their interaction partners. We used various means to significantly reduce the drift of the cantilever readout. Major improvements were achieved by tight control of temperature and mass transport which led to a faster system equilibration. Experimental protocols were improved to provide user-friendly and less time-consuming measurements. Further enhancements were achieved (i) by coating the entire cantilever array wafer with gold rather than individual cantilever arrays; (ii) by a directly implemented data analysis tool as real time feature of the measurement software. We succeeded to detect biomarker targets with high specificity in the picomolar range and we can easily distinguish perfect match from mismatches that hybridize with lower affinity.

We have demonstrated the detection of the biomarkers coagulation factor VII messengerRNA transcripts (F7) and microRNA-122 (miR-122) in proof of concept experiments with spike-in target in totalRNA background and cell lysates as well as the detection out of biologically relevant cell lysate samples with naturally occurring targets. Furthermore we have demonstrated the detection of miR-122 in acetaminophen treated rats' plasma and therefore prove the cantilever array technology to be a useful tool for the label-free direct detection of noncoding RNAs.

Biacore's surface plasmon resonance (SPR) system, the gold standard for label-free quantitative biomolecular interaction analysis, was used as reference parallel to the cantilever array technology (CLA). We compared the two fundamentally different systems, where the SPR measures the change in index of refraction in a boundary layer on the sensor surface and the CLA measures surface stress, in order to further support the interpretation of our results. The SPR can distinguish specific binding mostly by kinetic analysis and less by amplitude changes whereas the CLA offers to date less kinetic information but direct observation of amplitude changes. Plus, the CLA's dynamic range and sensitivity is higher.

Be still when you have nothing to say; when genuine passion moves you, say what you've to say, and say it hot.

D. H. Lawrence

Contents

List of Figures

List of Tables

Chapter 1

Introduction

1.1 Detection of Biomolecules

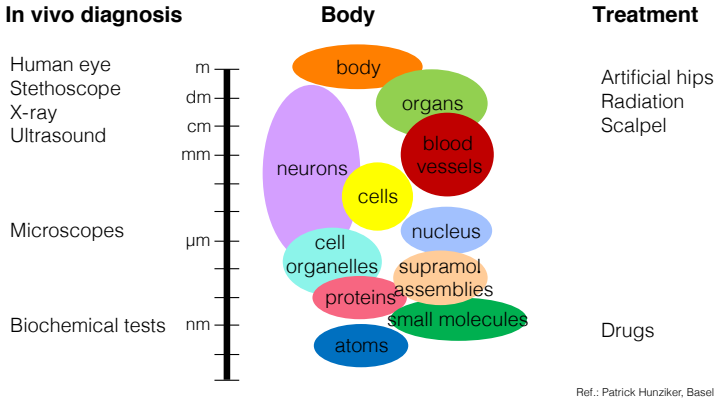

Figure 1.1: Biology in nanoscience: Most targets for pharma research are in the nanometer range (size of antibody $\approx 10\,\text{nm}$ regime). Nanoscience delivers new opportunities for better understanding of those disease related compartments and offers new tools to improve drug treatment. Especially in the context of personalized healthcare we have to understand and be able to analyze low level structures such as supramolecular assemblies (e. g. DNA-double-helix).

Nanoscience is a promising technology for drug development and clinical and non-clinical research. To understand the biology on a nanoscale level (see Fig. 1.1) with a wide range of research tools; for drug delivery of new medicines to address specific tissue and cellular targets; in "lab-on-a-chip" applications to enhance diagnosis and treatment selection; and in regenerative medicine with e. g. surface coatings and enhanced tolerability of implants.
Most of today's common detection applications in applied biology are based on an

amplified and labeled sensing. Two prominent members of this category are the Enzyme-Linked Immunosorbent Assay (ELISA) and the Real Time Quantitative Polymerase Chain Reaction (RTq-PCR or qPCR). The ELISA method is an Antibody (AB) based protein sandwich assay that triggers an enzyme linked color or fluorescent response upon detection. Real Time Quantitative Polymerase Chain Reaction (qPCR) is an amplification method for nucleic acids based on the Polymerase Chain Reaction (PCR) with the possibility for a quantitative readout. Where the ELISA is the gold standard for protein detection, qPCR is the state of the art detection method for Deoxyribonucleic acid (DNA) and Ribonucleic acid (RNA). To analyze biological samples for the presence of specific genes or proteins array based techniques have become common. For DNA/RNA the Affymetrix platform by Affymetrix Inc. is representative for such so called gene chips.

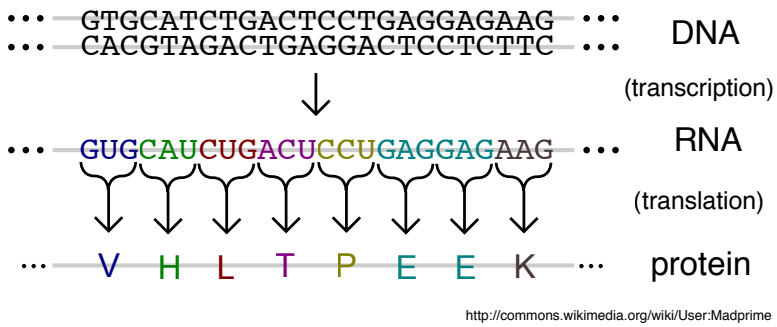

Figure 1.2: Gene expression: During gene expression DNA is transcribed into RNA and RNA translated into protein.

The key to all biological phenomena, our unique properties of living beings, the pathways and mechanism of all cellular processes is gene expression (Fig. 1.2). DNA is transcribed to RNA and RNA translated to protein. Therefore the most common RNA is the messenger RNA (mRNA) that contains the information for translation. Noncoding RNAs (ncRNAs) are a class of nucleic acids which do not code for protein such as mRNA. Members of this class of molecules are involved in many cellular processes and include highly abundant and functionally important RNAs, such as [1]:

- Transfer RNA (tRNA) that transfers the amino acid to the growing peptide chain during translation.
- Ribosomal RNA (rRNA) which is a component of the ribosome, the machinery behind the translation.
- Small interfering RNAs (siRNAs) and micro RNAs (miRNAs) expecting to have regulatory functions.

Along with these RNAs are some other ncRNAs. Their complete function is not fully understood yet. Besides tRNA and rRNA which are involved in protein synthesis, the functions of other ncRNAs are expected to be regulatory functions as said before.
The detection of such noncoding RNAs would be of high interest for monitoring miRNA or siRNA levels as biomarkers or for therapeutic approaches [2].

One of the present state of the art detection methods for low abundance RNAs is the branched DNA assay, or DNA ELISA. As in an ELISA assay, an immobilized capture probe binds the target sequence. Afterwards the sandwich structure is completed with a detection probe (annotated as label extender). This label extender then binds the branched DNA with label probe. The labeled branches ensure a strong enough signal for detection [3]. The advantages of the DNA ELISA is that no amplification is necessary and no reverse transcription such as that in qPCR is needed. Measurements can be done directly on cell lysates. The fact that time-consuming assay protocols are inherent for this ELISA type assay is a disadvantage. Time consuming protocols are especially critical in diagnostic tests for infectious diseases where a fast statement is very important. Furthermore there is one major limitation for all labeled assays: To attach the label we need a certain amount of nucleotides from the target strand which are not available for recognition and to ensure specificity. A label free direct binding assay can use the full strand length at a stretch for recognition, saves time-consuming wash and labeling or amplification steps and is free of expensive primer and labeling reagents.
State of the art methods are the Affymetrix platform and qPCR. Both techniques can be used for a broad miRNA screening or specific target analysis. Prominent qPCR assay is the TaqMan from ABI (Life Technologies) (Fig. 1.3). By reverse transcription complementary DNA (cDNA) is constructed, amplified and detected by the TaqMan label. Primers are normally $\sim$20 Nucleotide (nt) long. 10 nt would be sufficient for amplification but the shorter the sequence gets, the less specific the system is and errors might occur. Direct measurements such as the Cantilever Array (CLA) and other direct binding assays are preferred compared to amplified systems. Avoiding RNA isolation and amplification steps spares time and reduces errors. Especially very low concentrated samples such as miRNA detection in fluids would benefit from a highly sensitive and direct detection. Pre-amplification often induces errors due to lack in primer specificity or unequal amplification (PCR bias) of target and control [4, 5]. Especially in quantitative readouts the amplification under the mentioned aspect might be an additional source of error. Therefore a direct measurement is always preferred to a labeled and amplified one.
Major disadvantages of unlabeled direct binding assays is the lack of certainty in what the measured signal induced (did we really measure the target molecule or did we record a signal due to unspecific binding?) and the need for relatively

high "receptor occupancies" for signal response. The specificity problem can be overcome by feasible references. Where in most labeled assays the detected signal is amplified during readout (enzyme linked, Photomultiplier (PMT) in fluorescent readout, ...), the sensor response in unlabeled assays is dependent on sufficient binding efficiencies.

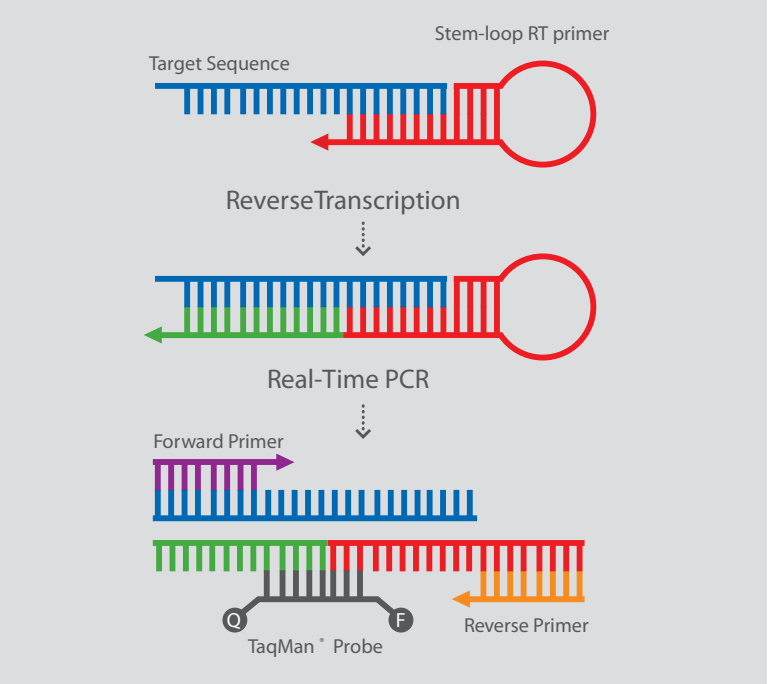

Figure 1.3: ABI (Life Technologies) TaqMan MicroRNA Assay: Small RNAs are isolated from the sample and reverse transcribed to make a cDNA library of the small RNA population. A target-specific stem-loop reverse transcription primer addresses the challenge of the short length of mature miRNA. The primer extends the 3' end of the target to produce a template that can be used in standard RTq-PCR or qPCR by amplifying the cDNA [Applied Biosystems, Publication 127BR03-01, 2010].

In case of short oligonucleotides such as siRNA and miRNA no commonly accepted assay exists. Even extremely elaborate sequencing technologies do not find favor. A technology to fill the gap is of high interest.

From the primary invention of the Atomic Force Microscope (AFM) in 1986 a great variety of new tools and a wide range of different applications evolved.
One of these devices is the CLA Sensor. Nanomechanical sensing systems based on cantilever arrays are a basic research tool for exploring label-free assays and can be used for a wide range of sensing applications. Investigators have shown

several static mode applications for the detection of biological binding partners such as DNA hybridization [6–8] and receptor-ligand binding [9–12].
Our focus lies on the label-free detection of noncoding RNAs for medium throughput assays where half automated processes and less time consuming protocols play an important role. Therefore our first intention was to set up a stable and reliable device for this application in the field of genomics.

For comparative measurement we refer to a publication that showed the label-free detection of biomarker transcripts in human RNA with a nanomechanical cantilever setup [13].
As proof of concept for a newly designed setup our goal was to detect a single stranded 21mer oligonucleotide at 100 pM in a physiological buffer solution.
For the detection of successful hybridization experiments we measured the transduced surface stress which accumulated depending on the amount of specifically bound single strand DNA (ssDNA) biomolecules. We operated our device in static mode and measured in liquid. The induced bending of the cantilever (which lies in the nanometer range) is measured by reflecting a laser beam on the top of the cantilever and pointing it towards a Position Sensitive Detector (PSD) as described in Ref. [14, 15] and Fig. 1.4.

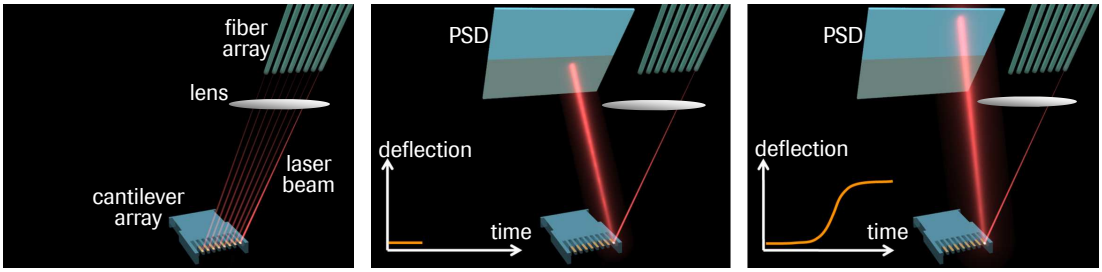

(a) (b) (c)

Figure 1.4: Schematic of deflection readout: (a) Time multiplexed sequential illumination of all 8 cantilevers. (b) Cantilever bending measured by detecting a reflected laser beam on a PSD. (c) Shift of detected laser beam on PSD due to cantilever deflection induced by a surface stress.

1.2 Surface Plasmon Resonance Technology

Today's state of the art label-free detection method for biomolecular interaction analysis in drug discovery is the Surface Plasmon Resonance (SPR) technology [16]. SPR has been used to study a variety of biological processes [17], including DNA hybridization [17–20], protein protein [21–24] and protein small molecule interactions [25, 26].

Surface plasmon resonance is the phenomenon where light stimulates the resonant oscillation of valence electrons in a metal layer. The induced electromagnetic waves propagate parallel to the interface metal/dielectric. Slight changes in the boundary layer between metal and dielectric, which is normally air or an aqueous solution, influence the SPR oscillations.
The most common principle to excite surface plasmons in a resonant manner is the so called "Kretschmann" configuration (Fig. 1.5).

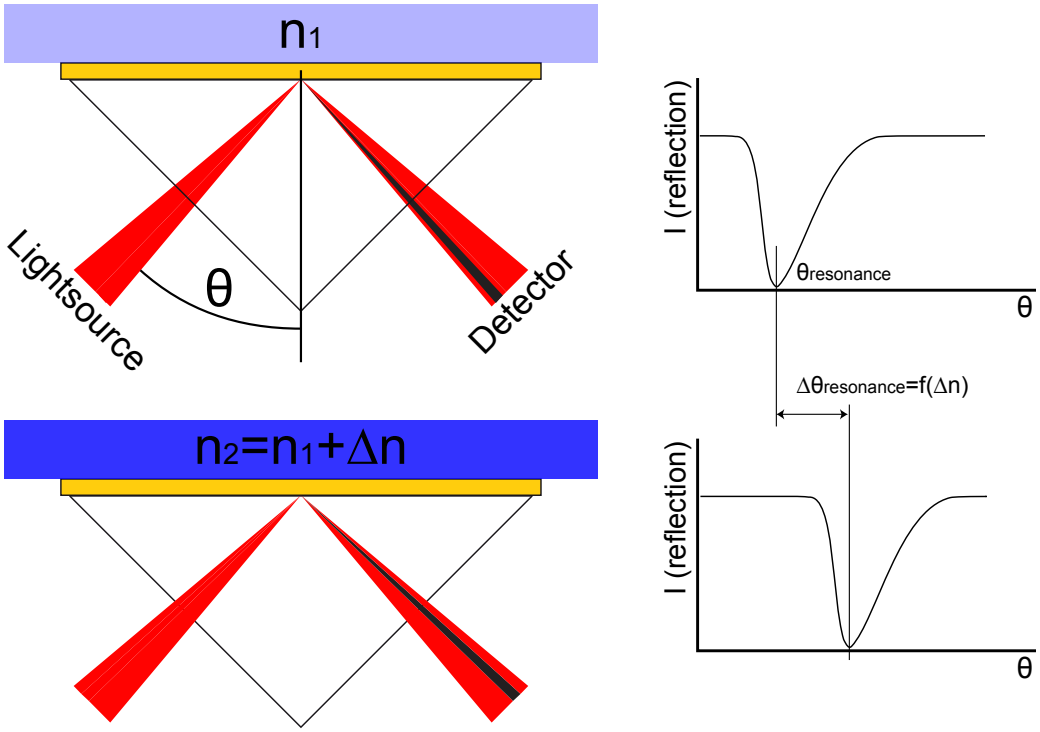

Figure 1.5: SPR setup in Kretschmann configuration: An additional mass load on the sensor surface leads to a change in index of refraction and to a shift in the angle at which the surface plasmon is brought into resonance.

SPR measures the shift of refractive index as average over an approx. 200 nm thick layer above the sensor surface. The origin of this shift is the polarisability of the biomolecules on top of the sensor surface. The polarisability of a biopolymer (protein, DNA or RNA) is based on the amount of polarizable groups in the

biomolecule — mainly the highly polarizable negatively charged moieties of the molecule. Therefore the SPR signal's origin is basically in a good approximation proportional to the ad-layer's mass. SPR shows a linear sensor response in terms of mass (pg/mm^2) even for a very small occupancy of the capture probes on the sensor surface. This is one of the SPR technology's basic advantages.

Biacore's SPR technology is capable of detecting ad-layers of target molecules of a few pg/mm^2.
The signal response is stated in "Resonance Index Units" (RIU) or in short "Resonance" or "Response Units" (RU). 1'000 RU correspond to a shift of 0.1° in the resonance angle or change in refractive index of 10^{-3}. 1'000 RU equates to a change of $\sim$1 ng/mm^2 in surface protein concentration [GE Healthcare Life Science, Real-Time Biomolecule Interaction Analysis, Biacore].

Due to the fact that the Biacore assay is in terms of chemical design (direct binding assay based on ssDNA on an Au surface) identical to a possible CLA assay, we used the SPR technology as a reference system. Biacore's unique properties as well as its importance in the label-free detection community will help to validate the novel CLA technology. The main benefit of the comparison of SPR and CLA are the different transducer properties (basically mass detection in SPR and stress detection in CLA), whereby both assays are carried out on similar gold surfaces.

1.3 Cantilever array technology[1]

A cantilever array chip is made by microfabrication out of silicon and consists of eight cantilevers with a thickness of typically 300 nm to 1 μm. The eight cantilevers can be differently functionalized and give an opportunity for reference measurements for differential read out.

The cantilever can be used in several kinds of modes as transducer for a sensing application. The two main operational modes are "static mode" and "dynamic mode". In dynamic mode the cantilever can be used as microbalance, for thermogravimetry or as biochemical sensor measuring liquid properties by tracking the damping. In static mode the change in surface stress is measured. Diffusion into polymers and bimolecular recognition are two subcategories of the static mode. Further categories can be set up such as "heat mode" (deflection due to temperature changes) by catalytic reactions or in calorimetry; "voltage control" to measure changes in potential on the cantilever surface. Different modes can be run in parallel in a so called "combined mode".

dynamic mode The principle of the dynamic mode sensors is based on oscillating the cantilever, where additional mass loading onto the cantilever interface results in a change of its resonance frequency. By tracking the resonance frequency (amplitude and phase-shift) either a real mass load on the cantilever surface or changes in the near cantilever environment influencing the damping of the cantilever can be measured.
The actual measured physical changes leading to a signal are similar as in other mass detection systems such as SPR or Quartz Crystal Microbalance (QCM). It is a mass load on the sensor surface.

static mode In static mode the cantilever deflection due to surface stress is measured. The technique is up to a certain point mass independent and therefore an interesting alternative to other mass detecting transducers. In static mode the measured quantity is the displacement Δx as shown in Fig. 1.6 of the initial state and bent state of the cantilever.

The correlation between surface stress σ and cantilever deflection is given by

[1]Partially published in Peter Noy *et al.*,"Instrument for Label-Free Detection of Noncoding RNAs", Journal of Sensors, vol. 2012, 2012.[27]

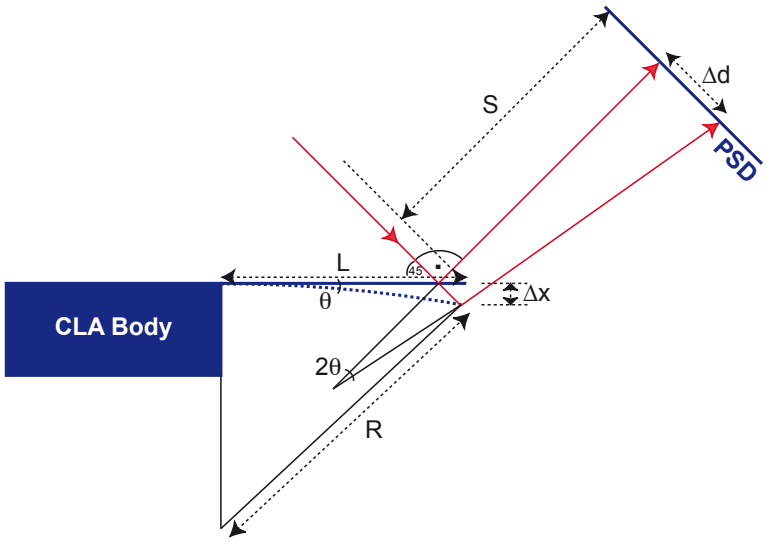

Figure 1.6: Static mode deflection readout. L: cantilever length; R: radius of curvature; θ: angle of deflection; Δx: deflection; S: distance between the PSD and the cantilever; Δd: shift on PSD

Stoney's formula [28] (Eq. 1.1):

$$\sigma = \frac{Eh^2}{6R(1-\nu)} \tag{1.1}$$

E and ν are elastic modulus and Poisson's ratio of the cantilever material. h is the thickness and R the bending radius of the cantilever. The deflection amplitude depends on the spring constant k (Eq. 1.2):

$$k = \frac{3EI}{L^3} \tag{1.2}$$

The "softer" (lower spring constant) the cantilever the larger the amount of deflection. $I = bh^3/12$ is the moment of inertia for a cantilever with the width b. L is the cantilever's length.
The position, respectively shift of the light spot on the PSD Δd is given by Eq. 1.3:

$$\Delta d = \frac{I_a - I_b}{I_a + I_b} \times \frac{l_{PSD}}{2} \tag{1.3}$$

Assuming the angle of deflection θ is very small, the bending angle is half the deviation of the deflected beam and the angle of deflection can be calculated as Eq. 1.4:

$$2\theta = \frac{\Delta d}{S} \tag{1.4}$$

where S is the distance between the PSD and the cantilever. Furthermore the relation between angle of deflection, deflection Δx and cantilever length L is given by Eq. 1.5 [29]:

$$\theta = \frac{2\Delta x}{L} \tag{1.5}$$

By substituting θ in Eq. 1.4 from Eq. 1.5 we receive:

$$\Delta x = \frac{\Delta dL}{4S} \tag{1.6}$$

The radius of curvature R of the cantilever with applied surface stress is expressed as circular curvature in Eq. 1.7:

$$R = \frac{L}{\theta} = \frac{2SL}{\Delta d} = \frac{L^2}{2\Delta x} \tag{1.7}$$

Hence the surface stress from Eq. 1.1 can be calculated.

A PSD is a resistive photo element with an isotropic sensor surface. This leads to a continuous position data. Light causes a local change in the resistance on the sensor surface. The position can be calculated by measuring the current through the device by the following equation 1.8:

$$x = \frac{I_a - I_b}{I_a + I_b} \times \frac{l}{2} \tag{1.8}$$

, which we already used for the calculation of the cantilever deflection. x is the position of the light spot on the psd; $I_a - I_b$ the PSD's differential signal; $I_a + I_b$ the PSD's sum signal; l the PSD length

Surface stress is induced by the interaction between immobilized biomolecules on the ssDNA bio-functionalized side of the cantilever bar and their interaction partners in an injected solution. Various forces such as intermolecular interactions, electrostatic forces and changes in the electronic density of the cantilever surface lead to the resulting surface stress [30].

By subtracting the deflection signal of a non-specific reference cantilever from the main signal as shown in the schematic drawing of the cantilever assay Fig. 1.7, parasitic effects such as drift due to small temperature changes and non-specific binding can be eliminated [30, 31].

Since measurable amount of signal drift is present in all known label-free detection methods we focused on its reduction by stabilizing the major external factors which affect drift in our nanomechanical setup. This was achieved by implementing a fast local temperature regulation system and measurement in con-

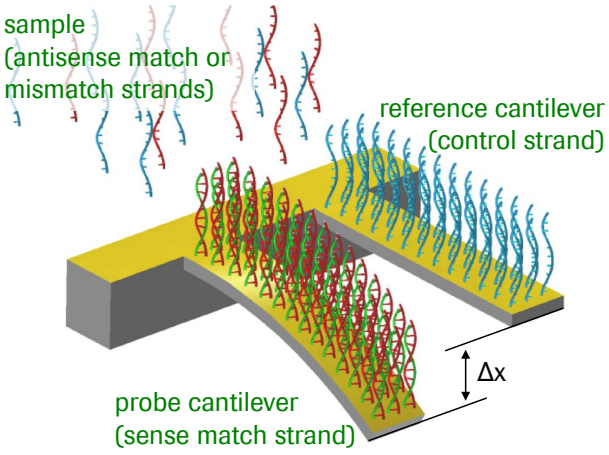

Figure 1.7: Schematic drawing of CL deflection due to DNA hybridization: We always measure differential signals. Differential deflection results are state as difference between the absolute bending of the probe cantilever minus the absolute bending of a reference cantilever. Dimensions of a cantilever are: 500 μm length, 100 μm width, 0.5 μm thickness. The drawing only shows a schematic principle. The size proportions of biolayer and cantilever thickness are not correct and the monolayer will never be that perfectly arranged.

tinuous liquid flow. Our goal was to optimize the system towards semiautomatic device handling, which is essential for industrial applications.
To assist the interpretation of the recorded data we developed a real time analysis software which applies simple operations and plots the results concurrently with the measurement.

We considered buying a commercially available device from the University of Basel. We decided instead to construct our own setup to provide the maximum flexibility to design the device for our specifications of the mentioned application. This also enabled a direct implementation of several improvements such as a new laser source, camera observation module and thermo-controller.

1.4 Assay Development

As implied in Fig. 1.7, we performed a simple oligo hybridization of an antisense strand in solution to a sense strand immobilized on a gold surface (Fig. 1.8). All 21 nucleotides are needed to be hybridized to ensure a specific detection of the target strand. There are not enough nucleotides in the antisense strand available for hybridization of a label. This is why the assay needs to be carried out label-free. The quantification of the antisense strand in cell and tissue lysates should technically be possible. The capture strand is easy to modify with a thiolated alkyl chain for immobilization on gold. This is a common technique also used for Biacore chips and other assays. Compared to the standard ligand binding assays on Biacore we do not have a dextran layer for surface stabilization and molecule fixation. The whole monolayer formation will be the first critical part for our assay. The higher ordered the monolayer is, the more accurate results are expected.

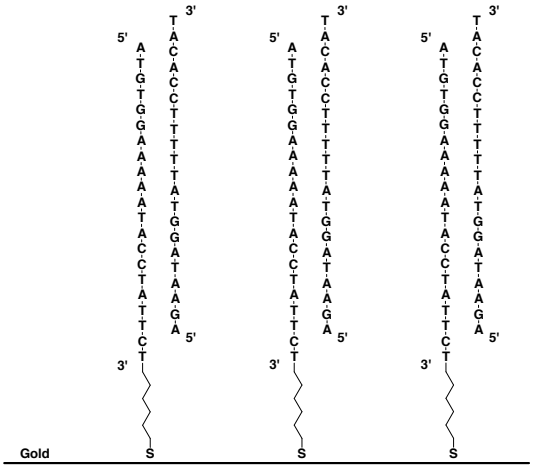

Figure 1.8: Schematic of the direct binding assay: Immobilized ssDNA strands bound by thiol chemistry on gold react with their complementary single strand oligo (DNA or RNA) in solution. In terms of terminology the bound thiolated strand is the "sense" or capture strand, which correlates to the passenger strand and the target in solution is the "antisense" strand, which is the guide strand.

Surface preparation in the assay development is critical for a successful detection of target hybridization. Probe density on the sensor surface affects the target hybridization efficiency. This was shown by several groups for SPR assays [32–34] as well as for cantilever based detection methods [6]. For both platforms there is an optimal probe density to achieve maximal hybridization efficiency and maximum response. Whereas, according to the mentioned literature, the cantilever platform requires a dense surface coverage for optimal signal response, the SPR platform does not seem to require this same coverage. The hypothesis from Ref. [6] for

the cantilever platform is explained by the required steric crowding to induce the contribution to one of the dominant effects leading to the nanomechanical signal. For the SPR platform steric hindrance is contra-productive and therefore a reduced surface coverage leads to a higher hybridization efficacy and higher signal amplitudes.
Due to this known fact we optimized the assay for all SPR measurements with a reduced immobilization density as shown in Fig. 1.9.

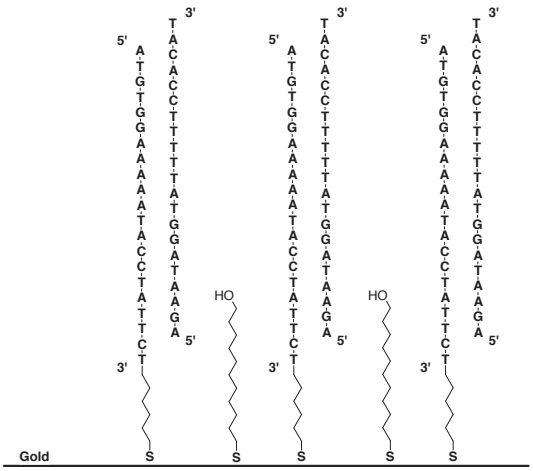

Figure 1.9: Schematic of the direct binding assay with reduced immobilization density: A certain percentage of immobilized ssDNA on the gold surface is displaced by shorter unspecific alkyl chains.

1.4.1 Assay Properties

In a direct binding assay, the sample is injected over the sensor surface and the analyte interacts with the immobilized biomolecule [35], which in our case is a ssDNA. The sensitivity in a direct binding assay depends on the interaction properties (k_a and k_d) of the reagents and on the injection time of the sample. The hybridization isotherms are quite complex and cannot be fit with simple kinetic models [32]. There is a strong dependence on probe density for both the efficiency of duplex formation and kinetics of target capture [32]. Hybridization of free target DNA strands (T) with capture probe strands (P) coupled to the sensor surface can be modeled by simple irreversible second order process [36]:

$$T + P \xrightarrow{k} P * T \tag{1.9}$$

P is the concentration of free (unbound) DNA probe on the surface, T is the concentration of free DNA target strand in solution and $P * T$ is the concentration

of probe-target complexes that form on the surface [36].
One of the few fitted adsorption coefficients for a direct binding assay based on surface plasmon resonance imaging measurements was achieved by Nelson *et al.* [17]. They reported an adsorption coefficient K_{ads} of $1.8 \times 10^7\,M^{-1}$.

1.4.2 CLA rear-side passivation

The cantilever's rear side is a potential source for drift and counter forces leading to a superposition of interactions on the CL which are difficult to interpret.
To avoid unspecific effects on the rear side of the cantilever the silicon surface had to be passivated. We commissioned SuSoS (see Sect. 1.6) to modify the surfaces of the CLA presenting two different materials: gold and silicon. The gold serves as basis for the sensing device, while the silicon should be rendered resistant against non-specific adsorption in order not to interfere with the measurement occurring on the Au-side. The company SuSoS has experience in modifying surfaces of various materials in order to reduce non-specific binding of biological molecules to the modified surfaces. The principle demonstrated in the Lit. Franks *et al.* (Ref. [37]) and modeled in Fig. 1.10.

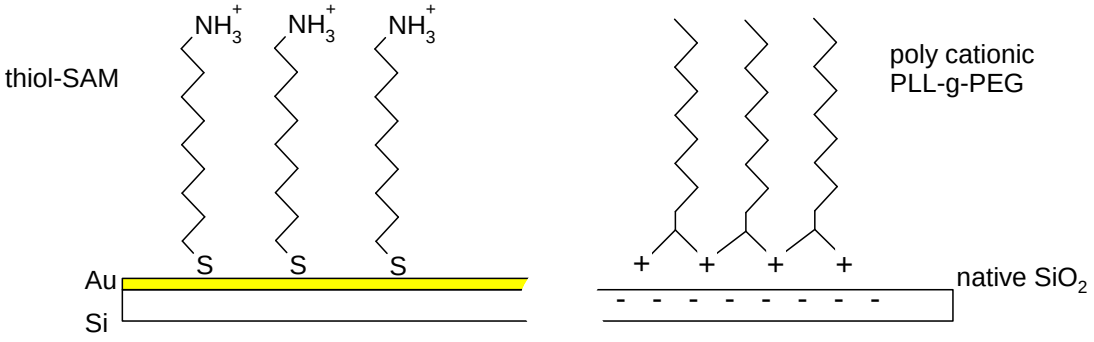

Figure 1.10: Selective treatment of Au/Si surfaces for functionalization according to Lit. [37]: Au is protected respectively functionalized by a thiol SAM. Si respectively native SiO_2 is functionalized by cationic binding forces.

Process step	**Au-side**	**Si-side**
Plasma or similar	Remove adventitious contaminations	Remove adventitious contaminations
Thiol-SAM	Assemble protective ad-layer	No effect
Non-fouling ad-layer (dipping and UV-curing)	Weak adsorption	Render surface resistant against non-specific protein uptake
Oxidation and rinsing	Removes thiol-SAM and assembled non-fouling ad-layer	No effect

Table 1.1: General idea to bi-functionalize a Au/Si bulk material according to SuSoS.

A general idea how to perform a bi-functionalization is given in Tab. 1.1.

1.5 Biology

In 1998 a new molecular mechanism called the RNA interference (RNAi) was discovered. Soon RNAi was used to study biological- and disease-related pathways; for target identification and target validation; as gold standard for efficiency of small molecules and biotherapeutics. Because of this the market size for reagents based on RNAi increased to more than 100 M $.
In 2006 Andrew Fire and Craig Mello received the Nobel Prize in Medicine "for their discovery of RNA interference — gene silencing by double-stranded RNA" ["The Nobel Prize in Physiology or Medicine 2006". Nobelprize.org. 11 Nov 2011 http://www.nobelprize.org/nobel_prizes/medicine/laureates/2006/].
Gene silencing by antisense-technique was not at all a new field. Regulating the protein synthesis by inducing a synthetic complementary RNA strand that forms a double strand with its target and therefore blocks the RNA translation was used before. In trials with nematodes (caenorhabditis elegans) Fire and Mello showed that gene silencing is much more efficient by applying double strand RNA (dsRNA) instead of just the antisense RNA. Today we know this is based on the RNAi mechanism [38].
Before the discovery of the RNAi, most known ncRNAs fulfilled relatively generic functions in cells, such as the rRNAs and tRNAs involved in mRNA translation, small nuclear RNAs (snRNAs) involved in splicing and small nucleolar RNAs (snoRNAs) involved in the modification of rRNAs [39].
A ncRNA is a functional RNA molecule that is not translated into a protein [1]. They are involved in many cellular processes (Fig. 1.11). Most of them are highly abundant and functionally important. The many classes of small RNAs are differentiated by their various aspects of origin, structure, associated effector protein and biological roles [2]. siRNA and miRNA are in phylogenetic and physiological terms the most important ones [2]. They are only known to be present in eukaryotic cells, although parts of their mechanism can also be found in prokaryotic species [2]. siRNA and miRNA are also the most interesting types of ncRNAs for pharmaceutical industry because of their mentioned roles as described in Chap. 1.1.

siRNA

siRNAs are small 21 to 22 nt long RNAs. They are produced by the cleavage of complementary dsRNA coming from the nucleus by an enzyme called Dicer (Fig. 1.12).
In comparison, the smallest mRNA has a size of min. 300 nucleotides which would lead to a protein of 100 amino acids. E.coli, one of the smallest organisms' proteins have 900–1'500 nucleotides in average.

The RNA fragments produced by Dicer can then form with Argonaute proteins

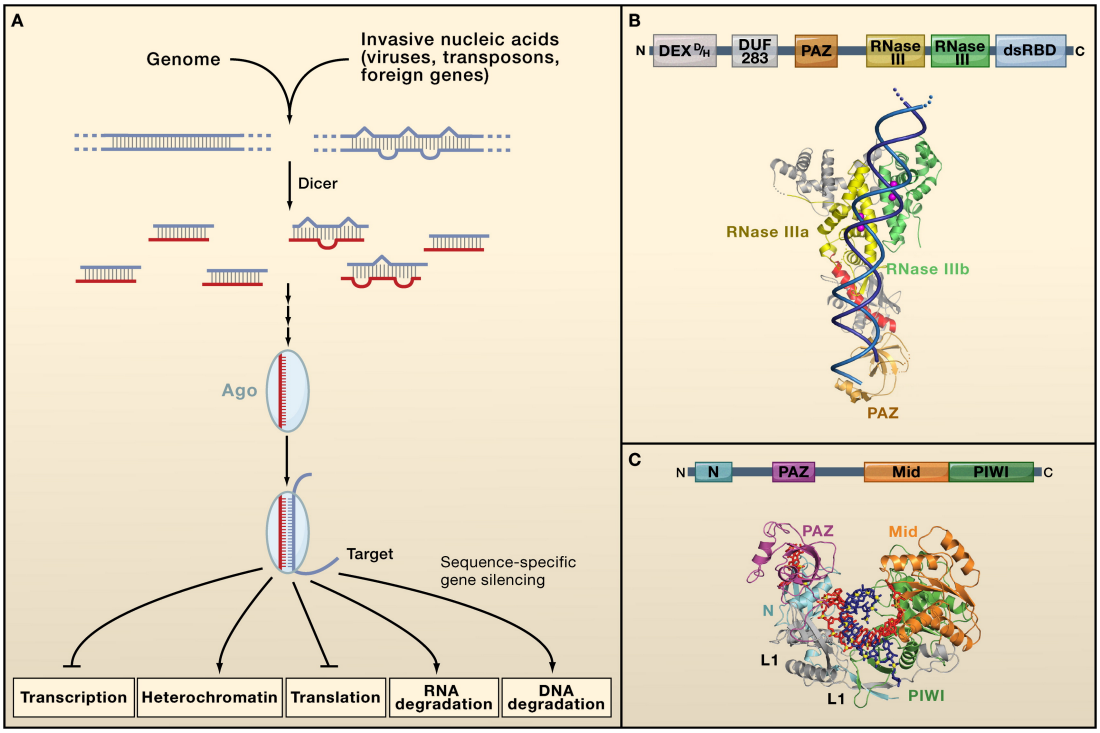

Figure 1.11: Core features of miRNA and siRNA silencing [2]: (A) Common aspects of all miRNA and siRNA pathways. dsRNA precursors are processed by a Dicer protein into short fragments. One strand of the processed duplex is loaded into an Argonaute protein, enabling target RNA recognition through Watson-Crick base pairing. Once the target is recognized, its expression is modulated by one of several distinct mechanisms, depending on the biological context.
(B) Dicer proteins cleave dsRNA precursors into characteristic lengths through the action of two RNase III domains.
(C) Argonaute proteins are RNA silencing effectors that are guided to their targets by short single-stranded nucleic acids. The canonical arrangement of Ago domains is given at the top. Below is a crystal structure of the Thermus thermophilus Ago protein, with a bound DNA guide strand base paired to an RNA target. The 5' end of the guide strand associates with a binding pocket in the Mid domain, and the 3' end binds the PAZ domain. The target cleavage site is juxtaposed with active-site residues in the PIWI domain, though in this case cleavage is suppressed by mismatches between the guide and the target. (Structure reprinted from Macmillan Publishers Ltd.: Wang *et al.*, Nature, 456, 2008.).

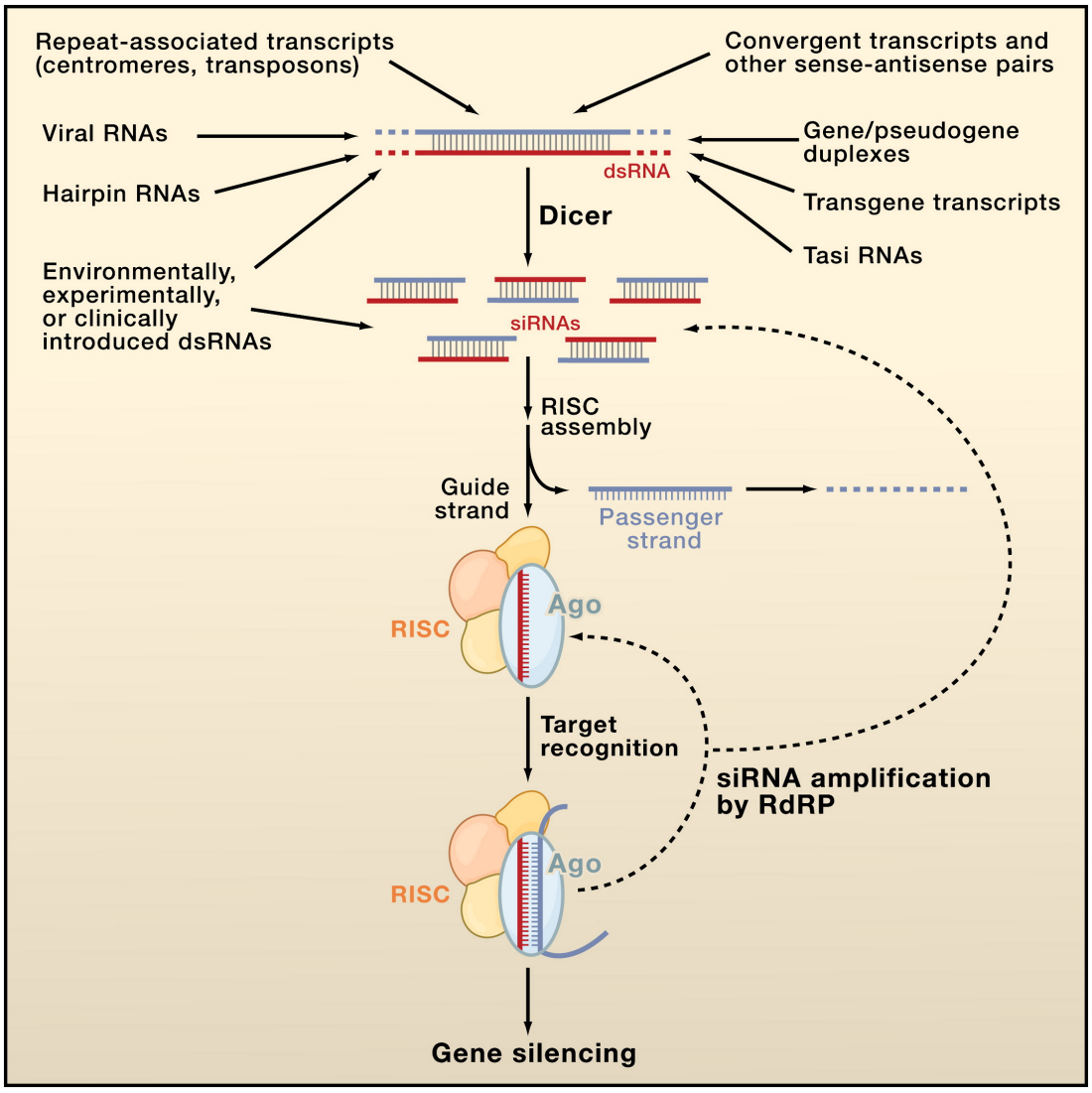

Figure 1.12: A diversity of siRNA sources [2]: Several different categories of transcripts can adopt dsRNA structures that can be processed by Dicer into siRNAs. These duplexes can be intra- or intermolecular, and although most are perfectly base paired, some (e. g., hairpin RNAs and gene/pseudogene duplexes) are not. A siRNA consists of a guide strand (red), which assembles into functional siRISC, and a passenger strand (blue), which is ejected and degraded. All forms of siRISC contain the siRNA bound to an Ago protein, and many if not most forms of siRISC contain additional factors. Target RNAs are then recognized by base pairing, and silencing ensues through one of several mechanisms. In many species, the siRNA populations that engage a target can be amplified by the action of RNA-dependent RNA polymerase (RdRP) enzymes, strengthening and perpetuating the silencing response.

a complex called RNA-Induced Silencing Complex (RISC). The fragments can then bind in a specific way to mRNA, cleaves the mRNA strand what leads to the degradation of the mRNA. This naturally occurring mechanism called RNA interference (Fig. 1.13) can be used for gene regulation, transposon control and defense against viruses [1].

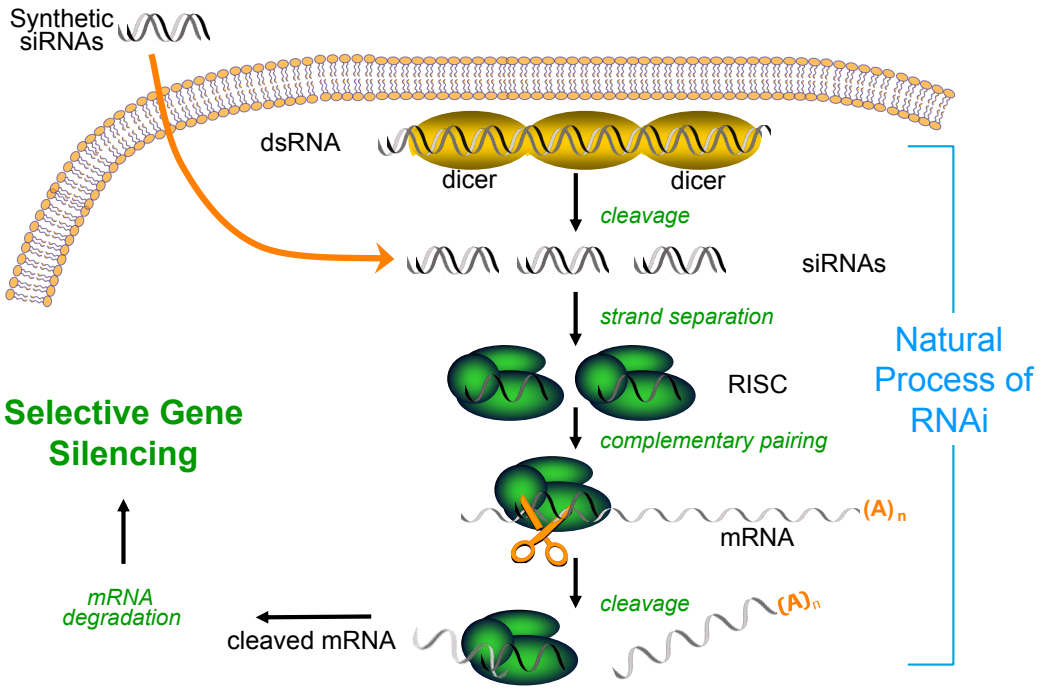

Figure 1.13: Mechanism of the RNAi [Figure by courtesy of U. Certa, F. Hoffmann-La Roche Ltd.]: An enzyme called dicer cleaves dsRNA into short fragments. Those fragments can bind with the RNA induced silencing complex in a specific way to messenger RNA, cleaves the complementary strand and leads to the degradation of mRNA. The naturally occurring process can also be achieved by synthetic siRNAs.

The same process works by an exogenous application of siRNA. For the pharmaceutical industry this would be a whole new drug class (see Sect. 5.1). Growth factors of tumors could be down regulated and due to a disease suppressed essential proteins promoted. Or as said above, siRNA could even be used as defense against all kind of virus infections.
The actual challenge is the delivery of the synthetically produced siRNA into the cell. Several strategies have been approached as shown in Fig. 1.14 with varying success.

F7 The RNAi effect as a new class of therapeutics that specifically suppresses gene-expression induced by small RNA, was attracting the attention of many researchers shortly after its discovery. In a short time, the field of applied RNAi therapeutics spread from the laboratory to the bedside. Many challenges and some concerns do still exist although some Phase I and Phase II studies were underway at the start of this thesis. Besides the mentioned difficulties of how to transport the siRNA target-orientated into the cell's cytoplasm, the possible triggering of off-target effects might occur.
Factor VII (F7) was already used as a model for hepatocellular application of siRNA and has properties which are of interest for *in vivo* analysis such as:

- exclusively expressed in hepatocytes
- secreted protein
- short half-life
- dose dependent suppression of the corresponding mRNA and their proteins (Ref. [41])
- continuing effect in rats and non-human primates (Ref. [41])

In studies at Roche for gene-expression analysis of off-target effects induced by siRNA against F7 which has an anticoagulating effect it was discovered that *in vitro* it had a reductive impact on the mRNA of chemokine (C-X-C motif) ligand 5' (CXCL5). A reporter assay (Luziferase) was developed to enable the suppression of CXCL5, F7 or the reporter itself by the siRNA and to test the dependency of the siRNA concentration.
[free translated from untitled, unpublished text of Frey Siegrist, Stefan Weis and Ulrich Certa, unpublished 2010.]

miRNA

Micro RNAs are a class of single-stranded RNA molecules 19 to 24 nucleotides in length and generated through a complex maturation process (Fig. 1.15) [1]. They are generally regarded as negative regulators of gene expression that inhibit translation and/or promote mRNA degradation by base pairing to complementary sequences within protein-coding mRNA transcripts [42].
Furthermore miRNAs represent a new class of biomarker. Biomarkers are measurable parameters to determine the health status. For example recent studies demonstrate an association of several miRNAs with various cardiac defects [42]. Known roles of miRNAs in heart development and function exist and it is expected that more miRNAs will be added to this growing list [42].

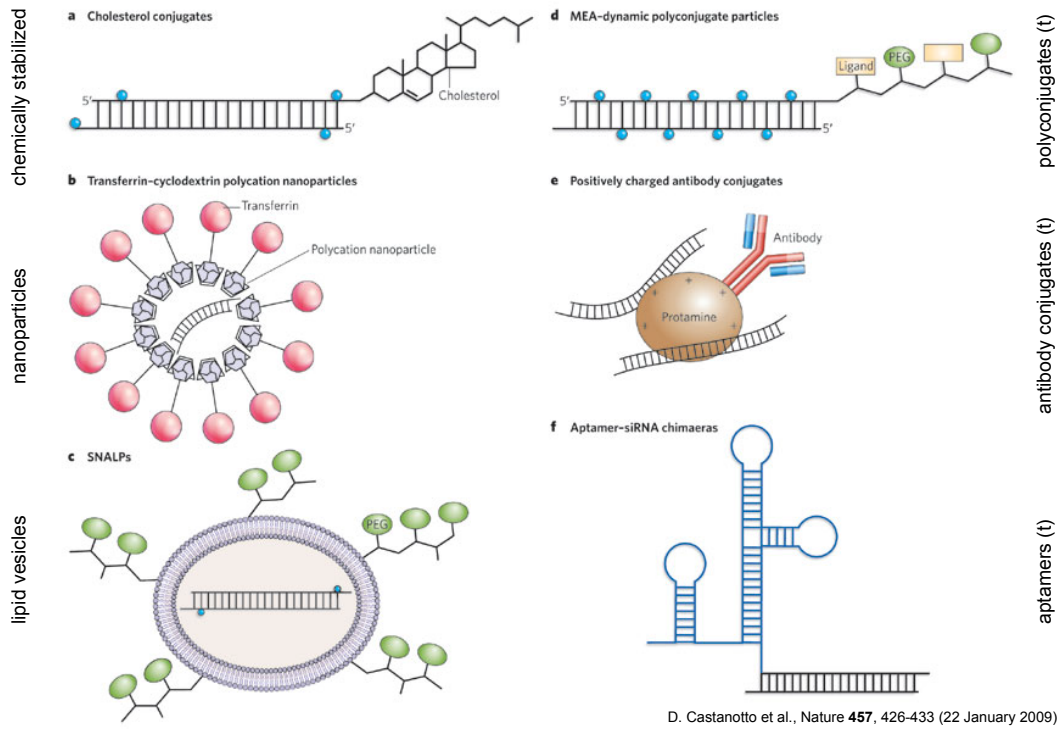

Figure 1.14: In vivo delivery strategies for therapeutic siRNAs [40]: Delivery strategies, respectively carriers or additives can be separated into different classes such as (a) chemically stabilized conjugates; (b) nanoparticles; (c) lipid vesicles; (d) poly-conjugates; (e) antibody conjugates; (f) aptamer based delivery. Stability enhancer such as 2'-O-methyluridine or 2'-fluorouridine substitutions (blue circles) are common siRNA modifications [40]. siRNA release can be triggered under specific conditions such as e. g. pH by pH-labile bonds. Targeted delivery would also be possible by systems such as (d), (e) and (f).

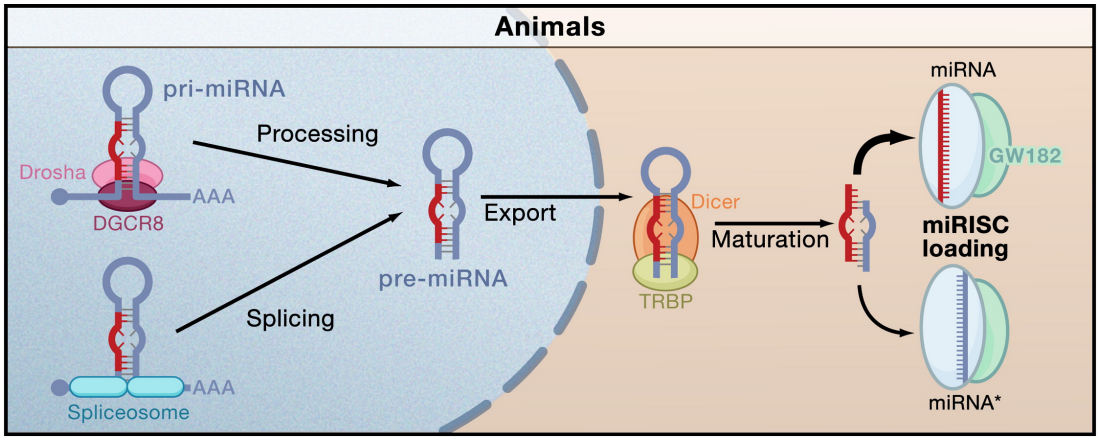

Figure 1.15: Biogenesis of miRNAs and assembly into miRISC in Animals [2]: Nuclear transcription leads to capped and polyadenylated pri-miRNAs. The pri-miRNA is processed by Drosha with the aid of DGCR8 to generate a pre-miRNA species. This is exported from the nucleus and processed by Dicer to form the mature miRNA/miRNA duplex. After processing, miRNAs are assembled into miRISC. Only one strand of the duplex is stably associated with an miRISC complex — the miRNA strand is usually more strongly favored than the miRNA* strand, although there are exceptions.

miR-122 miR-122 is a microRNA that is conserved between vertebrate species [43]. miR-122 is specific for liver tissue and is an established target for Hepatitis C (HCV) [44].

1.6 Disclaimer: affiliations

Names stated in this thesis belong to the following affiliations:

- Roche (F. Hoffmann-La Roche Ltd., Pharma Research and Early Development, Discovery Technologies, Switzerland)
- Rohit Mishra (CRANN - The Naughton Institute, School of Physics, Trinity College Dublin, Ireland)
- Martin Hegner (CRANN - The Naughton Institute, School of Physics, Trinity College Dublin, Ireland)
- IBM (IBM Research GmbH, Switzerland)
- SuSoS (SuSoS AG, Switzerland)

Chapter 2

Materials, Methods and Instrumentation

2.1 General remarks

Unless otherwise stated, the chemicals were analytical grade, used without any further purification and purchased from Sigma-Aldrich (Buchs, Switzerland).
We used Milli-Q H_2O for water if not otherwise stated. For RNA/DNA assays RNase and DNase free water was used (Distilled Water Dnase/Rnase Free #10977, GIBCO Invitrogen).
Prior to use we degased all running buffers by sonication under reduced pressure.
For all hybridizations we used Phosphate Buffered Saline with Calcium and Magnesium (PBS (+)) stated as Phosphate Buffered Saline (PBS) if not explicit specified.

2.2 Assay Development

Chemicals:

- "ECT" Eicosanethiol, 0.5 mM in abs. Ethanol (for hydrophobicity), $C_{20}H_{42}S$, MW 314.61, e. g. 3.14 mg in 20 mL of Ethanol (0.5 mM)
- "PEG" Thiolated Polyethyleneglycol, 1 mM in abs. Ethanol (for hydrophily), CH_3O-POE-NH-CO-$(CH_2)_2$-SH, MW 750, e. g. 150 mg in 20 mL of Ethanol (10 mM), Rapp Polymere GmbH, Germany

2.2.1 Detergent cleaning

To recycle Biacore SPR chips and for cleaning Au/Si micro devices, a detergent cleaning protocol developed by Gregor Dernick *et al.*, F. Hoffmann-La Roche Ltd. was used (Tab. 2.1).

1. Rinse substrate with 1× PBS.
2. Put the chips in the chip holder, fill it with 1× PBS, can be stored for a few days until cleaning procedure.
3. Fill chip holder with Deconex 12PA (Borer Chemie AG, Switzerland).
4. Put chips and holder in ultrasonic bath at 50 °C, sonicate for 15 min.
5. Rinse with water.
6. Put in wash bath with nanopure water and nitrogen bubbles for 10 min.
7. Fill chip holder with Deconex 20Ns (Borer Chemie AG, Switzerland).
8. Put chips and holder in ultrasonic bath at 50 °C, sonicate for 15 min.
9. Rinse with water.
10. Put in wash bath with nanopure water and nitrogen bubbles for 30 min.
11. Dry chips with nitrogen-jet, store protected from dust.

Table 2.1: Cleaning of Si/Au based microdevices after an experiment and/or prior to surface preparation.

2.2.2 Thermal denaturation in plate-shaker

To mix samples and to denature the DNA/RNA probes, we used a BioShake iQ high speed micro thermo shaker for SBS microplates, tubes and vials (BioShake iQ, QUANTIFOIL Instruments GmbH, Germany). For Eppendorf DeepWellplates 500 μL (Eppendorf AG, Switzerland) we mounted a customized adapter (#0030504.119, QUANTIFOIL Instruments GmbH, Germany). For 0.5 mL and 1.5 mL tubes an adapter 24× 1.5 ml and 15× 0.5 ml for BioShaker serial (QUANTIFOIL Instruments GmbH, Germany) was used. Validation is shown in Appendix B.1.

For improved DNA and RNA hybridization we denatured all probes prior to injection at 80 °C for 5 min followed by incubation on ice for 5 min.

2.2.3 XPS[2]

XPS analysis was performed using a PhI5000 VersaProbe spectrometer (ULVAC-PHI, INC.) equipped with an 180° spherical capacitor energy analyzer and a multi-channel detection system with 16 channels.
Spectra were acquired at a base pressure of 1×10^{-7} Pa using a focused scanning monochromatic Al-Ka source (1486.6 eV) with a spot size of 200 μm and 50 W. The instrument was run in the FAT analyzer mode. Pass energy used for survey scans was 187.85 eV and 46.95 eV on detailed scans.

Data were analyzed using the program CasaXPS (Version 2.3.15 www.casaxps.com). The signals were integrated following Shirley background subtraction. Sensitivity factors were calculated using published ionization cross-sections, (Scofield, J. H. J. Elec. Spec. Rel. Phen. 1976, 8, 129.) corrected for attenuation, transmission-function of the instrument and source to analyzer angle.

The measured amounts are given as apparent normalized atomic concentration and the accuracy under the chosen condition is approximately ±10 %.

All XPS measurements were performed at SuSoS by SuSoS technicians.

[2]Complete information received from SuSoS (SuSoS AG, Switzerland) as part of the purchase order for surface analysis and modification.

2.3 CLA Instrumentation

The cantilever deflection is measured by tracking a reflected laser spot on a PSD (1L10-10-A SU15, SiTek Electro Optics, Sweden). For detailed specs, refer to Appendix A.2. Due to the fact, that we are measuring in static mode we are only interested in DC signals. Therefore a 5 Hz Low-Pass filter was directly implemented in the PSD chassis. To run the PSD a ±15 V power supply with a VB 1/2/15 transformer (BLOCK Transformatoren-Elektronik GmbH, Germany) as core part was built. As laser source we chose pigtail lasers (LPS-635-CLEAVE-SP, Thorlabs GmbH, Germany) equipped with laser diodes 635 nm wavelength (HL6320G, Opnext Japan Inc., Japan), completed with SM600 fibers (Fibercore Limited, UK), flat cleave. To avoid electrostatic damage during device handling, we equipped all lasers with an Electrostatic Sensitive Device (ESD) protection and strain relief with DB9 connector (SR9A-DB9, Thorlabs GmbH, Germany). For testing purposes a benchtop LD current controller (LDC201CU, Thorlabs GmbH, Germany) was used. We established the stripping and cleaving procedure on bare SM600 single mode optical fibers with a fiber stripping tool T06S13 (Thorlabs GmbH, Germany) and fiber cleaver FkII (PK Technolgy, USA). For all measurements we operated the lasers in constant power mode. The effective optical output power was calibrated for each laser diode to 140 μW at the CLA's position with an optical power meter (E UNO, Gentec-EO, USA). By arranging the eight laser coupled fibers in a linear array we achieved readout of the eight cantilevers through their sequential illumination. The quality of the fiber cleave was visually checked by projecting the laser spot on a flat surface in wide distance as shown in Appendix B.2.
Alternatively several other laser sources were considered. In the original setup at the University of Basel and CRANN (Trinity College Dublin), Vertical Cavity Surface Emitting Laser (VCSEL) were used. The providing company, Avalon Photonics, Switzerland, did not exist anymore. Alternative companies such as Bookham AG, Switzerland or Philips Technologies GmbH ULM Photonics, Germany could not provide VCSEL arrays with the right specifications. Either wavelength, pitch size or beam divergence were not compatible or ideal for our setup. Instead of a sequentially illuminating eight lasers, an alternative of using one high-end laser could be used either mounted on a travelling stage (e. g. M-122.2DD, PI GmbH & Co. KG, Germany) or connected to a fiber switch for example by DiCon Fiberoptics Inc, USA.
The fiber dimensions were chosen to fit the cantilever array pitch size of 250 μm. This was achieved by a 1:2 optic (BFPL-12.7-25.0-C-633, BK7 singlet lens positive bestform, d=12.7 mm, f=25.0 mm, surface figure: lambda/10 at 633 nm before coating, antireflection coating 633 nm R<0.25 %, damage threshold: 10 J/cm^2, 8 nsec pulse, 1 MW/cm^2, CW at 1'064 nm typical, Melles Griot GmbH, Germany). Outer fiber dimension is 125 μm. A deflection mirror (02MFG001 with antireflective coating /023, Melles Griot GmbH, Germany) guides the laser towards the

PSD.
Our setup is divided into three parts. The main part is a temperature-controlled box containing the cantilever instrument and the fluidic system (Fig. 2.1 and Fig. 2.2). To keep the temperature at the cantilever array stable, we installed two controlled loops. (i) An external flow cycle thermostat (ministat 125, Peter Huber Kaltemaschinenbau GmbH, Germany) to stabilize the temperature inside the temperature-controlled box. (ii) The second temperature regulation module is a Peltier element (TEC1-1703, NTS electronic and components GmbH, Germany) mounted inside the measurement chamber at a distance of about 2 mm from the cantilevers. The Peltier element was regulated by a Peltier controller which is normally used for laser temperature stabilization (LDT-5525, ILX LIGHTWAVE, USA). For the ILX controller we chose a setpoint of 24.7 °C for best corresponding to room temperature. The flow cycle thermostat was set to 25 °C with −0.6 °C process temperature offset. For temperature feedback we installed several temperature sensors. The flow cycle thermostat measures the temperature with its external sensor (pt100 module) inside the post holding the flow chamber. The Peltier controller measures the temperature for feedback directly inside the flow chamber (SEMI833ET NTC thermocouple, HYGROSENS INSTRUMENTS GmbH, Germany). This value corresponds to the recorded temperature named "$T_{chamber}$". Furthermore the temperature inside a dummy probe vessel (T_{box}) and room temperature (T_{room}) are recorded (NTC thermocouple).

We performed all measurements in liquid phase. Two syringe pumps (neMESYS system, Cetoni GmbH, Germany) pull the system liquid and samples through the measurement chamber. The system consists of one base module (V2 NEM-B100-01 A CET-000987-1045) and two neMESYS dosing modules equipped with valves (14:1 gear NEM-B1010-02 B CET-001024-1045 to CET-001025-1045; see Appendix A.2). We used for slow flow speeds such as the system flow of 10 µL/min a 5 ml, 10.3 mm diameter Hamilton glass syringe (1005 TLL, 81520/01, Hamilton Bonaduz AG, Switzerland) and for faster flow speeds such as injections with >100 µL/min a 10 ml, 14.57 mm diameter Hamilton glass syringe (1010 TLL, 81620/01, Hamilton Bonaduz AG, Switzerland) with a BD plastic piston (piston from BD 10 ml syringe, REF 300912, BD, USA) to reduce stick-slip effects due to high friction forces with the original piston. To compensate for the pressure loss due to pulling we applied 80 mbar (nitrogen) overpressure on all sample vessels and the system buffer reservoir. Halar tubing (4030XL Tub Halar 1/16x.030, Ercatech AG, Switzerland) was used to reduce loss of probe molecules in the sample due to adsorption onto the tubing surface. The flow chamber is completely sealed and has a window (Mirogard Magic, 2 mm, SCHOTT AG, Supplier: Blaser Bauglas AG, Switzerland) to pass the laser beam. To automatically switch between a buffer reservoir and several probe vessels, we installed a VICI valve (C25 6180 EMHMA-CE, VICI AG International, Switzerland) in the flow path.

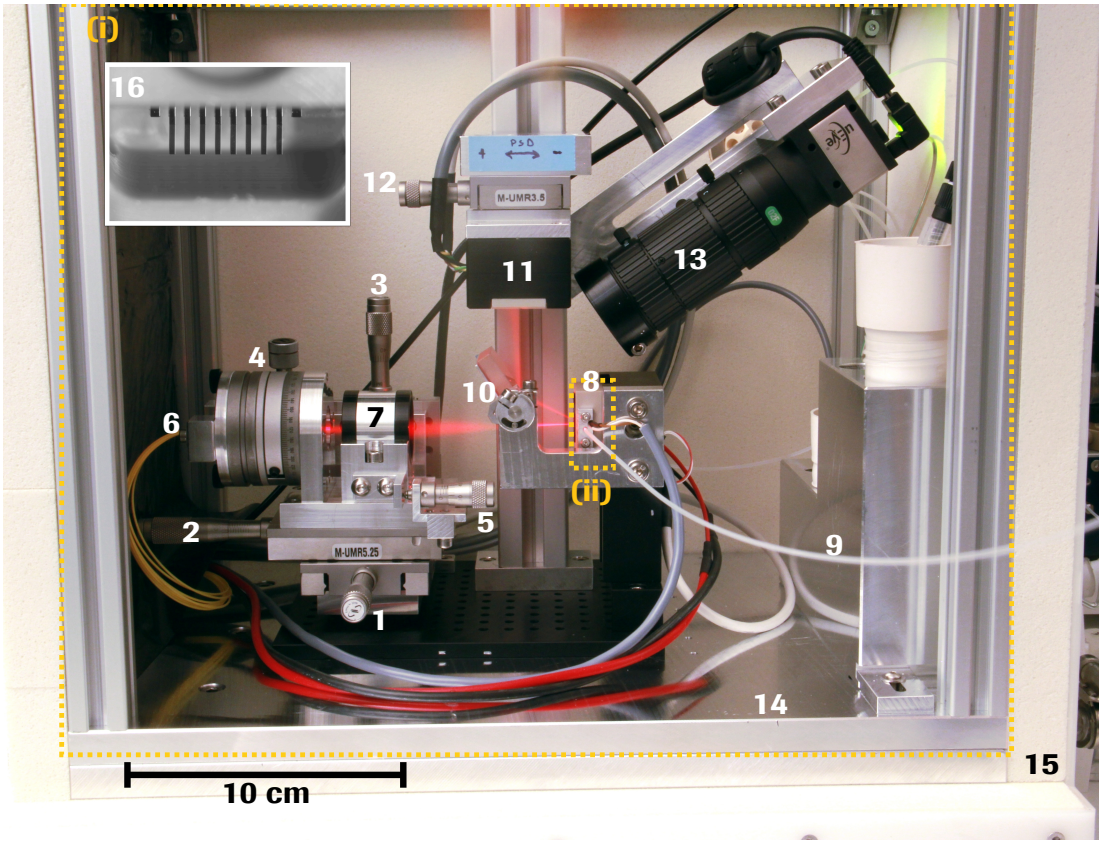

Figure 2.1: CLA instrument photo: View inside temperature controlled box containing the cantilever instrument. Laser ray-path visible due to slight haze. (1, 2, 3) x, y, z positioning; (4) parallel alignment of fibers to cantilevers; (5) longitudinal focusing on cantilevers; (6) optical fibers (laser sources); (7) lens; (8) flow-chamber (holds cantilever array chip); (9) tubing to syringe pump; (10) mirror with tilt function; (11) position sensitive detector (PSD); (12) PSD alignment; (13) camera module; (14) ground plate connected to flow cycle thermostat; (15) thermal insulated box; (16) inset of cantilever array image mounted in flow-chamber (8) taken with the camera module (13); (i) and (ii) illustrate the two temperature controlled zones.

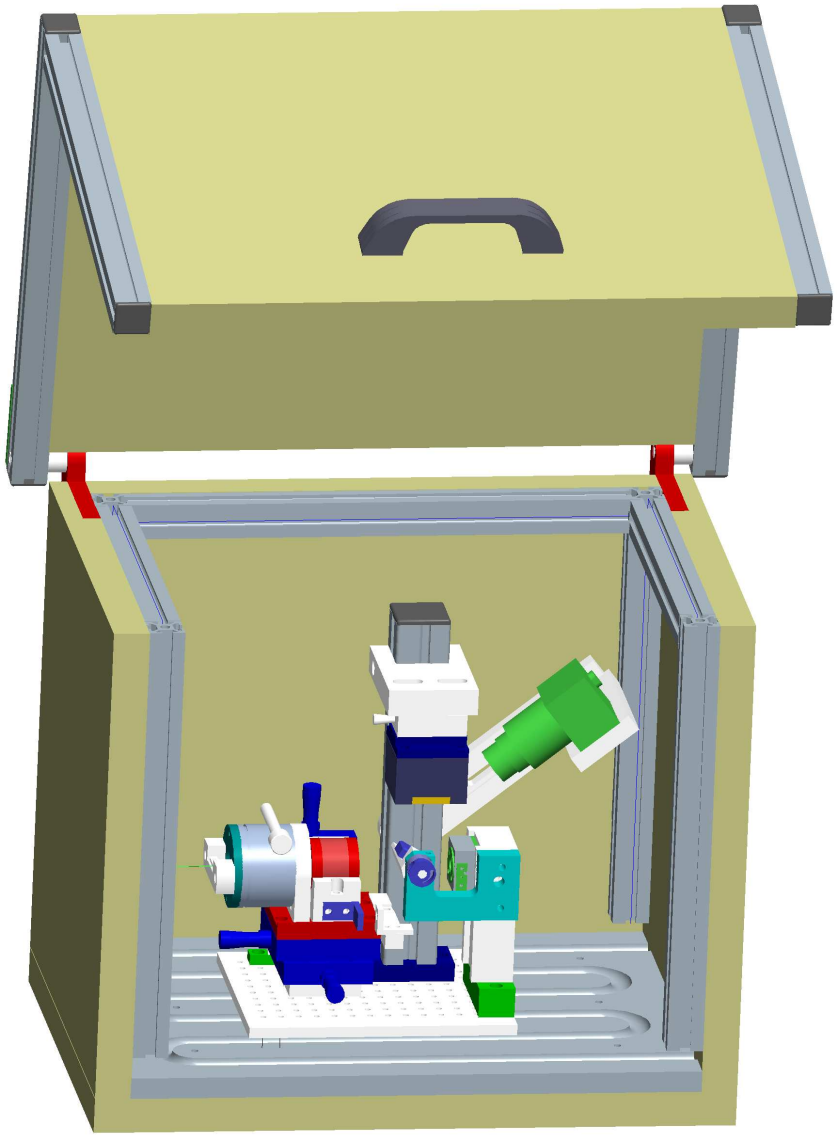

Figure 2.2: CLA instrument: CAD drawing for the construction of the instrument with a transparent bottom to show the pipes for heat exchange from the flow cycle thermostat.

To align the lasers and view inside the flow chamber, we installed a camera module (USB UI-1540SE, IDS Imaging Development Systems GmbH, Germany) with optics (MLM-3XMP, Computar - CBC (Deutschland) GmbH, Germany). To avoid oversaturation due to the strong laser light an additional short wavepass filter (SPF-550-25.0M, Melles Griot GmbH, Germany) was mounted in front of the camera lens.

For measurements the cantilever can be installed either under dry conditions or in a pre-filled system where the chamber and tubing are filled with buffer. In both cases we flush the system with CO_2 prior to filling with buffer. CO_2 dissolves 80 times better in water than nitrogen and leads to a gas bubble free fluidic system.
In addition to the temperature controlled box the setup comprises a 19" rack containing the laser controller and power supply for the PSD.

The setup is controlled by LabVIEW (NI PCI-6221 interface and LabView 8.0 software kit, National Instruments, Switzerland). A table with all connections is shown in Appendix A.2, Tab. A.1. All measured values are recorded and processed by LabVIEW software. The data analysis is based on algorithms which were tested and previously applied for kinetic microarray signals [45].

We used cantilever arrays with eight cantilever sensors pre-coated with 2 nm titanium 20 nm gold (IBM Research GmbH, Switzerland). External dimensions of these sensors are as follows: 500 μm length, 100 μm width and 0.5 μm thickness. To regenerate and clean the gold surface of environmental organics for subsequent ssDNA functionalization, the arrays were treated with UV ozone for 60 minutes (NIQ 40/18, Heraeus, Germany, radiation flux at 185 nm: $\sim$4 W; ambient O_2) prior to use [46]. An oxygen plasma treatment to clean the gold surface is not recommended due to the widely distributed electron energy leading to radiation damages and a poor controllability [46].

All measurements were performed under continuous flow (10 μL/min for equilibration before and after the injections and 100–150 μL/min for the probe injection and wash step) using the above mentioned syringe pumps. Cantilever arrays were functionalized with thiol modified ssDNA (Microsynth, Switzerland) for 60 minutes in 50 mM acetic acid - triethylamine solution buffer (Fluka #09748, Switzerland) in a home-built capillary device. Capillaries (KG-33, ID=0.18 OD=0.25, King Precision Glass Inc., USA) allow individual functionalization of the various sensors (Fig. 2.3).

The DNA sequences chosen for the proof of concept (Sect. 3.2) were `AGAATAGGTATTTTTCCACAT` for the biomarker target and `AGAATAGGTATAATTCCACAT` for the mismatch sequence. The chosen sequences do not tend to form hair-

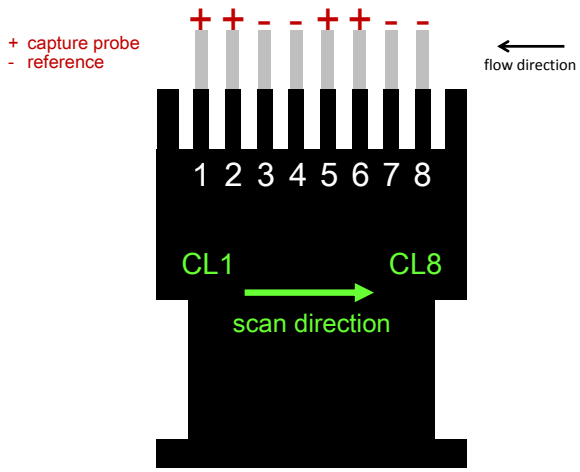

Figure 2.3: Schematic drawing of CLA showing the normally used pattern for functionalization: An even distributed pattern was chosen to avoid local effects during differential calculation. Two similar neighbors were chosen to minimize the risk of crosstalk during functionalization. Scan direction for the readout is from CL1 to CL8. Liquid flow in the chamber runs in direction CL8 to CL1 during measurements. Numbering of CLs as shown in the picture.

pins and do not dimerize. For proof of concept (Sect. 3.2) the following thiolated ssDNA oligonucleotides were used to functionalize the cantilever interface. (Sensor sequence: `ATGTGGAAAAATACCTATTCT`-C6 linker-SH, Reference sequence: `CTTACGCTGAGTACTTTGA`-C6 linker-SH). We used PBS with calcium and magnesium (Invitrogen #14040091, Switzerland) as running and hybridization buffer. Compared to Saline-Sodium Citrate (SSC) buffer we observe less salt crystal formation leading to coverage of the glass window and blocking of the light path. Furthermore the bivalent magnesium supports the hybridization.
For later experiments we used the corresponding sequences according to the target of interest. All sequences were provided by Microsynth, Switzerland and do not tend to form hairpins and do not dimerize. The full list of used oligonucleotides and their specifications is shown in Tab. 2.2.

2.4 SPR Technology

All SPR measurements were performed on a Biacore 2000 instrument (Biacore Life Sciences, GE Healthcare). As sensor chip we used either recycled CM5 or SM Biacore sensor chips or commercially bought Biacore Au sensor chips (BR-1005-42, Biacore AB, Sweden). To recycle the CM5 and SA chips we cleaned them according to protocol (see Sect. 2.2.1) with detergents and treated the chips prior to the functionalization with UV/O_3 for 10 min.

In most of the cases the SPR chip was functionalized outside the instrument. If not otherwise stated the oligos were immobilized onto the surface by pipetting 50 μL, 10 μM thiolated ssDNA in 50 mM TEAA buffer. The solution was incubated on the chip overnight (>10 h). The chip was washed by rinsing with TEAA buffer for 30 s, respectively 3× aspirated and pipetted with buffer.
Afterwards the chip was incubated for 1 h with 50 μL, 10 μM 11-Mercapto-1-undecanol (MCU) solution. The chip was washed by rinsing with H_2O for 30 s (3× aspirate and pipette), dried in an air-stream of N_2 and stored under Argon atmosphere at 4 °C.
Oligo solutions were prepared and stored in Biopur Safe-Lock reaction tubes 0.5 mL (Eppendorf #0030121.570). Samples were filled in either glass vials, Ø9 mm, 1.8 mL, borosilicate vials (Biacore #BR-1002-07) or plastic vials, Ø7 mm, 0.8 mL rounded polypropylene microvials (Biacore #BR-1002-12) to mount into the Biacore 2000. Vials were autoclaved in-house before use and closed with rubber caps, type 3 penetrable cap made of kraton G (SEBS) (Biacore #BR-1005-02).
In case the Biacore instrument was used before without any cleaning procedure in between, the system was cleaned by injecting 20 μL, 0.1 M HCl followed by injecting 20 μL, 1.0 M ethanolamine-HCl pH 8.5 on a maintenance chip.

For exploratory conditions either 0.1× SSC or PBS (PBS with Calcium, Magnesium, Invitrogen #14040091) was used for hybridizations. For standard conditions we used PBS (PBS with Calcium, Magnesium, Invitrogen #14040091). Sensorgrams were recorded with 5 μL/min flow through all channels if not otherwise stated. Injections were made by automated injection with the program "Inject" or "Kinject". In case of the kinetic inject program "Kinject" a distortion time had to be set.
Standard experiments with repeated conditions were later on run by written methods in a fully automated mode.
Under standard conditions 50 μL probe were injected with 5 μL/min flow. Regenerations were achieved by injection of 2× 5 μL urea (pulsed injection recommended by the manufacturer in case of harsh conditions to protect the tubing and microfluidics).

2.5 Biological Application

Thiolated oligo samples were shipped containing Dithiothreitol (DTT) for stabilization. DTT acts as strong reducing agent and avoids disulfide bonds between the several thiol groups. Before immobilization on gold the DTT hat to be removed. We processed a sample (200 μL) by extracting 3× with 1:1 diethyl ether, mixed in an Eppendorf tube and shook well. The aqueous (lower) phase was collected, aliquoted and evacuated for 20 min in an exsiccator. Afterwards the exsiccator was flushed with argon and the tubes closed under argon atmosphere. We sealed all tubes with Parafilm. The final concentration was checked by NanoDrop for one aliquot each.

2.5.1 totRNA fragmentation

As background and as pool of unspecific RNA we used universal human reference RNA (Stratagene #740000, Agilent Technologies, USA). To make the total RNA (totRNA) more competitive we fragmented the sample to receive ∼90 nt long RNA strands.
RNA samples were stored at −80 °C. We unfroze the samples and transferred them according to the Stratagene protocol into 50 μL H_2O (Appendix A.1). A 1:10 diluted sample was analyzed by NanoDrop (NanoDrop 2000, Thermo Fisher Scientific) resulting to 500,4 ng/μL. The stock solution (5 μg/μL) was diluted 1:5 in H_2O resulting in a 1 μg/μL solution. 5 aliquots with the 1 μg/μL fraction were fragmented according to the "Bauer Core Standard Protocol" (Appendix A.1) in an Eppendorf Thermomixer (Eppendorf AG, Switzerland) at 94 °C, 350 rpm. Each one tube was processed for 10 min, 20 min, 35 min, 45 min and 60 min and afterwards immediately cooled down on dry ice. After storing the probes for one night at −80 °C the samples were checked on an agarose gel (3 μL each). Before a Bioanalyzer (Agilent Technologies, Switzerland) test, we had to precipitate the RNA to get rid the fragmentation buffer. RNA was precipitated according to the Solid (Applied Biosystems, Life Technologies, USA) protocol. Samples were resolved in 20 μL H_2O and checked by NanoDrop. For the Bioanalyzer run we diluted 2 μL in an additional 2 μL H_2O. The run was performed on an Agilent total RNA Analysis ng sensitivity (Eukaryote) assay (Agilent Technologies, Switzerland).

2.5.2 Cell culturing

For the detection of ncRNA under realistic conditions (e. g. as toxicology screening test), we aimed to detect ncRNA out of cell lysates. For this purpose we cultured four different types of cell lines (see Tab. 2.3). Hep G2 and Hep 3B as model for F7-1 (F7 mRNA transcript) and HuH 7 and ME 15 as model for miR-122. Hep G2 is negative for F7 and Hep 3B positive. From the literature Ref. [47] we know

Sequence 5' → 3'	**Lot-No.**	**Name**	**Properties**
ATG TGG AAA AAT ACC TAT TCT-C6 linker-SH	932565, 1349394	F7 Sense Match	6'581.8 g/mol
ATG TGG AAT TAT ACC TAT TCT-C6 linker-SH	932566	F7 Sense Mismatch 1	6'564.0 g/mol
ATG TGG AAA AAT ACC ATA TCT-C6 linker-SH	932567	F7 Sense Mismatch 2	6'590.7 g/mol
AGA ATA GGT ATT TTT CCA CAT	932568	F7 Antisense Match	6'418.9 g/mol
AGA ATA GGT ATA ATT CCA CAT	932569	F7 Antisense Mism. 1	6'436.7 g/mol
AGA TAT GGT ATT TTT CCA CAT	932570	F7 Antisense Mism. 2	6'410.0 g/mol
CTT ACG CTG AGT ACT TTG A-C6 linker-SH	932571, 1349395	Control	5'947.6 g/mol
GAC TTA CCA GGA TTA CCA GGG ATT TAG CGT	932572	Scrambled	9'398.8 g/mol
Cy5-AGA ATA GGT ATT TTT CCA CAT	1022223	F7 Antis. Match Cy5	6'952.9 g/mol
Cy5-AGA ATA GGT ATA ATT CCA CAT	1022224	F7 Antis. Mism. 1 Cy5	6'970.7 g/mol
Cy5-AGA TAT GGT ATT TTT CCA CAT	1022225	F7 Antis. Mism. 2 Cy5	6'944.0 g/mol
CAA ACA CCA TTG TCA CAC TCC A-C6 linker-SH	1349396	miR-122 sense	6'883.6 g/mol
TGG AGT GTG ACA ATG GTG TTT G-C6 linker-SH	1349397	miR-122 control	7'168.0 g/mol
TGG AGT GTG ACA ATG GTG TTT G	1349398	miR-122 antisense	6'876.0 g/mol

Table 2.2: Table of used oligo nucleotide strands. Mismatch positions shown in color red.

that ME 15 is negative for miR-122 and HuH 7 highly overexpressing the target.

1 mL cell stock was seeded in a small cell culture flask (BD Biosciences) with 10 ml corresponding medium according to Tab. 2.3 (Gibco, Life Technologies Corporation). We checked the cells on a two daily basis if they are confluent. If not, we changed the medium. In case the cells were confluent, the medium was removed, the flask washed with 5 mL PBS, the PBS removed and 500 μL Trypsin (Gibco, Life Technologies Corporation) added. To dissociate the cells, they were incubated for 5 min with the Trypsin. We added 5 mL medium, aspirated the cells and transferred them in a medium flask. 20 mL medium were added to a total of 25 mL. To split the cells from the medium flask to two large flasks, after dissociation the cells with Trypsin, 10 mL medium were added and each 5 mL transferred to a large flask. We added 25 mL medium in each flask to a total of 30 mL. For dissociation in the medium flask, 1 mL Trypsin was added, in a large flask, 2 mL Trypsin were added. Cells were split from a large flask in a ratio of 1:3 to three new large flasks (4 mL cell solution in each flask plus 26 mL medium). To harvest the cells from the large flask, the medium was removed, the flask washed with 10 mL PBS, the PBS removed, 2 mL Trypsin added and incubated for 5 min. Afterwards 10 mL medium were added and the cells aspirated. All fractions were transferred in a 50 mL falcon tube (Falcon, BD Biosciences) and additional 25 mL medium were added to inhibit the Trypsin. With 10 μL solution we performed a cell count. Two fractions of cell solution containing each 10×10^6 cells were transferred to two 15 mL falcon tubes (Falcon, BD Biosciences). The tubes were centrifuged for 5 min at 400 rpm. We removed the buffer and resuspended the pellet in 10 mL 1× lysis-buffer (8 mL H_2O + 2 mL Lysis-buffer (Promega Passive Lysis Buffer 5×, #E194A, Promega)) to a final concentration of 10^6 cells/mL.

Cell lysates were normalized on their total protein concentration. To get the total protein concentration we did a Bradford assay. As calibration line we used a BSA standard (Albumin Standard #23209, Thermo SCIENTIFIC). Bradford Assay Reagent (BIO-RAD-PROTEIN ASSAY #500-0006, BIO-RAD) was diluted 1:5 with H_2O. Cell lysate samples were diluted 1:1, 1:2, 1:5, 1:10, 1:20, measured in doubles with 10 μL probe. 10 μL of each standard and probe (in doubles) were transferred in a 96-well plate. 240 μL assay reagent were added. Signal was measured in a MTP-Reader (BioTek Synergy 4, BioTek Instruments) at 595 nm.

2.5.3 Peltier Test

To prove the consistency over several injections with the same cantilever we performed repeated Peltier peak tests. We record prior to each experiment a heat induced stress test — Peltier test. The temperature in the chamber (Peltier element) was increased for 10 s at 30 °C. The resulting cantilever deflection peaks were used for cantilever normalization to compensate for differences in mechanical

Name	No.	Cell type	Properties	Medium
Hep G2	ATCC 92, ATCC 91, ATCC HB-8065 CLBA170	Human liver carcinoma cell line	Negative for F7	41090 + 10 % FBS
Hep 3B	ATCC 170	Human liver carcinoma cell line	Positive for F7	41090 + 10 % FBS
HuH 7	CLBA00398 loBA_08	Human liver carcinoma cell line	Positive for miR-122	41965 + 10 % FBS
ME 15	Rachel Scott's stock 02.04.2007	Human melanoma cell line	Negative for miR-122	RPMI 1640 w/Glutamax-I, non-essential AS, Sodium pyruvate (1 mM), 10 % FBS

Table 2.3: Table of used cell lines.

properties or as control to check their functionality. By repeating this test before each injection and at the end of the whole series we monitored the functionality of the array plus consistency for several sample injections, respectively regeneration steps.
Sample graphs are shown in Appendix B.4.3.

Chapter 3

Results and Discussion

The following sections describe the experimental results towards the final goal, the label-free detection of noncoding RNA.

3.1 Assay Development

The general section "Assay Development" describes the Research & Development (R&D) of the assay which then later was used for the Biacore SPR and CLA experiments. Specific assay validations are partial described in the separate result sections for each corresponding topic.
Appendix B.1 shows the results from the plate-shaker validation.

3.1.1 Surface analysis and CLA rear-side passivation[3]

To avoid unspecific effects on the rear side of the cantilever the silicon surface had to be passivated.
In a first attempt a protocol was established and the resulting surface characterized in order to render the silicon surface resistant against unspecific adsorption and to provide a clean and reactive gold surface. In a second step the protocol was transferred to be applicable on the IBM cantilever arrays.
Two polymers were tested as non-fouling layer: (i) Polyethylene glycol (PEG) and (ii) Polyvinylpyrrolidone (PVP). Problems with crystallization occurred with the PEG polymer. Therefore PVP was favored. It was possible to coat the cantilevers with SuSoS protocol, but a few parameters had to be optimized, such as concentrations of coating solutions to obtain a desired thickness. Nevertheless a first proof of concept could be obtained. In none of the cases the cantilevers brake, but if the coating was too thick, a permanent bending in the dry state was

[3]Results achieved in collaboration with SuSoS (SuSoS AG, Switzerland) as part of the purchase order for surface analysis and modification. Text partially free translated from untitled, unpublished protocol and results of SuSoS, unpublished 2011.

observed. An XPS spectra of a thick versus thin layer proofs the presence of the coating in both cases with a higher amount of gold from the substrate detectable for the thinner coating as expected. Thick layer means a denser ad-layer than the thinner one. The shape of the C 1s signal is as expected for PVP. Wash steps had to be adapted to the microdevices, because the common known protocols were too harsh for the fragile structures.

XPS analysis of surfaces from commercially bought clean Au Biacore sensor chips and the IBM cantilevers are similar and therefore comparable bases for the two assays. Nevertheless some impurities were detected on the CLAs (Si, Au, O, F, Ca) with very high chip to chip variabilities. Impurities from manufacturing are less critical on the upper side, because the last step is the gold coating that should cover all the remaining particles. For passivation the Si rear-side impurities can be critical. Impurities can impair a full adsorption of the non-fouling layer.

Further trials were performed with the addition of a thiol protection step (to protect the Au side from uptake of the Silicon side adhesion promoter). These trials were successful and resulted in training for the coating process. These samples were then taken to Roche for experimental work, and returned to SuSoS for analysis.

It was observed that after EtOH wash and drying in ambient air or desiccator, the CLs are mostly fully bent (180°) and do not relax reproducibly. Most of the CLs relax after a certain time period up to hours. Worst is the situation if water is used as last wet step. There all the CLA were bent and only few relaxed. A positive effect was observed by drying the arrays in an air-stream. The actual protocol for the selective functionalization of Si/Au cantilever is stated in Table 3.1.

The cantilevers of one fully passivated CLA chip were functionalized with DNA. After washing in immobilization buffer (TEAA), the array was dried in an air-stream (all according to the protocol). After drying all CL on the passivated chip were broken somewhere in the middle region whereas a reference chip not treated for passivation did survive the functionalization as usual.

An XPS survey spectra and detail spectra of C 1s, O 1s, Si 2p, N 1s, S 2p, Fe 2p, Ca 2p, N 1s, F 1s and Au 4f were acquired on a wide set of cantilevers (sometimes on multiple positions as specified) except 'as received' Au side cantilevers where only a survey was acquired. In addition, P 2p was measured on a set of SPR chips. Table 3.2 shows a brief overview of the analyzed samples. Fig. 3.1 shows the measured binding energy spectra for the mentioned samples. Full XPS results can be found in the Appendix B.1.

The following results were achieved by the XPS analysis for the CLA chips

1. Plasma (O_2, 2 min)
2. Dip in EtOH
3. Dry in desiccator under vacuum
4. Dip in thiol (HS C11 NH_2 HCl, 0.25 mg/mL in EtOH, 1 h)
5. Dip in EtOH
6. Dry in desiccator under vacuum
7. Dip in adhesion promoter, HVA (0.1 mg/mL in 3:2 EtOH/H1, 30 min)
8. Dip in 3:2 EtOH/H1, twice
9. Dip in ultra-pure water
10. Dip in EtOH
11. Dry in desiccator under vacuum
12. Dip in PVP (1 mg/mL in EtOH, 2 min)
13. Dry overnight in air
14. UV-C (2 min)
15. Rinse o/n in ultra-pure water
16. Fresh dip rinse in ultra-pure water
17. Dry in desiccator under vacuum

Table 3.1: Coating process for Au/Si microdevices according to SuSoS: Additional wash steps after (16.) with 50 % EtOH and 100 % EtOH can be implemented. By drying the CLs in an air-stream (N_2 puriss) a sticking of the cantilevers to the CLA body (bent state for 180°) can be avoided. Furthermore drying the chip from a H_2O rise is too slow and therefore leads to more sticking cantilevers compared to a final EtOH rinse.

No.	**Substrate**	**Conditions**
1	Si Side Array 10/5 Position 1	As received (plain)
2	Si Side Array 10/5 Position 2	As received (plain)
3	Si Side Array 9/5 Position 1	As received (plain)
4	Si Side Array 9/5 Position 2	As received (plain)
5	Si Side Array 9/5 Position 3	As received (plain)
6	Si Side Array 10/4	As received (plain)
7	Si Side Array 9/3 Position 1	As received (plain)
8	Si Side Array 10/3	As received (plain)
9	Si Side Array 9/4 Position 1	As received (plain)
10	Au Side Array 10/1 Position 1	Only thiol coating step
11	Au Side Array 10/4 Position 1	PVP
12	Si Side Array 10/4 Position 1	PVP
13	Si Side Array 11/3	PVP, UV/O_3, oligo
14	Si Side Array 11/4	No PVP, UV/O_3, oligo
15	Au Side Array 11/1	No PVP, UV/O_3
16	Au Side Array 11/2	PVP, UV/O_3
17	Au Side Array 11/3	PVP, UV/O_3, oligo
18	Au Side Array 11/4	No PVP, UV/O_3, oligo
19	SPR Chip 1	Au chip, UV/O_3, oligo, MCU
20	SPR Chip 2	CM5 chip, UV/O_3
21	SPR Chip 3	CM5 chip, UV/O_3, oligo, MCU
22	SPR Chip 4	CM5 chip, UV/O_3, oligo
23	CLA Au side	1 μm chip, UV/O_3, oligo

Table 3.2: Catalog of XPS analyzed substrates: Preparations according to 3.1. PVP: PVP coated (incl. all necessary steps in advance); UV/O_3: 10 min UV/O_3 treatment at Roche; oligo: 1 h oligo functionalization for CLA and >10 h for SPR; MCU: 1 h MCU post treatment.

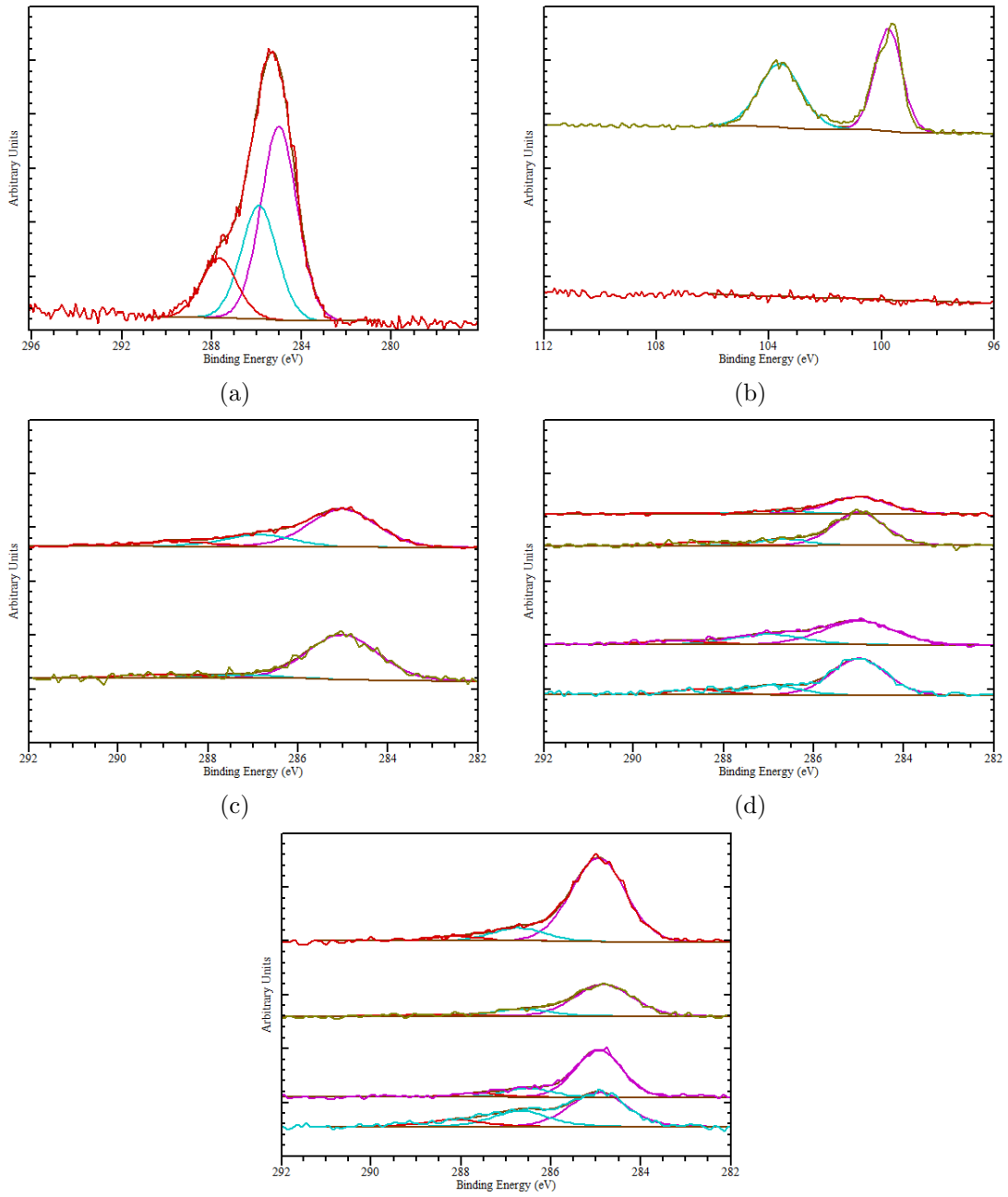

Figure 3.1: XPS results: (a) Tab. 3.2: #12, C 1s region of PVP coated Si side of cantilever showing typical PVP peak shape (pink C-C, blue C=O, red CON). (b) Overlay of Si 2p region for 'as received' Si side cantilever (Tab. 3.2: #8, upper) with PVP coated Si side (Tab. 3.2: #12, lower). (c) Overlay of C 1s region for Tab. 3.2: #13 (red curve) and Tab. 3.2: #14 (green curve), Si side treated cantilevers. (d) Overlay of C 1s region for Tab. 3.2: #15-18 (red to blue curve), Au side treated cantilevers. (e) Overlay of C 1s region for SPR chips #19-22 (red to blue curve) (Tab. 3.2, upper to lower) fitted peaks from right to left: C-C, C=O, CON/COO.

(Numbers refer to Tab. 3.2):

- Thiol coated Au side analysis by XPS does not show the presence of thiol (no S) but perhaps the concentrations are below detection limit.
- PVP successfully coated onto cantilevers Si side (good PVP C 1s signal and ratio, N, little or no substrate (Si) components). The reproducibility between samples could be improved.
- PVP is also present on the Au side in very small amounts (but not so convincing with the C 1s peak components).
- The Roche treated microdevices PVP coated ones have a different C 1s signal. Perhaps the PVP is partially attacked by the UV/O_3 treatment. Some F is present (perhaps from the adhesion promoter underneath).
- #15 Au side has a lot more C than expected (not clean), this then probably has an influence on the coating processes used. #15 also had P which is unexpected.
- It would be expected that the Si side of #15 is also similarly C contaminated.
- #16 Au side has less and not the expected C components for PVP, which is perhaps partially destroyed by the UV/O_3 treatment. The C contamination is slightly less than on #15, although this is difficult to say exactly.
- It would be useful to have the data for the Si side of #16, with expected PVP.
- #13 Au side, it would be expected to have the oligo present, there is P but no difference from some non oligo treated samples. It is difficult to determine this compared to the PVP composition (both contain C-C, C-O, C-N).
- #13 Si side contains PVP as expected (also some P, which is not expected).
- #18 Au side has a similar composition to #17, but with no P (which should be present).
- #18 Si side still contains quite a lot of C, but not PVP (as expected).

The following results were achieved by the XPS analysis for the SPR chips (Numbers refer to Tab. 3.2):

- It is expected that #20 is a clean Biacore chip. This chip still has around 25 normalized At.-% C, but less than the other chips. There also is some P present, which is not expected.

- Chip #22 has more C and more P (slightly), which is expected as the chip has immobilized Oligo1.

- Chip #21 has a lot more C than #22 as expected, as the chip, as well as immobilization of oligo also has the MCU spacer. The amount of P also decreases as expected when compared with #22.

- Chip #19, the original Au chip is similar in composition to #21 as expected (both have oligo and MCU spacer) but #19 has slightly more P.

- #23 was only measured one cantilever (position not known) so there is difficulty concluding anything from this measurement. It seems there is oligo immobilized (C-O and N) but slightly odd that no P was detected.

Besides the fragile structure and device handling difficulties due to its size, the CLA assay has a further disadvantage compared to the SPR. Where in the SPR setup only the sensor surface is exposed to the analyte, in the CLA setup the whole cantilever is surrounded by liquid. This implicates that effects on the cantilever rear-side can interfere with the ongoing measurement on the actual sensor surface — the upper side.
For static mode experiments, already during functionalization of the CLA chip we must apply a selective immobilization of capture probes on only one sensor surface (usually the upper-side). Only one side might be functional to avoid canceling the forces from opposite directions. This is achieved by gold coating the upper CL side and a selective thiol chemistry to apply the capture probes.
Although silicon has a "neutral" appearance to biomolecules a certain affinity is given. Especially with the recently gained knowledge about the origin of forces leading to a cantilever deflection (see Sect. 1.3), we have to be cautions and effects occurring on the CL rear-side cannot be neglected.
A passivation of the cantilever's silicon rear-side might lead to a closer comparability with the one-side SPR system and will impair parasitic effects on the rear-side.
With a selective treatment of upper and rear-side we might be able to reduce the remaining drift even more. A non-fouling ad-lyer (good omniphobe functionalization) would be a good solution to passivate the Si rear-side. The question of gain in sensitivity remains. With an assumption of a high drift value of 10 nm/min drift and a low signal of 100 nm we might be able to reduce the drift for 50 %. In terms of signal win, the gain would only be 5 %. As long as it is not proven that the chemical-physical conditions do have a significant influence on the drift, it is not necessary to passivate the cantilever's rear-side. Furthermore we expect the parasitic effects on the rear-side to be canceled by subtracting the reference cantilever which does experience the same effects.

The protocol by SuSoS recommends a UV-curing application of the non-fouling polymer on top of the Si surface (UV-linker to attach the hydrophilic brush forming polymer). Several advantages compared to other commonly known methods are given:

(i) A functionalization by applying a poly lysine PLL-PEG layer would add charge on top of the surface respectively neutralize the negatively charged SiO_2. The stability of this binding, respectively the charge during an experiment with different buffer and salt concentrations might be questionable.

(ii) Polyelectrolytes do swell under certain pH conditions and differing ionic strength.

(iii) A silanization would not be reproducible enough because the chemical properties significantly change with humidity.

3.2 CLA Instrumentation[4]

3.2.1 Proof of concept

With the described setup, we could detect a 100 pM antisense strand (F7) and differentiate between a perfect match and mismatch sequence. Fig. 3.2 shows the overlay of two consecutive experiments. Before each injection a stable baseline was recorded to ensure that all cantilevers were equilibrated (phase (I)). Due to the automated injection program the timing for the following injection steps was the same for each experiment. This allowed the overlay of the two sequential experiments shown in Fig. 3.2. The effect of switching the valve from running buffer reservoir to the probe container and changing the flow speed from 10 μL/min to 100 μL/min is visible at the beginning of the sample injection in phase (II). It takes about 3 minutes until the sample reaches the chamber with the cantilevers. This explains why the slope did not change significantly until mid phase (II). The heavy fluctuations can be explained by the change in refractive index, flow effects and the exchange of molecules in the chamber before a new equilibration is set. After 10 min the sample (1'000 μL) is completely injected, the valve switches back to running buffer and the flow speed is decreased to 10 μL/min (transition to phase (III)). In phase (III) the chamber is still filled with probe solution. A stable equilibrium is not reached during this incubation period. Several reactions leading to a cantilever deflection as described in Ref. [30] tend to occur. To remove the remaining probe solution and wash the chamber the buffer flow was increased (phase (IV)) to 100 μL/min. We flushed with 1'000 μL buffer. Here we see again the delay before the probe solution in the system was fully replaced by buffer (change in slope). The peak at the changing point can be explained by the change in electrostatic conditions of the plain buffer solution compared to the buffer solution with probes. Fast effects such as valve switching and bulk buffer changes cannot be fully recorded due to the comparatively slow data acquisition (0.25 Hz) and therefore sequential injection traces are not completely identical. Finally the program switches back to the standby conditions (10 μL/min buffer flow) and the resulting deflection values are monitored. Compared to the end point of the deflection in phase (III), the start point of phase (V) is slightly higher ($\sim$50 nm) although we have the same flow speed in phase (III) and (V): 10 μL/min. A small amount of deflection is lost due to the dissolution of weakly bound strands (not fully hybridized) during the washing step. The two injections shown (red curve and black curve) were recorded sequentially. First the negative probe (mismatch configuration) was injected and after a new equilibration the match injection was monitored. Finally the two starting points of the baselines were shifted to zero and the graphs plotted in an overlay. The resulting net deflection of $\sim$200 nm for the 100 pM matching probe

[4]Partially published in Peter Noy *et al.*,"Instrument for Label-Free Detection of Noncoding RNAs", Journal of Sensors, vol. 2012, 2012.[27]

injection is repeatedly measured in our experiments. The resulting surface stress of about $9\,\mathrm{mN\,m^{-1}}$ is relatively high compared to previous experiments such as Ref. [13] (Young's modulus (Si): 130 GPa, Poisson ratio: 0.28). Reasons therefore could be due to longer cantilever functionalization times and due to different buffer properties which affect steric hindrance and ionic repulsion of the molecules.

3.2.2 Drift Analysis

By means of temperature stabilization and continuous flow measurements drift in the raw deflection signal was reduced from ∼12 nm/min to ∼2.5 nm/min as shown in Fig. 3.3. The described setup and protocols represent a significant drift reduction by a factor 5 compared to previous experiments with readout in stationary fluid before and after sample injection. The gain in accuracy is especially of importance for the hybridization measurement with reaction times >1 min. The typical drift shown in Fig. 3.3 was observed in all actual measurements.

In an experiment with a bare Au chip without any immobilized molecules we could show that reactions on the CL surface do have a significant drift effect. Although temperature and sum signal were absolutely stable we observed massive drift >10 nm/min (constant flow of 10 µL/min to avoid diffusion effects). An open question is how much deflection results from effects on the Au surface and how much from the silicon backside.

3.2.3 Electronics

In terms of electronic parts we used state of the art components. The amplifier has a noise level of approximately 1 µV, the PSD ∼3 µV (Bandwidth (BW) = 100 Hz). The analogue digital converter NI PCI-6221 with ∼122 µV noise level is therefore the main source of electric disturbance (values from datasheet stated in V_{RMS} to illustrate the critical components). Therefore we adjusted the full range scale to the maximum signal voltage and took the average over several measurement points (1'000 samples in 500 ms). This is possible due to the slow reaction time (>1 Hz) compared with the sampling rate characteristics of the electronic parts. The precision of the National Instruments (NI) card is dependent on its dynamic range. For ±5 V detection voltage range, the random noise is 122 µV and the sensitivity 48.8 µV. For ±10 V dynamic range, the random noise is 244 µV and the sensitivity 97.6 µV (see Attachment A.2). Furthermore we optimized the settling time of the laser controller and adjusted the data processing to let the laser stabilize after switching. Before averaging we discard the first half of the data points to be sure to have a stable laser signal. The remaining 500 samples are still enough for noise reduction by averaging. Due to the sequential readout a too long sampling time might lead to missing a reaction event.

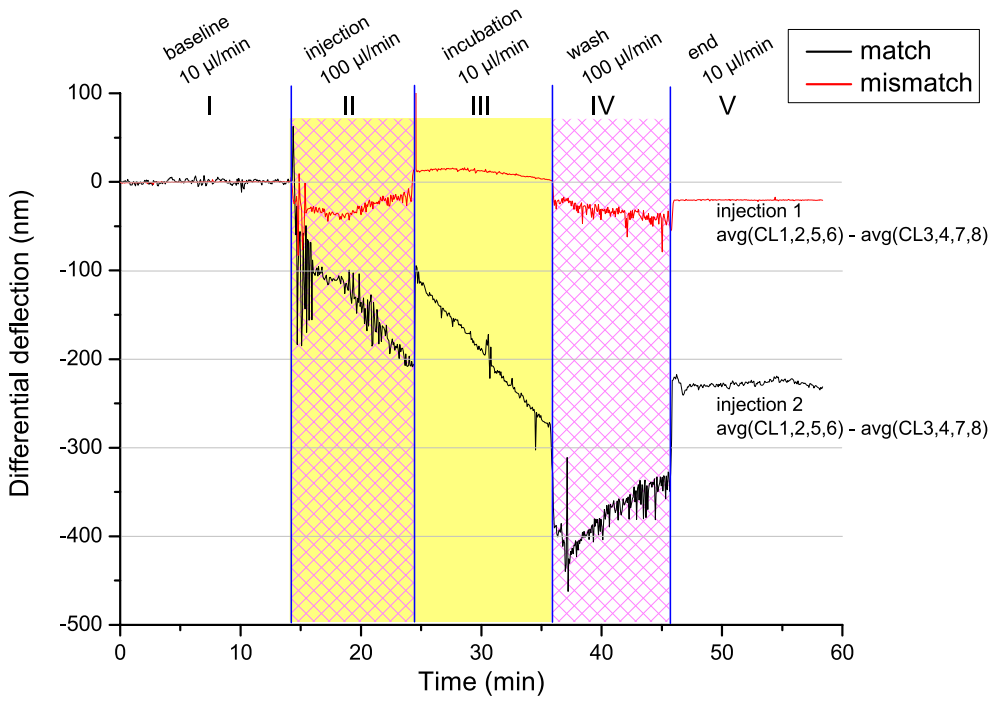

Figure 3.2: Overlay of two consecutive experiments to prove the detection of a 100 pM antisense strand: The graph shows the significant difference between an injection of 100 pM antisense match strand (black curve) and an injection of 100 pM antisense mismatch strand (red curve, the mismatch has two nonmatching base pairs in the center of the target). Injecting the match sample induces approx. −200 nm differential deflection whereas the injection of the mismatch configuration leads to almost no differential signal. Phase (I) shows the recorded baseline at 10 μL/min buffer flow. (II) 1'000 μL sample injection at 100 μL/min. (III) incubation phase at 10 μL/min. (IV) flushing with buffer 100 μL/min. (V) resulting differential deflection after injection cycle is completed (10 μL/min buffer flow). Curves correspond to the differential deflection signal of positive minus reference CL. Therefore the bending of the cantilevers are not absolute but differential deflections. The two injections were performed in series on the same cantilever array chip. A baseline correction, normalization, averaging and differential signal calculation (probe minus reference) were done according to the literature [45]. Hatched area highlights the increased flow speed during injection and wash phase. Colored area indicates the presence of probe molecules in the flow-chamber.

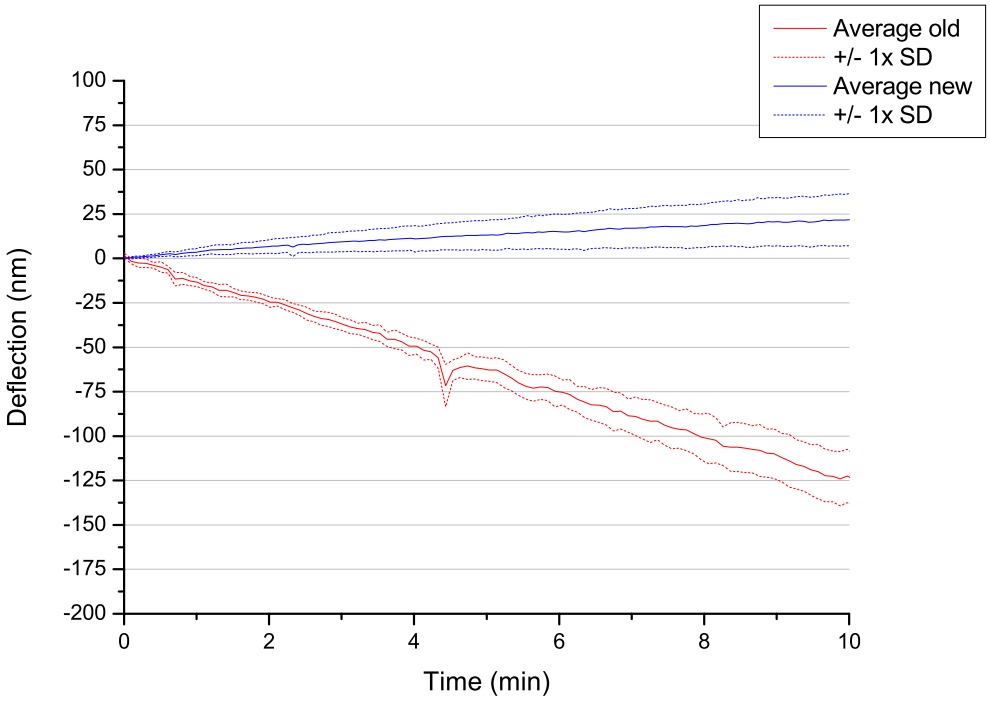

Figure 3.3: Typical drift before (red curve) and after implementation (blue curve) of means for drift reduction (continuous flow, temperature regulation etc. as described in this thesis): Curves show the average of the raw data from 8 recorded cantilevers and the corresponding standard deviation. Curves have an offset at zero. Red curve measured under stationary conditions (flow: 0 μL/min). Blue curve measured in flow (10 μL/min).

Super luminescent diodes might lead to a more stable laser signal due to their characteristics.

3.2.4 Temperature

By placing a temperature controlling element close to the cantilever array we obtained a controlled loop with very short time constant for temperature equilibration. Time to regulate the temperature in the chamber from 21 °C room temperature to 25 °C setpoint is approx. 0.5 min (Fig. 3.4 (b)). The much slower flow cycle thermostat regulation loop than that of the Peltier element leads to a stable temperature for all probe vessels, the buffer reservoir and surrounding elements. In addition, a large (23 × 35 × 2.5 cm) aluminum ground plate provides a good heat exchange. To regulate the temperature from room temperature to setpoint by the flow cycle thermostat it takes ∼50 min (Fig. 3.4 (a)). Even by opening the box for a few minutes (<7 min) the temperature in the box (T_{box}) is not affected (Fig. 3.4 (c)). The chamber temperature $T_{chamber}$ remains stable even by opening the box for 30 min. Once the flow cycle thermostat reaches equilibrium it only takes ∼25 min to restabilize T_{box} after closing the box. Although we did not want to risk any temperature fluctuations by injecting not perfectly equilibrated solutions. Therefore we always waited long enough until a stable temperature was recorded for T_{box}.

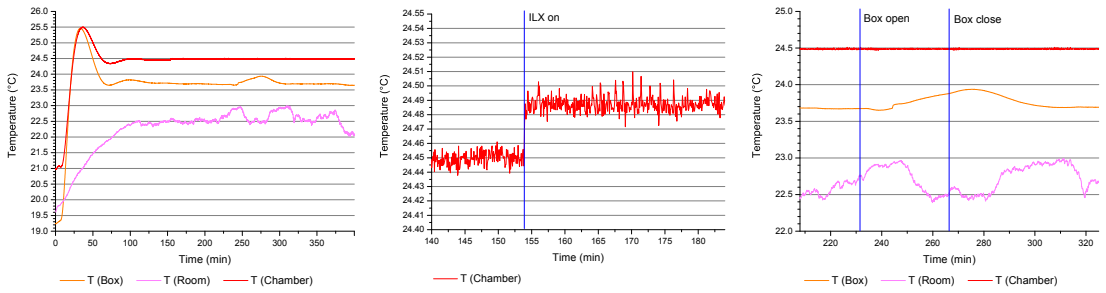

(a) (b) (c)

Figure 3.4: Temperature characteristics: (a) After switching on the flow cycle thermostat. ILX controller was not on until minute 154. (b) After switching on the ILX temperature controller the setpoint is reached almost instantaneously. (c) Compensation of T_{box} after box was opened.

A Negative Temperature Coefficient Thermistors (NTC) thermocouple element changes its resistance depending on the temperature. In a specific range this behavior is linear. To receive the temperature in degree Celsius (°C) a calculation

with a linear regression is necessary. From the reference curve Fig. 3.5, the following formula is received:

$$T = -1.0642 \times \frac{68}{\frac{U_{ref}}{U_T} - 1} + 72.351 \tag{3.1}$$

, where U_T is the measured voltage at the temperature sensor and U_{ref} an applied reference voltage.

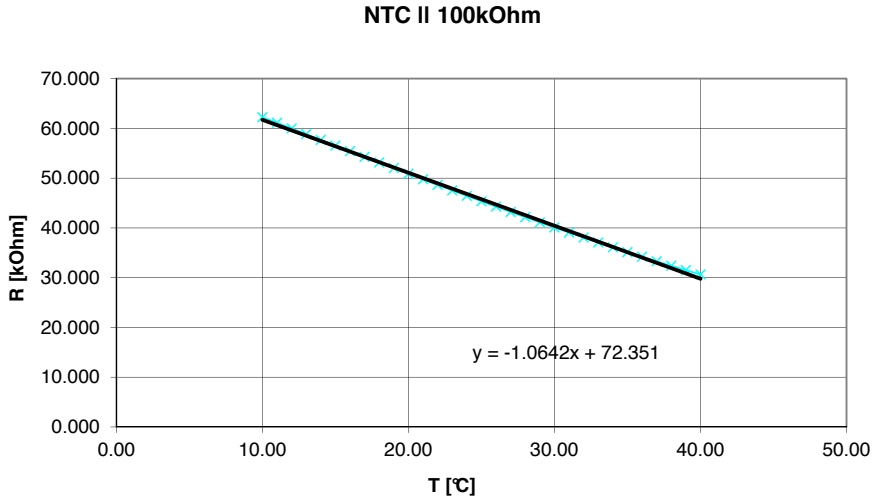

Figure 3.5: Thermocouple characteristics: Calibration curve for the NTC thermocouple element. With a linear fit we determine the characteristics for the temperature calculation for T_{room} and T_{box}.

The ILX temperature controller in combination with the NTC thermocouple has a polynomial correlation between measured voltage and temperature. To calibrate the LabVIEW software for correct temperature display we performed a measurement series with a calibrated reference temperature sensor and applied a polynomial fit to the recorded data (Fig. 3.6).

We decided to run all experiments at room temperature although an increased temperature is favored for hybridization experiments. Hybridizations at room temperature are possible as demonstrated in Ref. [13]. For temperature sensitive

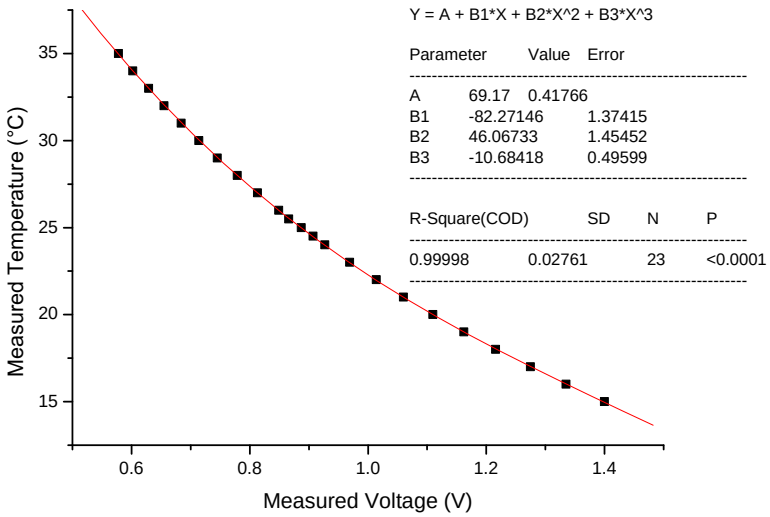

Figure 3.6: ILX characteristics: Calibration curve for the ILX temperature controller in combination with a thermocouple element. With a polynomial fit we determine the characteristics for the temperature calculation for $T_{chamber}$.

transducers such as the CLA and SPR it is also a technical issue. It is much easier to keep the temperature stable inside the enclosed box close to room temperature than an increased value.
Although our instrument is highly improved in terms of temperature regulation it still takes slightly more than 3 hours to get a stable temperature of 35 °C. Furthermore, keeping this increased temperature stable during sample exchange (opening the box) is much more difficult. Sample exchange without temperature drop, respectively long restabilizing times, is absolutely possible for the newly built setup for measurements close to room temperature.

3.2.5 Fluidics

The stated 10 µL/min flow speed corresponds to approximately one chamber volume per minute (approx. chamber volume = 4 mm × 2.35 mm × 1.5 mm = 14.1 mm^3 = 14 µL. The injection flow speed of 150 µL/min has its origin in the experience of Martin Hegner's group to achieve a feasible time until the probe reaches the chamber and until the sample in the chamber is completely exchanged with injected probe.
The two pulsation-free syringe pumps were embedded in our LabVIEW control software. With two dosing modules an endless flow could be programmed, even for running measurements overnight. Besides electronic and temperature drifts

the main portion of the overall drift visible in the deflection signal is drift due to diffusion effects (for example ionic exchanges between the cantilever surface and the surrounding liquid). The continuous flow led to a fast equilibration between the cantilever surface and the surrounding liquid which is diffusion independent. One feature which has to be taken into account when measuring in flow is the effect of the laminar flow on the cantilevers, as we see a deflection due to flow forces. In experiments with readout in stationary fluid before and after sample injection the liquid phase is moving during the injection process as well. This leads to significant flow induced deflections (see for instance in Ref. [13]). Depending on the position of the sensors relative to the liquid chamber channel the flow forces will be different for the eight cantilevers, inducing different additional bending that could potentially affect the measured deflection values. By measuring the baseline and the actual hybridization signal at equivalent buffer flow speeds, the comparability is given. The typical flow induced bending by switching from stationary fluid to 10 μL/min is up to 7 nm (see Fig. 3.7 (a)). For the increased injection flow rate the induced bending is up to 400 nm (see e. g. Fig. 3.7 (c) or Fig. 3.2). For the differential deflection signal the flow induced bending is completely reversible as visible in Fig. 3.7 (right). Stop flow read out with only a short stop phase to record the data points (much smaller time period than the drift kinetics) could add additional improvement.

Due to instrument design restrictions (flow path, lack of space and temperature sensibility) we decided to set up the flow with a syringe pump in pulling mode. The disadvantage with this pulling method is the risk of sucking air into the flow path. Small air bubbles will stick to the cantilever array and lead to an abortion of the measurement. By compensating the pressure loss with a positive pressure on the probe side we avoided these problems. We applied 80 mbar. The value was estimated by a rough calculation for the pressure loss over tubing distance (Appendix B.2, Tab. B.1).

Additionally, Halar tubing was chosen to avoid gas diffusion into the system. The gas permeability value for oxygen for Halar is similar to PEEK and ∼30 times less than Teflon (according to the specification guide from the provider: Appendix B.2, Tab. B.2). Moreover, Halar tubing is almost as flexible as Teflon tubing, in contrast to PEEK which would otherwise be a perfect material in terms of gas diffusion and low affinity for biomolecules.

3.2.6 CO_2 Sparging

Air bubbles tend to stick in small corners in the fluidic path and require a time consuming procedure for their removal. CO_2 sparging allows a fast fluidic system priming without any bubbles. The buffering characteristics of the solution, and closing the CO_2 connection after priming, ensure that the effect of the CO_2 on

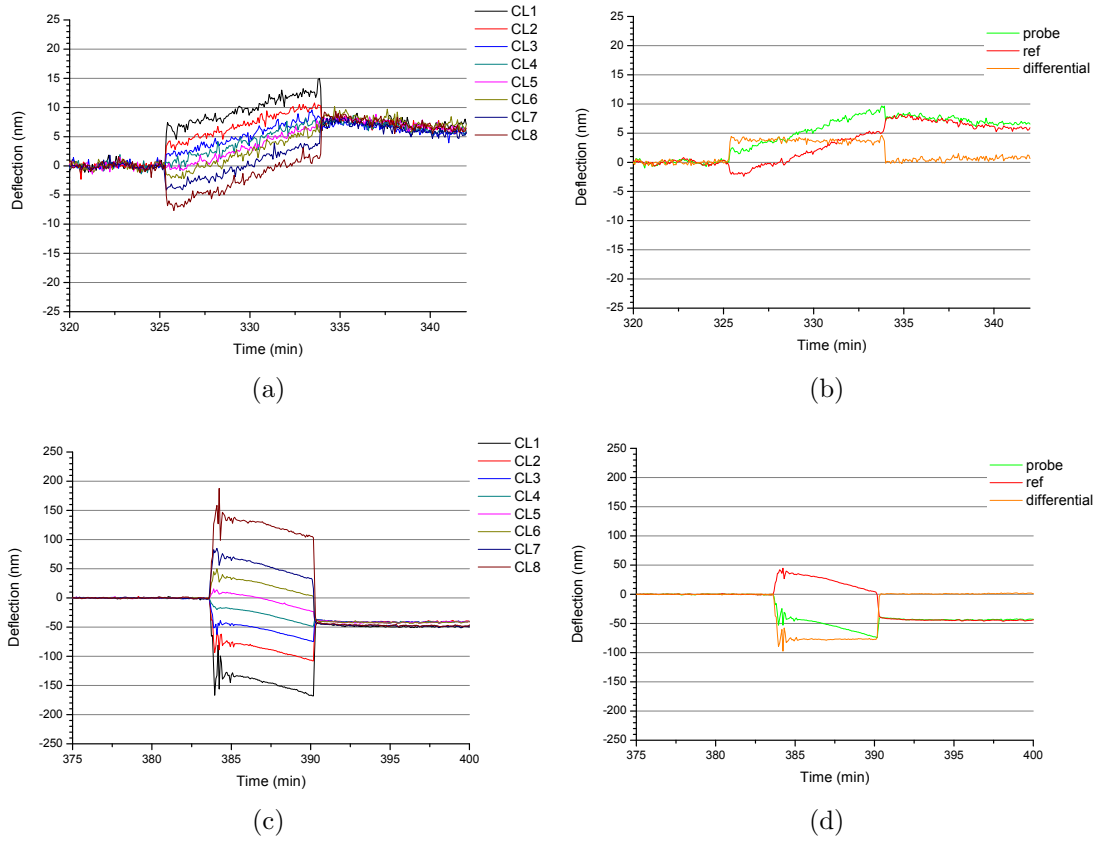

Figure 3.7: Flow force influence: Flow induced deflection for (upper) 10 μL/min, (lower) 100 μL/min. Both for the baseline corrected raw signal (left) and averaged signal and differential signal (right).

the acidity of the buffer is negligible.

3.2.7 Laser stability

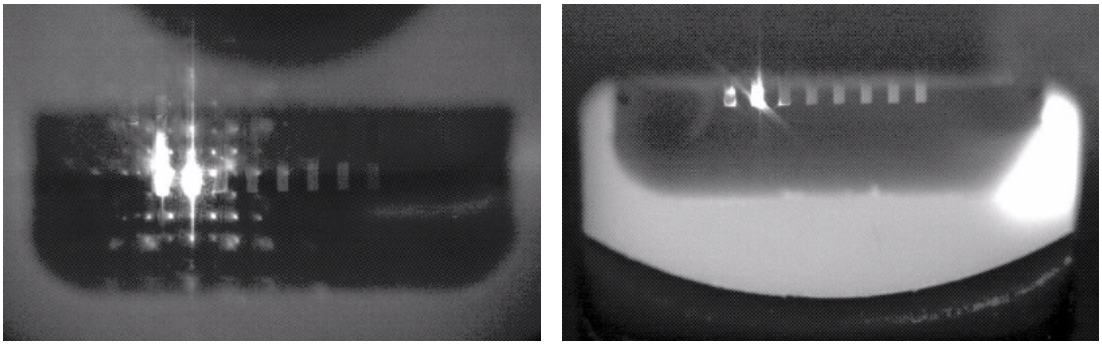

(a) (b)

Figure 3.8: Photo of laser reflection on CL in flow chamber: (a) Interference pattern with normal setup after implementation of bandpass filter in front of camera module. (b) Setup without parallel optical surfaces. Cover glass was removed and bandpass filter slightly tilted.

To avoid interference patterns as visible in Fig. 3.8 (a) we prevent parallel planar optical surfaces. An inspection has shown that the source for the interference pattern visible in Fig. 3.8 (a) is the bandpass filter in front of the camera module. Due to the fact that this optical element does not belong to the path of the actual measured laser beam for deflection readout, this is not crucial. No interference patterns can be achieve by tilting the bandpass filter and avoiding any parallel optical surfaces leads as shown in Fig. 3.8 (b).

In most of the experiments the PSD sum signal is quite stable for CL2–8. The PSD sum signal for CL1 has a significant drift as shown in Fig. 3.9 (a) representative for a randomly picked experiment. This behavior can be observer in more or less all experiments. By comparing the slope of the drift of the sum signal with the matching deflection signal we do not see any correlation. Slow drifts in the sum signal do not seem to have an influence on the deflection values which is expected from the PSD formula (Equation 1.8). Slow fluctuations in the sum signal do not affect the final deflection result. Fast fluctuations do have an influence as shown in Fig. 3.10. Nevertheless the influence on the differential deflection signal is negligible.

Laser stability might be affected by fluctuations in the room temperature as shown in Fig. 3.11. Furthermore we can see in Fig. 3.11 (minute 230 to minute 260)

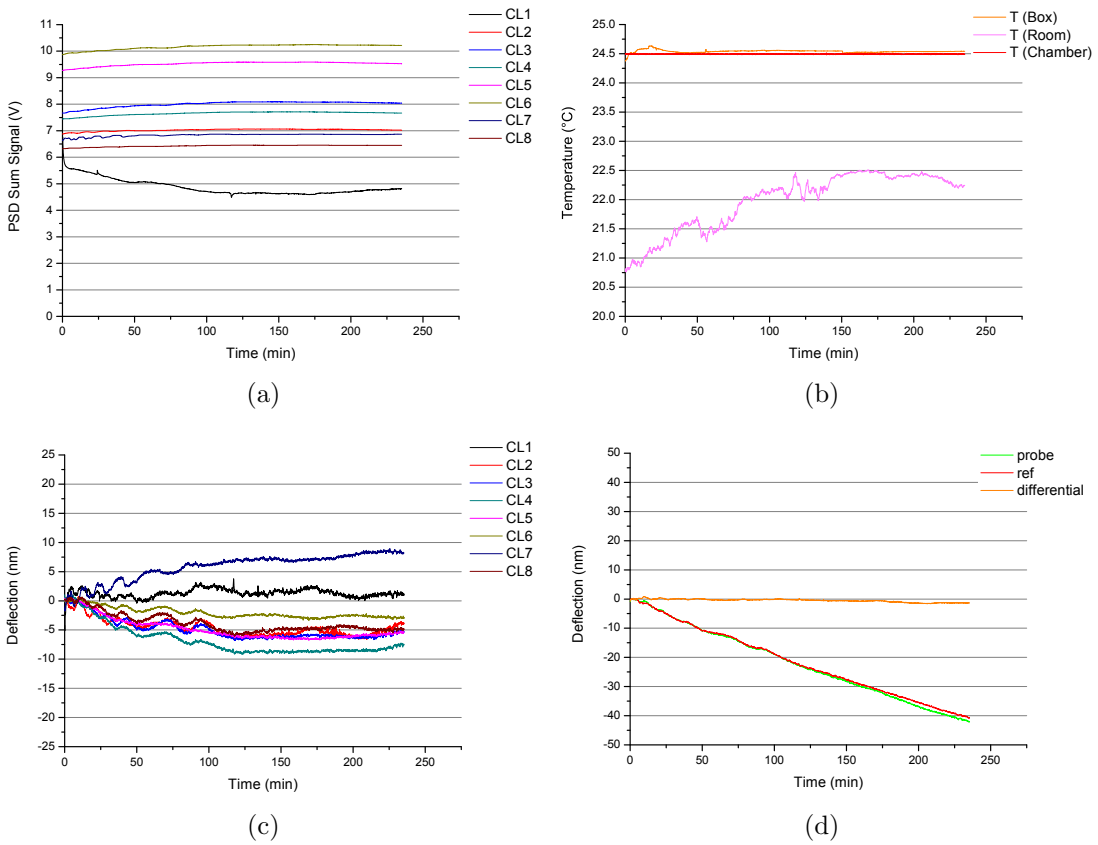

Figure 3.9: PSD sum signal drifts: PSD sum signal (a), temperature development (b) and resulting deflection signal (raw (c) and averaged (d)) from a control experiment. Measurements performed on a 180 ° rotated CLA chip to measure on a stable CLA body. Therefore the measured signal does not has its origin in cantilever deflection. (a) Visible drop of CL1's laser sum signal compared to stable signal for all other CLs. Drop might correlate to increase of room temperature over time (b). No effect on deflection signals either raw (c) or averaged (d) is visible.

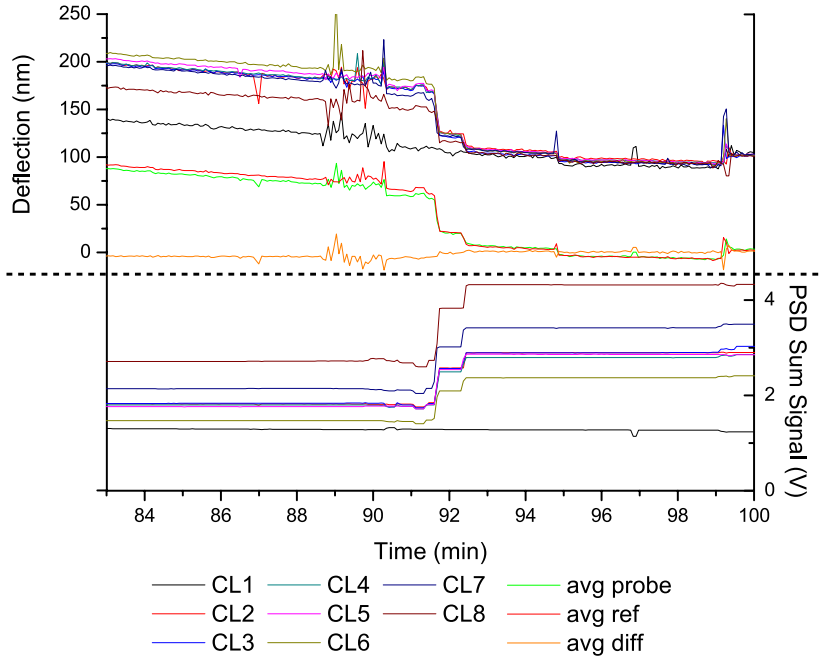

Figure 3.10: Influence of fast and high sum signal fluctuations on the measured deflection as well as averaged differential deflection: The figure shows a combined graph of the PSD sum signal (right axes and data in the lower third), the baseline corrected deflection signal (left axes and date in the upper third) and the averaged deflection of probe and reference cantilever as well as the calculated differential deflection (left axes and date in the middle third). At minute 91.7 and 92.7 the laser power was increased. The laser for CL1 was not affected thereby. The influence of the fast fluctuation in sum signal on the deflection signal can be seen in the graph.

what happens when we open the box and ambient light shines on the PSD: The sum signal increases and a lot of fluctuations are induced. If we zoom in we can see the 50 Hz from the ambient light source.

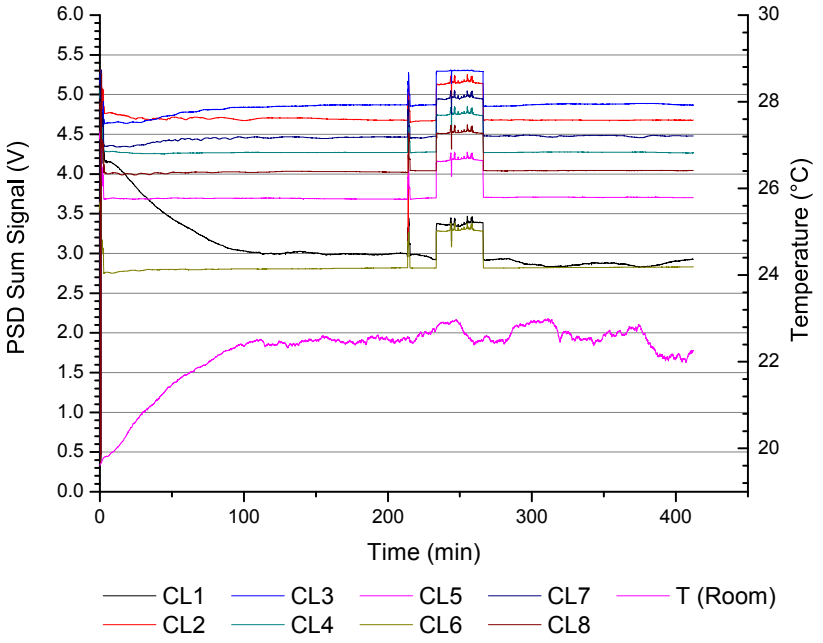

Figure 3.11: Room temperature influence on laser power: Correlation between T_{room} and drifts in the PSD sum signal especially with the unstable laser diode for CL1. Peak at minute 216 is due to a realignment of the PSD. Artifacts at minute 230 to minute 260 are due to the open box.

3.2.8 PSD

After assembling the PSD its functionality and especially linearity were tested in a liner setup. Therefore we mounted the PSD on a linear micro positioning stage and pointed a focused laser beam perpendicular towards the vertical center of the PSD area. The sum and differential signal were recorded while shifting the PSD horizontally from beyond one end to the other. The values were plotted against the absolute position of the micro positioning stage (Fig. 3.12).

For the sum signal we performed an analogue experiment (Fig. 3.13). A linear region of ±3 mm from the center of the PSD is given. This value correlates with the spot size of ∼6 mm because beyond that limit too much light is pointed not

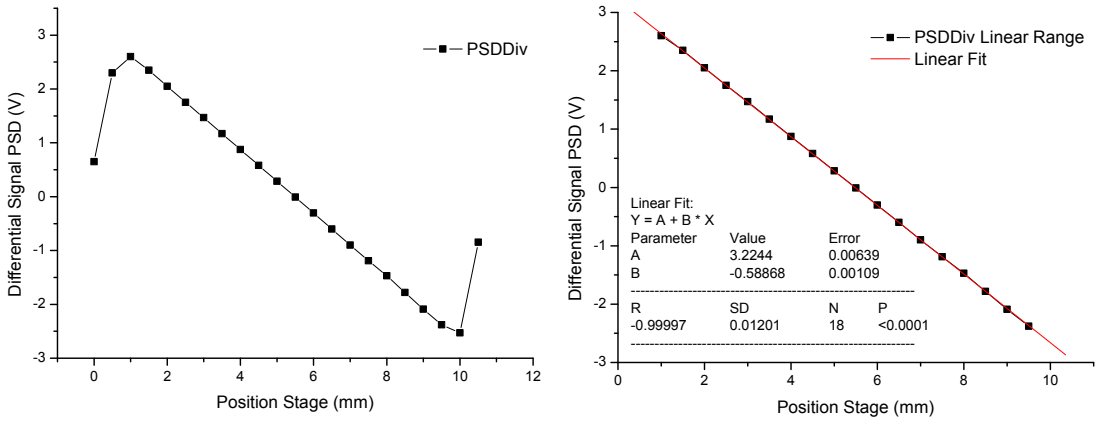

(a) (b)

Figure 3.12: PSD differential signal vs position: (a) Recorded differential signal of PSD output while the PSD was shifted horizontally versus a perpendicular laser beam pointing towards the sensor area. Measurement started with laser spot beyond the sensor area. (b) Plot of linear region from dataset shown in (a). A linear fit proves the linear behavior of the PSD differential signal (b).

on the sensor area. This leads to a loss of sum signal that influences the position. Plus, the center of the light spot is falsified due to the fact that not the whole spot is represented on the sensor area.

3.2.9 Optical Fibers

The proper cleavage of optical fibers plays an important role for the quality and quantity of the light guided through the fiber. Several badly cleaved fibers were recognized by checking the shape of the projected output (Appendix B.2) and inspecting the fiber with a binocular. A perfect cleaved fiber has a round shaped light projection and shows no cracks or other damages on the core and cladding (Appendix B.2, Fig. B.1).
By newly cleaving all fibers we achieved a clean fiber cut with perfectly shaped output (final results not shown).

Two criteria have to be fulfilled for the alignment of the laser spots on the CLA: (i) the pitch from one spot to the other has to be the same as the 250 μm pitch between two cantilevers and (ii) the CL should be in focus, thus in the narrowest beam waist. To achieve this we reduced the laser light with a neutral density filter for better visibility of the laser spot with the camera. Then the distance from the laser to the chamber ((2) in Fig. 2.1) and the distance from the laser to the lens ((5) in Fig. 2.1) were set in an iterative way. After the visual

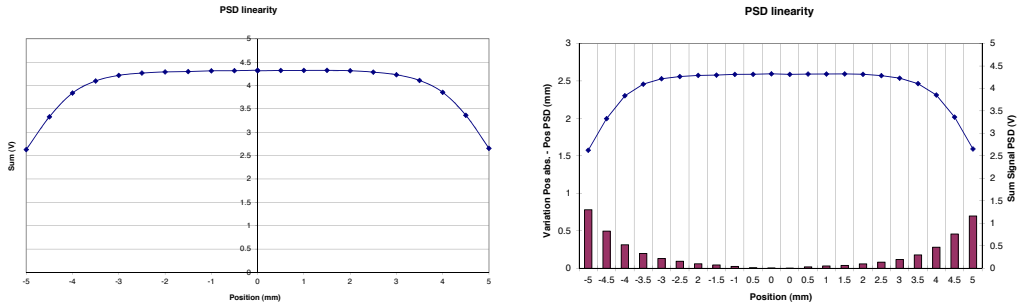

Figure 3.13: Results from the experiment to check the linearity of the PSD: On the left side the PSD sum signal versus absolute position adjusted with a micro positioning stage. On the right side additionally the variation of the absolute position from the micro positioning stage to the calculated position received from the PSD.

impression of a good result, we verified the focal distance by a simple experiment. The laser was shifted horizontally across one cantilever. Thereby the sum signal was recorded by the PSD (Fig. 3.14). This was repeated for a slightly changed distance between laser and CLA in a plus and minus direction. The slope at full width at half maximum indicates the size and sharpness of the laser spot. With the settings $z_{laser-lens} = 2.90\,\text{mm}$ and $z_{laser-CLA} = 8.58\,\text{mm}$ we have the best result.
A theoretical disquisition to calculate the spot size can be found in Appendix B.2.3.

Touching, respectively moving the optical fibers has an influence on the sum signal. This is not due to increased or decreased couple efficiency. This was excluded by observing the same effect with fixed fiber ends. Furthermore we know that the influence is due to movement and not due to a temperature change, because the same effect is observed if we touch the fibers with bare fingers or with a tool. Further investigations with a test setup resulted as follows: The laser light is polarized. The polarization changes by moving/bending the fiber. This was shown in the test setup with a polarization filter. Thus the position/curvature has an influence on the polarization of up to 10 mV PSD sum signal.
In an ideal setup we should align, respectively rotate each fiber to end up with an identical polarization direction and protect all fibers against movements. The polarization becomes critical, because all optical planes such as the Au cantilever surface do not reflect p-polarized and s-polarized light identically.
The fibers were never aligned like mentioned. This due to the enormous effort to fulfill this task and due to the fact that we never observed any direct influence during a measurement. Section 3.2.7 proves that small changes in the sum signal are negligible because they do not have an influence on the differential deflection

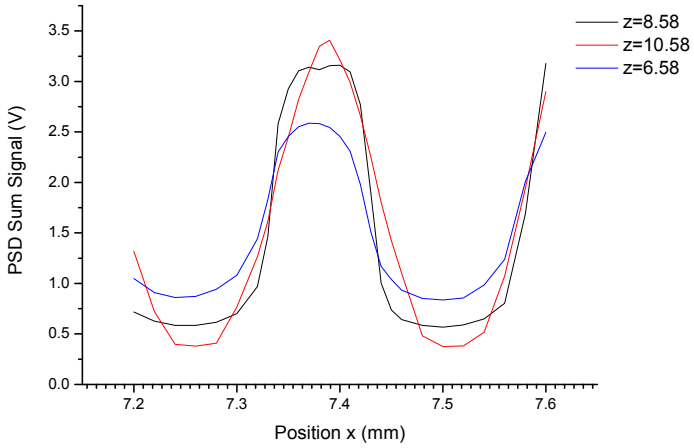

Figure 3.14: Recorded PSD sum signal while shifting a laser spot horizontally across a cantilever: The slope correlates directly with the laser spot size and shape quality.

signal.

3.2.10 Software

To control the CLA instrument an adaption of the original NOSE software by W. Grange was used (developed in M. Hegner's group and adapted to the new instrument at Roche). We realized some deficits during the first period of measurements. Short term fluctuations were up to ∼100 nm. For a feasible detection they should be in the 1 nm range. Major improvements were achieved by letting the laser stabilize before measurement. E. g. discarding the first 500 recorded datapoints before averaging as described in 3.2.3. Furthermore we implemented faster controlled loops for regulating the lasers. Finally the software was improved by reprogramming all allocations. Global variables were exchanged by absolute connections, because they can delay in complex programs.
Over time the whole software was reprogrammed and only a few core-parts such as temperature and deflection display were copied from the original NOSE software. A module to restore all parameters, one to control the syringe pumps (neMESYS) and a separate Virtual Instrument - A LabVIEW program (VI) for the whole data analysis were programmed and implemented step by step during the thesis. Additionally a VI to overlay two consecutive experiments and display plus store the results was programmed.

Software Memory

We experienced several times a software crash from a memory overflow in the neMESYS control module. The LabVIEW support document ID 2T9ICKTL describes the problem and offers a solution. According to the document the software error was due to high memory usage and wrong memory allocation. To check the memory usage we ran a "profile analysis". As expected the result showed a high memory usage in several neMESYS module blocks. Especially the sub-module VI "NCS_GetFloUnitString.vi" which handles the option to choose the flow unit such as [l], [ml] and [μL] seemed to use a lot of resources. This correlated with the LabVIEW document, which tells us that saving and passing "strings" are very memory intensive. In a new version we removed all unnecessary functions and set the flow unit to the fix unit in [μL.]

3.2.11 Cantilever arrays

All cantilever arrays were provided by IBM (IBM Research GmbH, Switzerland) as described in the material and methods section (Sect. 2.3). IBM offers several chip designs such as with or without protection bars on one or both sides. We have chosen a standard chip design as shown in Fig. 3.15 without protection bars. The chosen wafer design has the best yield of arrays per wafer with the right dimensions (chip-type A) for the application of interest.
IBM processed a batch of wafers (2 wafers of a total of 3). One with 500 nm cantilever thickness and one with 1 μm cantilever thickness. The third wafer went to M. Hegner.

The two wafers for Roche were kept at IBM and stored for further processing. A batch of 5 cantilever arrays was gold coated (2 nm Ti, 20 nm Au) by IBM and sent to Roche for quality check. The main concern was the initial bending that gold coated cantilever mostly have. The gold coating process induces a force on the cantilevers. Depending on heat dissipation from the sputter source and distance between source and target, the influence is different. Good quality chips do have less initial deflection, which makes it easier to image the laser spot in the CLA instrument on the PSD.
Initial bending values from the two IBM batches were: $<3\,\mu$m for the 1 μm wafer and $<15\,\mu$m for the 500 nm wafer. Those values are comparable to arrays processed by M. Hegner and in tolerance for the instrument.
After proofing the successful Au coating by IBM, the whole wafers were gold coated. Due to problems during the 500 nm wafer processing, the Au coating had to be stripped and the coating process renewed. Therefore the yield of complete arrays was lower than expected ($\sim$100 pieces). Initial bending values were in range and not higher as the values stated before.

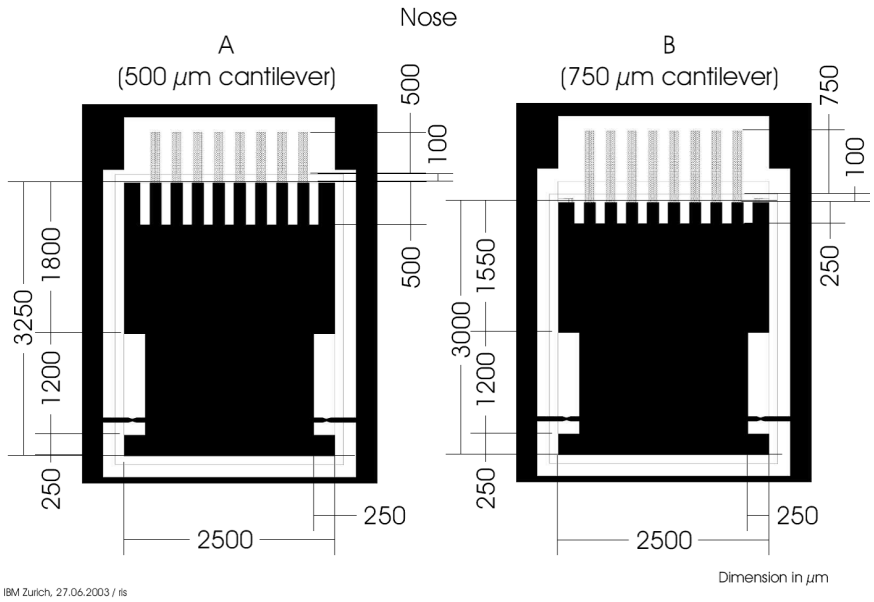

Figure 3.15: IBM mask layout for static arrays: Mask division 80 % 500 μm and 20 % 750 μm length. Target thickness: 500 nm respectively 1 μm. Tolerance within a wafer: $\pm$60 nm. Tolerance within a chip: $\pm$10 nm. Minimum good chips per wafer: 200 for 500 nm respectively 250 for 1 μm thickness.

M. Hegner detected some impurities on their CLAs. The impurities were only visible under a darkfield microscope or by scanning electron microscopy. We had the concern that impurities might have an effect on the stiffness of the cantilevers and therefore might lead to different results in referenced measurements. The concerns were not confirmed and no further research was initiated.
Cleaning the arrays in Piranha solution did not dissolve the impurities (results from M. Hegner *et al.*). An overall analysis of the entire wafers of the IBM batch mentioned before, as well as a former batch from 2007 showed randomly distributed clean and contaminated areas (results from M. Hegner *et al.* and Roche). Fig. 3.16 show images of the mentioned impurities on randomly picked CLAs from M. Hegner *et al.* and Roche.

Due to the fact that the impurities are only on a small percentage of the cantilever area the effect is expected to be minor.
Additional information was given by IBM: Before gold coating the Roche CLAs were stripped in 1:100 HF for 30 s which removes $\sim$5 nm of the silicon oxide. Contact angle measurement would result in the change from $\sim$5° hydrophilic to >80° hydrophobic due to the fact that the SiOH is stripped and converted into SiH. Afterwards the wafer was cleaned in Piranha solution before gold coating. The HF etches inorganic oxides. Therefore the Roche CLAs, Au coated by IBM,

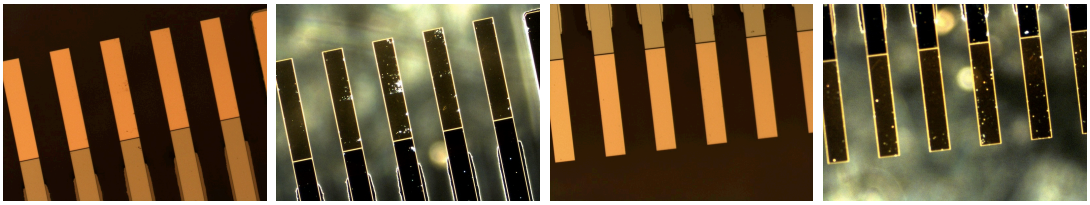

(a) M. Hegner: 0.5u fresh BF

(b) M. Hegner: 0.5u fresh DF

(c) M. Hegner: 1u Piranha cleaned BF

(d) M. Hegner: 1u Piranha cleaned DF

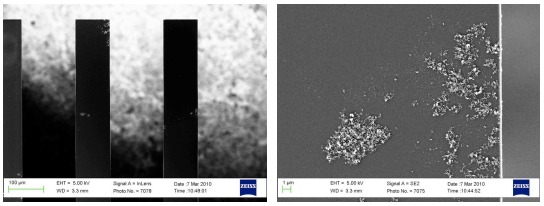

(e) M. Hegner: 0.5u Piranha SEM

(f) M. Hegner: 0.5u Piranha SEM (zoom)

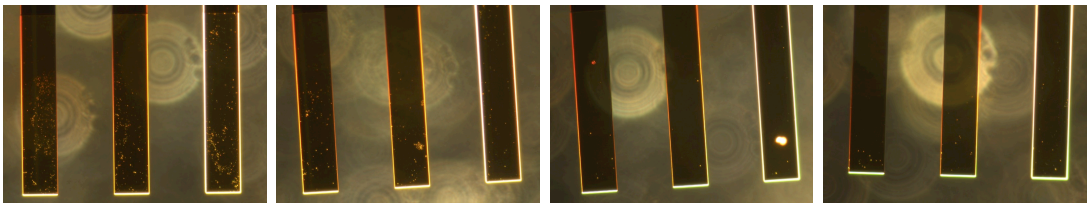

(g) Roche: 0.5u fresh DF

(h) Roche: 0.5u fresh DF

(i) Roche: 1u fresh DF

(j) Roche: 1u fresh DF

Figure 3.16: BF, DF and scanning electron microscopy images of contaminated CLAs: (a) and (b) BF and DF image of untreated 0.5 μm M. Hegner CLA (typical sample for heavily dirty cantilever). (c) and (d) BF and DF image of Piranha cleaned 1 μm M. Hegner CLA (typical sample for moderately dirty cantilever). (e) and (f) SEM image plus magnification of Piranha cleaned 0.5 μm M. Hegner CLA. Piranha cleaning was performed without salt solution cleaning steps to avoid crystal formation on the CL surface. Contaminations did marginally reduce after three times wash. (g) and (h)DF images of untreated 0.5 μm Roche CLA. (i) and (j) DF images of untreated 1 μm Roche CLA.

do have fewer impurities than the ones from M. Hegner who only does the Piranha cleaning without the HF etching step.

The impurities on the CLAs might have their origin in the manufacturing process. IBM uses a "Novolack" photo-resist which is normally stripped of during etching. This could be the source of impurities on the CLs.
To get rid of the impurities on the CL the following steps could be applied: RCA cleaning might remove inorganic contaminations. This is not applied at IBM till now. An oxygen plasma or CF_4 would oxidize impurities and might help to get rid of them.
Further investigations could be made. For our purpose this should not be necessary. By the Peltier test a sufficient uniformity can be observed. Furthermore no irregularities were ever observed during all experiments.

In an experiment where 500 pM antisense match respectively mismatch was hybridized on one of the new IBM cantilever arrays, we prove that their functionality was intact. The results were analogue to previous experiments with individually functionalized gold surfaces. We could not detect any differences in the hybridization signal (sensitivity) nor specificity (no differential deflection signal for the mismatch injection).

3.2.12 Cantilever Functionalization

The literature proposes several different functionalization times and strategies (Ref. [32–34]). A long functionalization time seems to be favored to receive highly ordered SAM. Small volumes used during functionalization by immersion the CLA into capillaries lead to a fast evaporation of the solution. For our application the solution volume needed for the functionalization is not even critical, because we use synthetic DNA oligos which are available in sufficient amounts. Therefore we set up a functionalization station (Fig. 3.17) with a reservoir to avoid the drying-out of solution in the capillaries. Additionally we placed the whole functionalization station in an enclosure. A water bath in the enclosure leads to a high relative humidity that increases the dew point.

Plasma treatment of the capillaries prior to use for functionalize the CLA chip leads to an enhanced hydrophilicity which is an advantage for a good filling of the capillaries. In return it is a disadvantage in terms of cross-talk. Liquid might flow on the outside of the capillaries and the different immobilization solutions might merge.

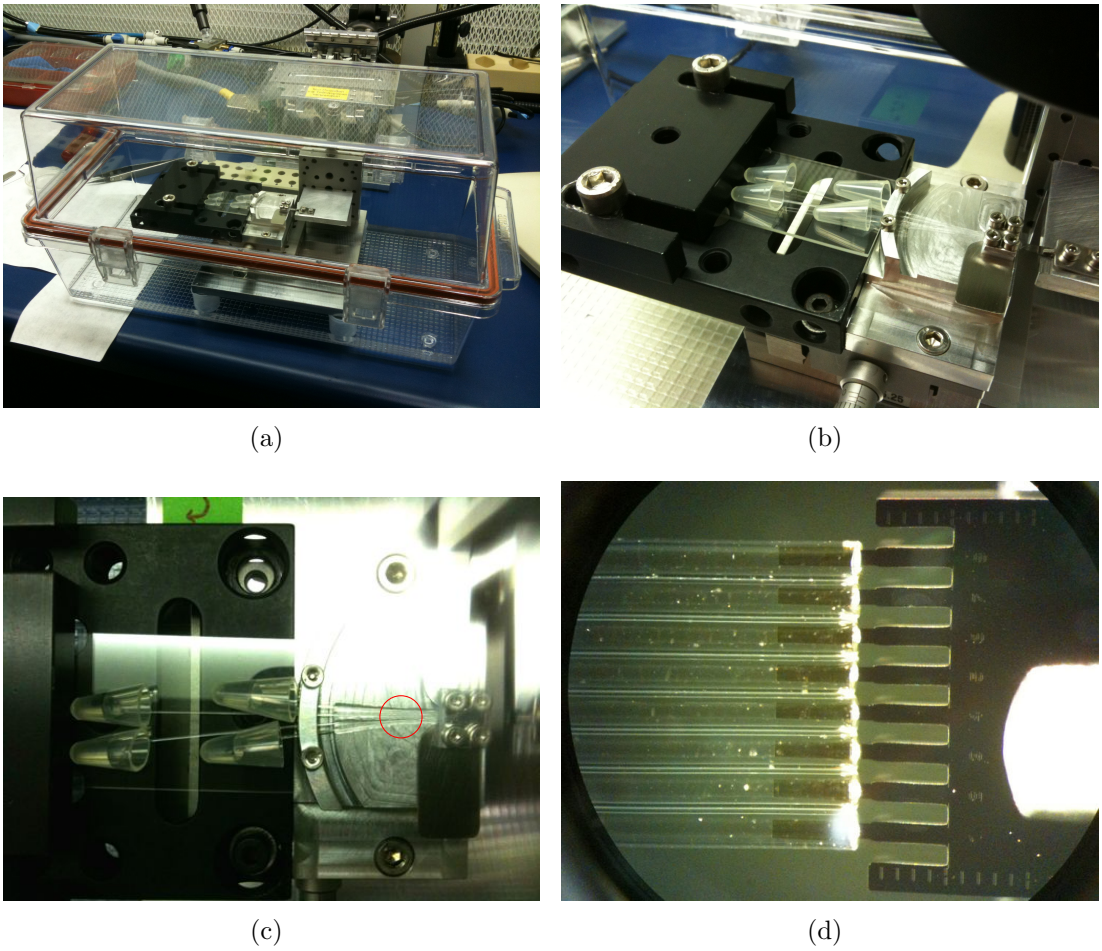

(a) (b)

(c) (d)

Figure 3.17: Photos of improved capillary functionalization device for long term functionalization: (a) Setup is placed in a tight enclosure with a water bath to avoid evaporation. (b) The capillaries ends are placed in tubes acting as reservoir for the immobilization solution. Depending on the functionalization pattern two or more tubes are required. (c) To avoid cross contamination by flow on the outside of the capillaries a droplet of vacuum grease was placed on the support table around the center of the capillaries. (d) The cantilever is aligned by an x, y, z micro positioning stage and immersed into the capillaries till the hinge. Before filling the capillaries, respectively reservoirs the chip was retracted a tiny bit to avoid wetting of the cantilever support and a possible cross contamination by liquid flowing around the cantilever support up to the chip body.

3.3 Surface Plasmon Resonance Technology

3.3.1 Biacore chip preparation

For SPR experiments we used recycled Biacore Dextran sensor chips (type CM5 or SA). The idea was to strip the Dextran layer and end up with plain Au surfaces. This was achieved by a cleaning protocol described in Material and Methods Sect. 2.2.1. First we washed the chips by sonification in detergent. Covalently bound monolayers and other organic remaining where then finally removed by UV-ozone or plasma treatment.
To verify the result we analyzed the surface with three different methods: (i) Contact angle measurement (rough analysis), (ii) in dark field, (iii) by vapor condensation.
We determined 60 s plasma treatment to be the upper limit before damaging the polymer chip holder. After the treatment an extremely good wetting with H_2O was observed as expected. Before plasma treatment we measured contact angles of $\sim 60°$. After plasma treatment we ended up with an extremely hydrophilic surface (contact angle $<30°$. After the first stripping we functionalized the Au surface with ETC for 2 min. An absolutely hydrophobic surfaces with contact angle $>90°$ was formed. We were able to remove the hydrophobic functionality by stripping the ETC SAM by plasma treatment (30 s). After plasma treatment we measured contact angles similar to before the functionalization of $<30°$.
The same result was achieved by a 10 min UV/O_3 treatment as shown in Fig. 3.18.

Observing the cleaned Biacore sensor chip in dark field does not show any residues on the sensor surface. To validate the chip cleaning process we experienced a vapor condensation test to be the best method. By condensing vapor on the surface of the sensor chip we could immediately see if the cleaning process was successful. Vapor tends to condense first at remaining molecules on the otherwise absolute perfectly clean surface. This leads to a different pattern for clean and dirty areas. With this method we could distinguish between clean and substandard sensor chips. In most of the failed cleaning processes the Biacore flow channel stamp was perfectly visible by the mentioned vapor condensation test.

UV/O_3 treatment was determined to be the favored cleaning process compared to plasma treatment as described in Sect. 2.3 and in Ref. [46].
Increased time during UV/O_3 treatment lead to thermal radiation damages to the plastic Biacore chip body. Therefore we used a reduced time for the SPR chip preparation compared to the CLA. Furthermore we manufactured a special aluminum frame to protect the plastic parts from UV radiation and for increased heat dissipation.

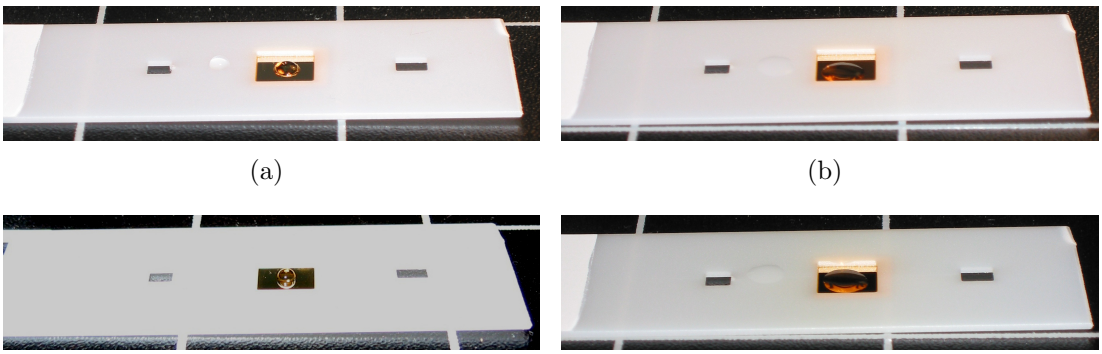

(a) (b)

(c) (d)

Figure 3.18: Biacore sensor chip regeneration: (a) Taken photograph of a water droplet on a recycled Biacore sensor chip. The chip was cleaned with detergent before and stored for several days at ambient air. The resulting contact angle is ∼60°. (b) Resulting contact angle of <30° after 5 min UV/O_3 radiation. (c) After a second 5 min exposure to UV/O_3 the Au surface was functionalized with ETC for 2 min. The resulting contact angle is now >90° due to the hydrophobic functionalization. (d) By 10 min UV/O_3 treatment we could completely remove the hydrophobic properties and a contact angle of <30° can be observed leading to the conclusion that UV/O_3 radiation removes organic monolayers from the chip surface.

3.3.2 DMSO series

To validate the recycled Biacore sensor chips (see Sect. 2.4) we checked the signal quality and stability during a standard DMSO concentration series experiment (Fig. 3.19). We mounted a cleaned chip with expected bare gold surface in the Biacore device and injected ten differently concentrated samples of DMSO diluted in SSC buffer. By plotting the amplitude of the injection response versus the DMSO concentration a linear dependency can be observed. Furthermore we can see a slight drift.

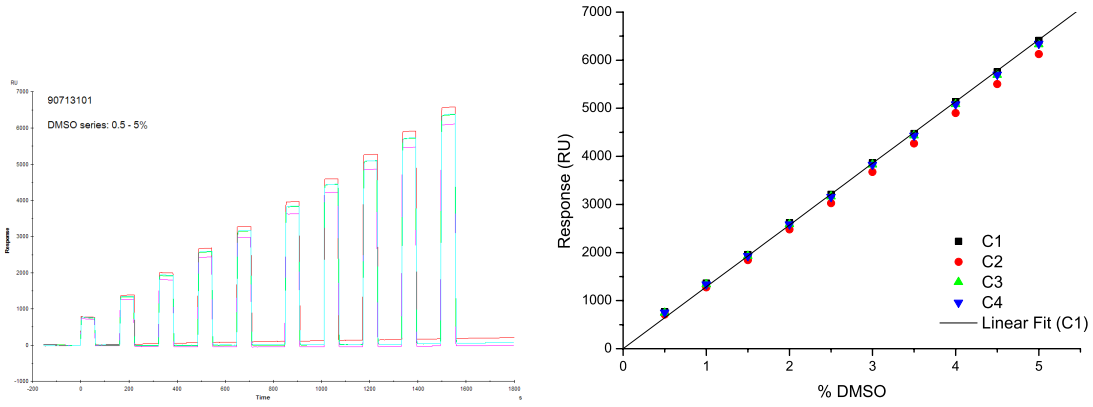

(a) (b)

Figure 3.19: (a) Recorded sensor response during the injection of a series of DMSO (0.5 %–5 %) in SSC buffer on a recycled Biacore SPR sensor chip. (b) Expected linear behavior of signal peaks proves the correctness of the chip response. Besides a slight drift, the recycled chip does not show any irregularities. Therefore the recycling process will be applied for further experiments.

In the graph we can see the measurement of a series of DMSO dilutions in our hybridization buffer. Due to linear increase of the concentration of DMSO, the signal should also increase linear. Unfortunately we have a small drift in our baseline signal, which should not be. We extracted the ten peaks and plotted their amplitude in a new graph. The concentration series should behave linear. As expected we can show the linear behavior with a linear fit. Although the slight drift we could prove that we do not have any unexpected background noise from a bad sensor chip. The chip recycling seems to be acceptable and can be used for further experiments.

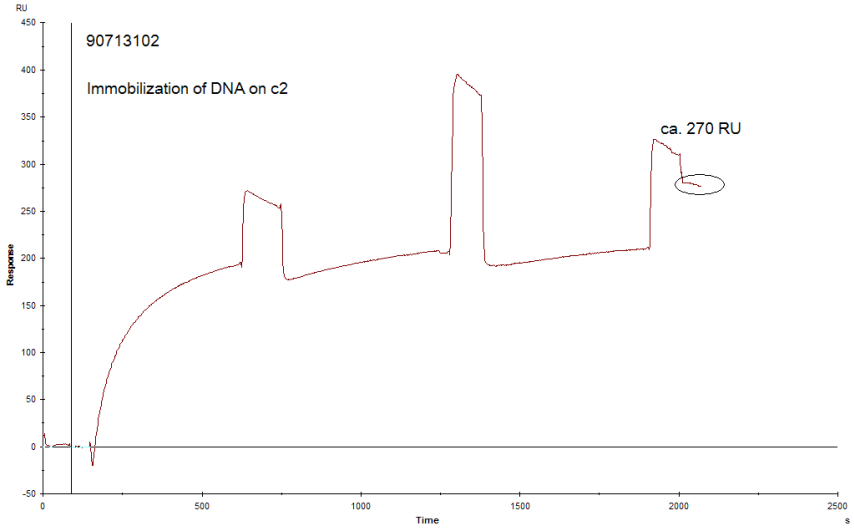

Figure 3.20: Immobilization of thiolated DNA on Biacore sensor chip: The mass increase was recorded in situ in the Biacore device. 25 μL, 50 μM thiolates oligo sense match in 50 mM TEAA buffer were injected. Saturation was finally reached at ∼200–250 RU. The value of ∼2–2.5×10^{10} oligos/mm^2 correlates with the value from the reference literature Zhang *et al.* [13] were they reported an immobilization value of 2×10^{12} oligo/cm^2. Signal does not significantly drop even by washing with buffer (peaks visible in graph). Signal drifts quite strongly.

3.3.3 Immobilization in Biacore instrument

DNA immobilization was performed in situ in the Biacore device in a test series (Fig. 3.20). 25 μL, 50 μM thiolates oligo sense match in 50 mM TEAA buffer were injected onto a cleaned gold sensor chip. The mass increase was tracked by recording the RU versus time. By washing several times with buffer we tested if the adsorbed mass was effectively bound to the sensor surface.
The resulting ∼200–250 RU correspond to ∼0.2–0.5 ng/mm^2. This value correlates with the reported 2×10^{12} oligo/cm^2 by Zhang *et al.* from the reference literature [13].
Immobilization ends in saturation. Even after washing with buffer, the signal stays at the reached value. In all future experiments the chip functionalization was done outside the instrument for more flexibility in terms of chosen buffers and immobilization times.

General Discussion

Whereas for the SPR platform many studies exist determining the optimal surface coverage for probe molecules [32–34], for the CLA platform only a few data exist showing that probe density on the sensor surface affects the signal amplitude. The optimal immobilization density for CLA measurements is somewhere between the highest dense coverage and reduced coverage. The optimal setting has an increased hybridization efficiency without losing the steric repulsion leading to cantilever deflection.

An open question remains how the changes in conformation of a SAM over time do have an influence on the SPR signal. Concrete, how much of the measured 300 RU is due to mass adsorption and how much is due to changes in conformation in the ad-layer over time.

3.3.4 Proof of concept

Our attempts to detect DNA hybridization on the Biacore SPR system were not successful until we changed the hybridization buffer from SSC to PBS. The reason for this observation is not clear yet. In previous experiments on a microarray platform (results not shown) several hybridization buffers such as SSC (0.1×, 0.5×, 10×), PBS, PBS (+), SSC 5× with 50 % Formamide, as well as an Affymetrix buffer (Affymetrix Inc.) and an Illumina buffer (Illumina Inc.) were validated. PBS with magnesium and calcium ions (PBS (+) stated as follows as PBS) resulted to be one of the favored hybridization buffers. The bivalent ions give thereby an additional support for the hybridization.

After switching to PBS as hybridization buffer successful results were achieved

Fig.	Chip type	Preparation	Immobilization buffer	Hybridization buffer	Injected sample
Fig. 3.21 (a)	CM5	UV/O_3 + EtOH	NaCl-TE	SSC (not shown), PBS	25 µL, 1 µM antisense match in PBS, 5 µL/min
Fig. 3.21 (b)	CM5	UV/O_3 + EtOH	KH_2PO_4	PBS	50 µL, 1 µM antisense match in PBS, 5 µL/min
Fig. 3.21 (c)	SA	UV/O_3	NaCl-TE	PBS	25 µL, 1 µM antisense match in PBS, 5 µL/min
Fig. 3.21 (d)	SA	UV/O_3	KH_2PO_4	PBS	30 µL, 1 µM antisense match in PBS, 5 µL/min

Table 3.3: Experimental conditions referring to Fig. 3.21.

as shown in Fig. 3.21. We tested several different functionalization protocols listed in Tab. 3.3. All assays were functionalized with reduced density (implemented MCU spacer) of capture molecules for improved hybridization as recommended by the literature (Sect. 1.4 and Ref. [32–34]).

For the established hybridization experiment with 1 µM target we observe saturation after injecting 25 µL probe (Fig. 3.21 (a)). The resulting signals differ for the four experiments shown in Fig. 3.21. Reason therefore might be the different functionalization protocols or chip types used for recycling. For a final statement too many parameters were changed and therefore no absolute conclusion could be made.

3.3.5 Regeneration during SPR

After the study of immobilization and hybridization we focused on regenerating the chip after hybridization.

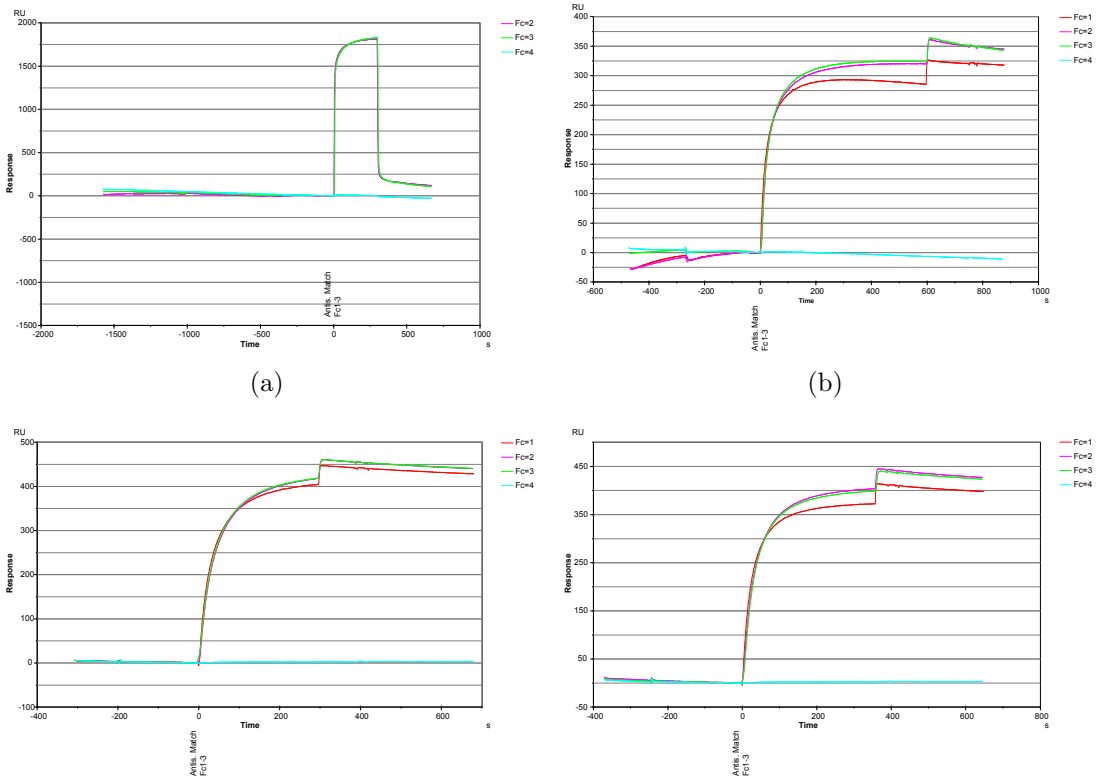

Figure 3.21: DNA hybridization on SPR chip: (a) Response units versus time during the injection of 25 μL, 1 μM, 5 μL/min antisense match DNA in PBS on a recycled CM5 chip immobilized with sense match DNA in NaCl-TE buffer. Chip cleaned according to protocol with detergents, UV/O_3 and immersed in EtOH. Injection was performed after a first attempt of hybridization in SSC buffer without any result. Fc4 (blue curve) was used as reference without sample injection. (b) Sensorgram of the injection of 50 μL, 1 μM, 5 μL/min antisense match DNA in PBS on a recycled CM5 chip immobilized with sense match DNA in KH_2PO_4 buffer. Chip cleaned according to protocol with detergents, UV/O_3 and immersed in EtOH. (c) Sensorgram of the injection of 25 μL, 1 μM, 5 μL/min antisense match DNA in PBS on a recycled SA chip immobilized with sense match DNA in NaCl-TE buffer. Chip cleaned according to protocol with detergents, UV/O_3 without immersion in EtOH. (d) Sensorgram of the injection of 30 μL, 1 μM, 5 μL/min antisense match DNA in PBS on a recycled SA chip immobilized with sense match DNA in KH_2PO_4 buffer. Chip cleaned according to protocol with detergents, UV/O_3 without immersion in EtOH. In (a) the change in refractive index during the injection is abnormally high due to the fact that SSC was used as running buffer and PBS as hybridization buffer.

A Biacore CM5 sensor chip was recycled by cleaning according to protocol with detergents and UV/O_3. 1 μM thiolated sense match DNA was immobilized on the chip in NaCL-TE buffer overnight. We reduced the functionalization density by post-processing with an MCU immobilization for 1 h. Figure 3.22 shows the signal response versus time while hybridizing and regenerating the immobilized biomolecules. For hybridization we injected 25 μL, 1 μM, 5 μL/min antisense match DNA in PBS. As regeneration agent we used HCl and injected once or twice 10 μL, 0.1 M at 5 μL/min.

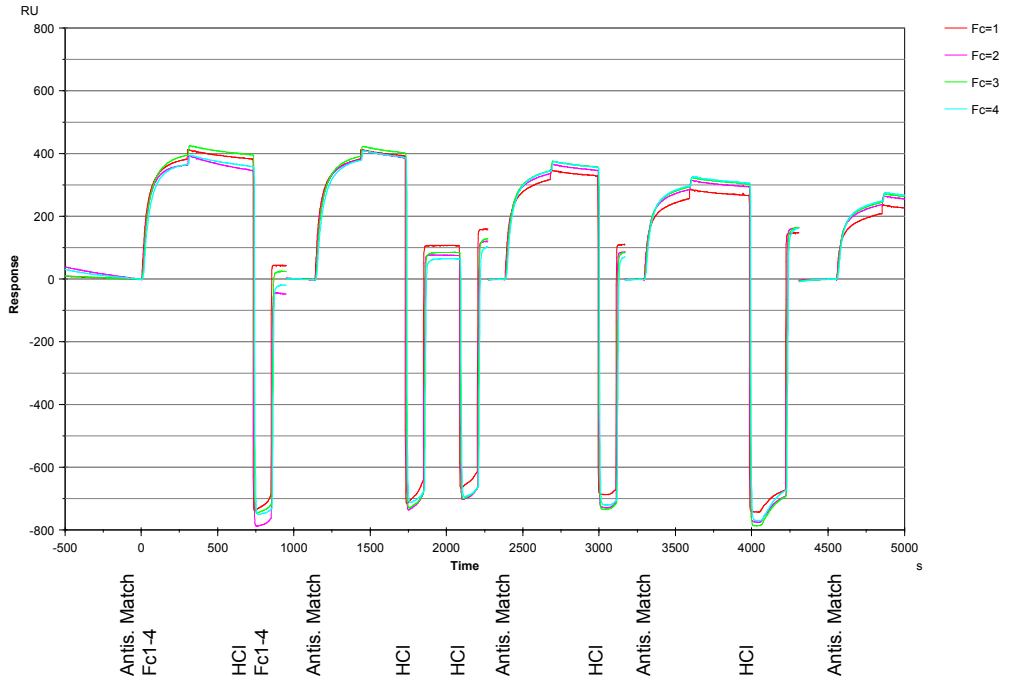

Figure 3.22: Repeated hybridization and regeneration of DNA on the Biacore chip sensor surface: Hybridization was achieved by injecting 25 μL, 1 μM, 5 μL/min antisense match DNA in PBS. Regenerating was achieved by injecting one or twice 10 μL, 0.1 M, 5 μL/min HCl. The baseline was corrected to zero before each cycle for each channel. The graph shows the decrease in hybridization efficiency: less amplitude for each renewed cycle after probe hybridization. Regeneration efficiency is not 100 %: endpoint of each cycle is slightly higher than the recorded baseline at the beginning.

The graph proves that HCl leads to a partial recovery. The recovery cannot be repeated for several times as shown by the superposition of the signal over several cycles. Mass seems to accumulate on the surface over the several cycles (increase of RU signal). Even two injections of HCl lead to a slight increase of signal. This leads to the conclusion that not only mass accumulates but that HCl might alter

the sensor surface or the biolayer on top. Furthermore the recovery is not 100 %. A certain ad-layer is not removed from the surface, visible by the discrepancy of baseline and endpoint. The differential signal from each hybridization cycle decreases by each repetition after regeneration.

For further measurements standard conditions and protocols as described in Sect. 2.4 were used. Furthermore most injections were performed by a scripted program operating the Biacore instrument.

After testing the chip regeneration by HCl leading to a non-satisfying result, we switched to a different regeneration agent. Figure 3.23 shows the overlay of an extract of 88 repeated cycles of hybridization and regeneration by urea. All hybridizations were performed on the same Biacore sensor chip. For each cycle we first recorded a stable baseline. Then we injected 25 μL, 1 μM, 5 μL/min antisense match DNA in PBS. After a short dissociation time 2$\times$ 5 μL, 8 M urea, 5 μL/min were injected. The graph shows the response signal versus time for the cycles 10 and 13 at the beginning and 67 and 78 at the end of the experiment.
After each regeneration the signal ends on the same level as the baseline at the beginning. This proves that the regeneration by urea is feasible. Furthermore the loss of signal amplitude in hybridization 78 compared to hybridization no. 10 is minor and can almost be neglected. Assay functionality (amount of binding partners and affinity) did not decrease, which is crucial for a successful regeneration. The loss in signal after 88 hybridizations is 4 %.
The "nose" in the signal right before saturation is an irregular effect and seems to disappear after repeated hybridizations/regenerations. A possible reason is explained in Sect. 3.3.7.

3.3.6 Specificity

With a functional assay and the possibility to perform several hybridization in series on the same Biacore sensor chip with regeneration in between we next wanted to focus on the specificity of the Biacore assay. Where the cantilever might experience a different force for unspecific adsorption and therefore respond with less signal (see Fig. 3.2), an SPR instrument cannot differ between "real" bound molecules and unspecific adsorbed mass on the sensor surface. Both will lead to the same shift in refractive index if the mass is similar.

Figure 3.24 shows the overlay of three consecutive experiments. The Biacore sensor chip was recycled from a former SA chip by cleaning it according to protocol with detergents and UV/O_3. Functionalization was done by incubation with 1 μM thiolated sense match DNA in NaCl-TE buffer overnight and post-processing with 1 h MCU spacer incubation to reduce the immobilization density for improved hybridization. Before each injection a stable baseline was recorded to ensure

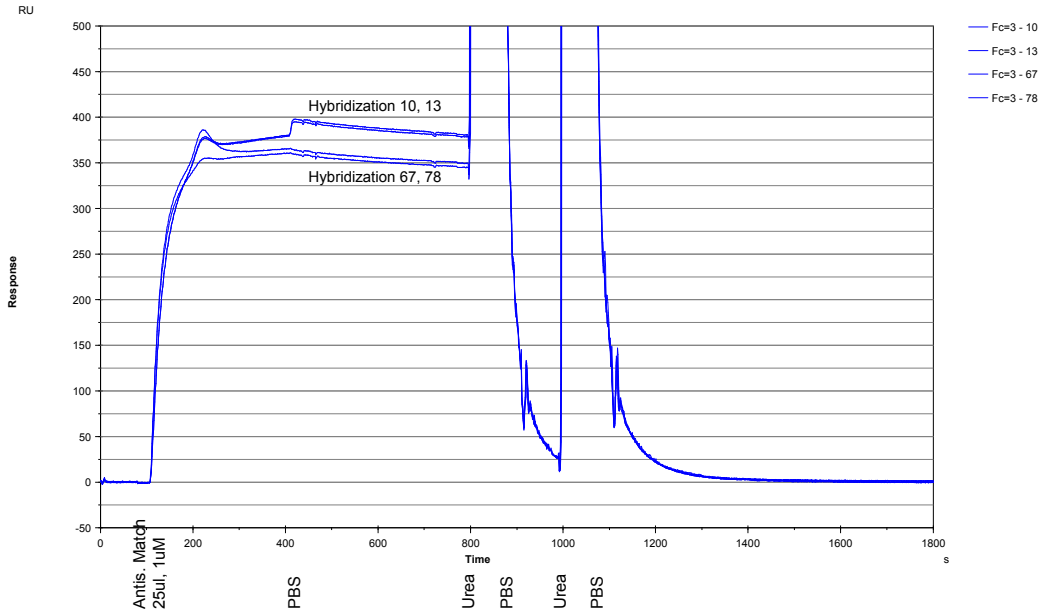

Figure 3.23: Overlay of an extract of 88 repeated hybridizations with followed regeneration by urea: All injections were performed on the same Biacore sensor chip. The chip was recycled from a former SA sensor chip by cleaning according to protocol with detergents and UV/O_3. Functionalization was done by incubation with 1 μM thiolated sense match DNA in NaCl-TE buffer overnight and post-processing with 1 h MCU spacer incubation to reduce the immobilization density for improved hybridization. Only a minimal loss of signal in a series of over 50 hybridizations is visible. Furthermore the baseline is absolutely consistent after each regeneration (endpoint on same level as recorded baseline at the beginning). For each injection the recorded baseline was corrected to zero.

that the system was equilibrated. Then 25 μL, 1 μM, 5 μL/min antisense DNA in PBS were injected. After injection the system switches back to buffer flow (PBS 5 μL/min). After 1 h dissociation time, the chip was regenerated by injecting 2× 5 μL, 8 M urea, 5 μL/min (not shown in Figure). First we injected the fully matching antisense match strand (green curve). After dissociation and regeneration the process was repeated for two kinds of antisense mismatch strands (blue and red line). The mismatch configuration 1 had two mismatch sites in the center of the strand. Mismatch configuration 2 had three mismatch sites in the first halve of the strand (see Tab. 2.2: F7 Antisense Mism. 1 and F7 Antisense Mism. 2).
The graph shows the mass adsorption after injecting a fully or partially matching antisense DNA by hybridizing to an oligo on the sensor surface and its dissociation over time. Where the signal amplitude for all injections is besides a slight decrease for Antisense Mism. 2 almost the same, the dissociation is different for the matching and non-matching strands. Antisense Mism. 2 has the fastest dissociation, followed by Antisense Mism. 1 and Antisense Match does almost not dissociate. With the shown experiment we could prove that the differentiation between specific (antisense match configuration) and unspecific (antisense mismatch configurations) is possible by observing the dissociation kinetics.

By changing the stringency we should be able to wash away partially bound strands due to the fact that unspecific bound ssDNA has less affinity to the sensor surface compared to full matching targets. Before proving our hypothesis, we had to show that a wash step with H_2O does not affect fully hybridized strands.
Figure 3.25 (a) and (b) show the signal response during a H_2O flush. Both experiments were performed on the same Biacore sensor chip in series. The chip was prepared as described before. In (a) we injected 25 μL, 1 μM, 5 μL/min antisense match DNA in PBS. The typical reaction pattern for oligo hybridization can be observed. After the injection was finished and the program back to standby conditions (5 μL/min buffer flow), we injected in channel Fc1–3 10 μL, 5 μL/min H_2O. The change in buffer stringency will induce a stress and therefore removes not well bound oligos from the sensor surface. Fc4 (pink curve) was not flushed with H_2O as reference. The graph shows that the loss of specific bound target is less than 5 % by flushing with H_2O. The drop during H_2O injection time in the reference curve Fc4 is due to changes in the flow and fully recovers after the injection is completed. The reference curve does not show any loss of target as expected. A slight drift leads to a decrease of the signal even in the reference curve, but can be neglected. At the end channel Fc1–3 were washed with urea for regeneration. In (b) the experiment was repeated with 25 μL, 1 μM, 5 μL/min antisense mismatch (Antisense Mism. 1) DNA in PBS for Fc1–3. Fc4 was kept in hybridized state, respectively fully bound with perfect match. We injected 2× 10 μL, 5 μL/min H_2O (all channels) and finally Fc1–3 were regenerated with urea. Where the signal in the reference channel with the specific bound match strand did not drop more than 5 % per H_2O injection, the signal for Fc1–3 with

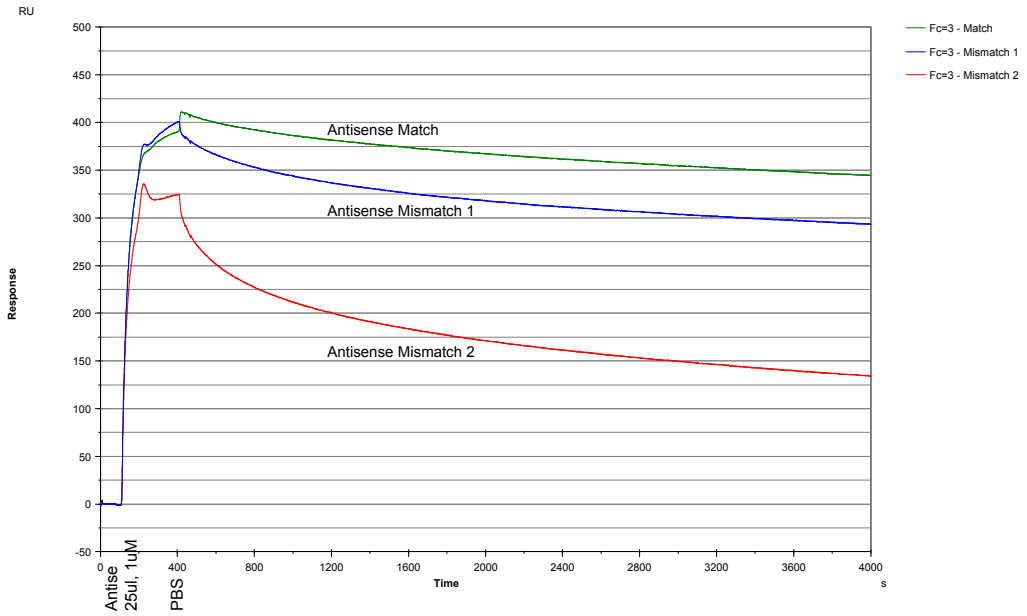

Figure 3.24: Reaction kinetics of match and mismatch configurations: The differentiation between specific and unspecific bindings to a single strand oligo on a Biacore sensor surface can be done by tracking the dissociation. The graph shows the binding of a full matching strand (green curve) and two kinds of mismatching strands (blue and red curve) to an oligo on the sensor surface. The Biacore sensor chip was recycled from a former SA chip by cleaning it according to protocol with detergents and UV/O_3. Functionalization was done by incubation with 1 μM thiolated sense match DNA in NaCl-TE buffer overnight and post-processing with 1 h MCU spacer incubation to reduce the immobilization density for improved hybridization. After injection the hybridization can be observed by the increase of signal response. The mismatch configuration 2 (red curve) with three non-matching bases led to slightly less deflection than the mismatch configuration 1 (blue curve) with two non-matching bases and the fully matching strand (green curve). To distinguish between the three configurations, the dissociation has to be observed. Where the signal amplitude right after the injection is almost identical for match and mismatch 1, the dissociation is for all three samples different. The fastest dissociation can be observed for the mismatching configuration with three mismatch sites.

not fully specific bound antisense strands decreased more than 15 % by flushing with H_2O during the first injection. A repeated H_2O wash step did not lead to the same decrease than before (second: ∼12 %). This might be due to the fact that during the first H_2O wash already very badly bound strands were removed whereas during the second H_2O wash only better hybridized strands remain.

3.3.7 Sensitivity

In the previous subsections we have shown the specific detection of antisense oligos on the described Biacore assay and its feasible regeneration by urea. Next we want to check the sensitivity of the Biacore SPR assay.
In a first experiment we injected several concentrations of 25 μL, 5 μL/min antisense match DNA in PBS. The assay was prepared as described before: The Biacore sensor chip was recycled from a former SA chip by cleaning it according to protocol with detergents and UV/O_3. Functionalization was done by incubation with 1 μM thiolated sense match DNA in NaCl-TE buffer overnight and post-processing with 1 h MCU spacer incubation to reduce the immobilization density for improved hybridization. Before each injection we recorded a stable baseline to ensure that the system was equilibrated. Eleven samples with concentrations between 1'000 nM and 0 nM were injected in series with urea regeneration in between. Samples were diluted in 1:2 steps.
Figure 3.26 (a) and (b) show the signal response during the injection of the titration series on the described assay. The typical reaction curve can be observed for the 1'000 nM sample. After each injection the program switches back to standby conditions (5 μL/min buffer flow). The switching leads to a rapid signal increase induced by switching the valves and slight changes in buffer conditions. After a short dissociation phase, 8 M urea was injected twice for regeneration. The endpoint perfectly ends at the same level like the baseline proving that the regeneration was successful (as shown before in Fig. 3.23). In (a) a baseline corrected (baseline set to zero) overlay of the data for the eleven injected samples is shown. The data is only shown for Fc3. In (b) the reference injection (1 nM respectively 0 nM) is subtracted from each curve which reduces the refractive index conditional steps by buffer changes. Where in the rising phase in (a) a "nose" is visible (at about s 200) this artifact is almost eliminated in (b) leading to the conclusion this artifact might be due to buffer changes. In (b) therefore the reaction curves are easier to interpret. The explanation that the "nose" is a superposition of hybridization signal (actual mass adsorption on the surface) and changes in refractive index due to buffer changes correlates with the fact that running buffer and probe solution do slightly differ.
With 1 nM concentration we clearly reach saturation after injecting the 25 μL sample. This might also be the case for the 500 nM injection whereas at lower concentrations saturation is not reached.
With Fig. 3.26 we have proven that the differentiation between concentrations is

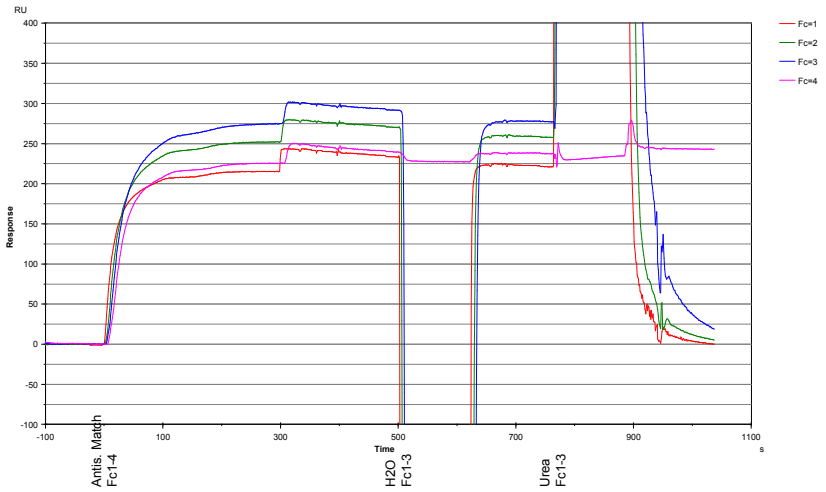

(a)

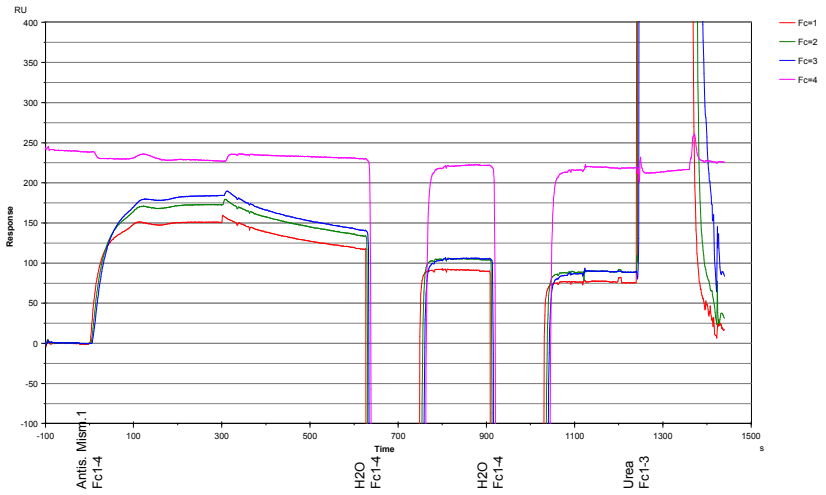

(b)

Figure 3.25: Effect of stringency on match and mismatch configuration: Both figures show the hybridization of a single strand oligo to the immobilized ssDNA on the sensor surface under similar conditions than before. In (a) a perfect match antisense strand was injected and hybridized specifically to the capture probe. Injecting H_2O does almost not affect the binding (loss $<5\,\%$). Fc4 (pink curve) acts as reference and was not flushed with H_2O, therefore does not show any loss of signal respectively bound material. In (b) Fc1–3, a mismatch sequence with two non-matching bases was injected. The target is expected to bind unspecific respectively partially specific to the immobilized ssDNA on the sensor surface. By flushing with H_2O we induce enough stress to partially remove unspecific bound material (loss $>15\,\%$ during first H_2O flush). In contrast the reference Fc4 with a perfect match is almost not affected by the H_2O flush. This proves that the affinity of our assay is significantly less for unspecific bound oligos and therefore we can distinguish between specific target and unspecific binding effects.

possible. For further statements a series of experiments at lower concentrations had to be set up.

3.3.8 High sense SPR detection and assay conditions

Finally we wanted to gain insight in different assay conditions to improve the sensitivity of the assay. Several variables were altered to check their influence on the sensitivity: (i) chip source (recycled or new), (ii) immobilization time (1 h or >10 h), (iii) immobilization post-treatment with MCU to reduce the immobilization density (none or 1 h). As analyte we chose target concentrations around the actual lower limit of detection from the experiment shown in Sect. 3.3.7. Besides the hybridization of a perfect match oligo we injected in each series a mismatch control to observe the signal behavior.
Results are shown in Tab. 3.4, 3.5 and 3.6. The Biacore sensor chip was either recycled from a former CM5 chip by cleaning it according to protocol with detergents and UV/O_3 (stated as CM5), or as commercially bought clean Au chips activated by UV/O_3 treatment (stated as Au). Functionalization was done by incubation with 1 μM thiolated sense match DNA in TEAA buffer for 1 h or overnight (stated as >10 h). TEAA was chosen although slightly better results were achieved with NaCl-TE buffer in previous experiments. This decision was made to have direct comparability to the CLA experiments and reference experiments in Martin Hegner's group. Certain chips were post-processed by incubation with a MCU spacer for 1 h to reduce the immobilization density for improved hybridization.

Each column in Tab. 3.4, 3.5 and 3.6 belongs to one sensor chip. Multiple samples were injected in series with urea regeneration in between. Before each injection we recorded a stable baseline to ensure that the system was equilibrated. 50 μL, 5 μL/min sample were injected for each hybridization. The increased sample volume compared to previous experiments was chosen due to the fact that saturation was not reached at 25 μL sample volume for low concentrations (as shown in Fig. 3.26).
We recorded the response signal for each injection. Tables 3.4, 3.5 and 3.6 show the resulting amplitudes for each hybridization, as well as the drift plus mentioned assay conditions. The stated drift corresponds to an average value of the first injection cycle. Drift normally decreases over time.

The experimental series displayed in Tab. 3.4 proves a positive effect of the MCU post-treatment on the drift. The recycled chips do also have less drift. In terms of signal amplitude no significant statement can be made by comparing the described assays. The chip to chip variability is very high and therefore we cannot conclude which immobilization protocol leads to the most sensitive result so far.

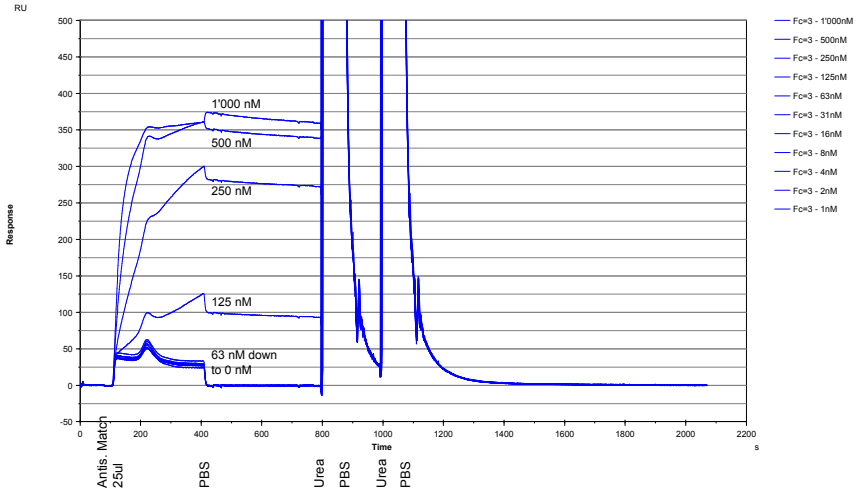

(a)

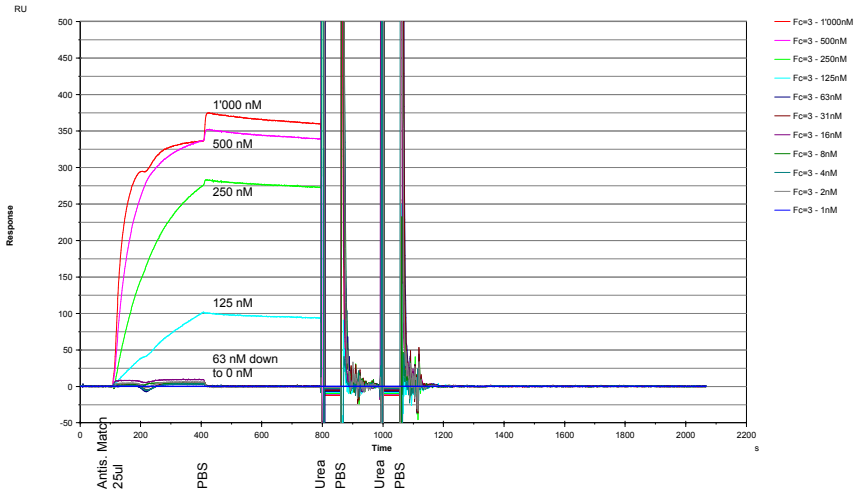

(b)

Figure 3.26: Concentration series on SPR assay: Both graphs show the identical experiment of a series of injections of various samples with differently concentrated targets. The 11 samples were injected sequentially on the same chip which was prepared as described before. The data is shown as an overlay of each injection for Fc3. After each hybridization the chip war regenerated by injecting 2× urea. In (a) only a baseline correction was applied to set all baselines to zero. In (b) the reference injection (1 nM respectively 0 nM) was subtracted for each curve. The decrease of signal for lower concentrated samples can be observed. 1'000 nM and 500 nM seem to reach saturation and therefore do have similar amplitudes. Expected decrease by $\frac{1}{2}$ due to the 1:2 dilution steps is not visible. For lower concentrations (<125 nM the signal seems to suddenly break down. The differentiation between concentrations is possible.

Chip	Au	CM5	CM5
DNA immobilization	1 h	>10 h	>10 h
MCU post-treatment	no	no	1 h
Drift	6 RU/min	2.4 RU/min	∼0 RU/min
antis. Match 100 nM	70 RU	65 RU	80 RU
antis. Match 50 nM	<10 RU	8 RU	3 RU
antis. Match 100 nM	55 RU	70 RU	43 RU
antis. Mism. 100 nM	55 RU	50 RU	75 RU fast dissociation
antis. Match 100 nM	45 RU	70 RU	67 RU
antis. Match 50 nM	-	20 RU	3 RU

Table 3.4: SPR results for different chip functionalization times and MCU post-treatments.

Chip	CM5	Au
DNA immobilization	>10 h	>10 h
MCU post-treatment	1 h	1 h
Drift	∼0 RU/min	∼0 RU/min
antis. Match 100 nM	90 RU	60 RU (peak 285 RU)
antis. Match 50 nM	70 RU	20 RU
antis. Mism. 100 nM	60 RU	15 RU
antis. Match 100 nM	80 RU	60 RU
antis. Match 50 nM	80 RU	55 RU
antis. Mism. 100 nM	60 RU	15 RU

Table 3.5: SPR results to compare a recycled CM5 chip and a commercially bought Au Biacore sensor chip.

The detection of low concentrations (<100 nM) is still challenging and the signal tends to fall below the lower limit of detection. Differentiation between match and mismatch sequences can only be done by observing the kinetics (dissociation). The signal amplitude is almost identical for 100 nM antisense match and 100 nM antisense mismatch probes.

In the experimental series displayed in Tab. 3.5 the previous findings were directly implemented. Therefore both chips were post-treated with MCU. The focus lays on the difference between a recycled CM5 Biacore sensor chip and a commercially bought clean Au chip. In terms of drift both chip types do show very stable signals. This was expected due to the previous findings with the MCU post-treatment. Both chips lead to feasible results even for 50 nM. The chip type to chip type variability is not very high. By trend the recycled CM5 chip

Chip	CM5	CM5	Au
DNA immobilization	>10 h	>10 h	>10 h
MCU post-treatment	1 h	1 h	1 h
Drift	<0.5 RU/min	∼0 RU/min	∼0.3 RU/min
antis. Match 100 nM	75 RU	110 RU	40 RU
antis. Match 50 nM	15 RU	5 RU	5 RU
antis. Match 10 nM	7 RU	3 RU	3 RU
antis. Match 1 nM	0 RU	0 RU	0 RU
antis. Mism. 100 nM	8 RU	70 RU	15 RU
antis. Match 100 nM	60 RU	105 RU	45 RU
antis. Match 50 nM	3 RU	7 RU	5 RU
antis. Match 10 nM	3 RU	5 RU	3 RU
antis. Match 1 nM	0 RU	0 RU	0 RU
antis. Mism. 100 nM	12 RU	60 RU	20 RU

Table 3.6: SPR results from measured concentration series down to low concentrations (1 nM matching target strand): Results listed for three experiments on two chip types with identical immobilization conditions.

led to higher signal amplitudes. Compared to measurements on assays without MCU post-treatment we measured slightly higher signals. This correlates with the literature. Therefore the MCU post-treatment is favored for this type of assay and can lead to higher signal responses under ideal conditions.
The chip to chip variability is very high. The intra chip variability is much smaller. Several injections on the same chip with regeneration in between do show similar results.

Hybridization signal amplitudes shown for the CM5 chip in Tab. 3.5 are surprisingly high compared to previous experiments. Even the 50 nM antisense match injection signal is above the lower limit of detection.

In terms of comparability with the CLA assay there is one major difficulty. The long functionalization times we use for the SPR protocol cannot be applied on the cantilevers. Long immobilization times lead to high initial deflections. CLA with strongly bent CL cannot be used for proper readout due to technical reasons. Therefore we had to adapt the SPR protocol several times to the CLA protocol.

The set of experiments shown in Tab. 3.6 focuses on relatively low target concentrations in SPR. Two recycled CM5 Biacore sensor chips were used to check the chip to chip variability. Furthermore a clean Au chip was used to compare it with the recycled ones.

The results did not show any unexpected behavior. Drifts were small as expected for the assay with MCU post-treatment. Recycled chips lead to slightly higher signal amplitudes compared to the Au chip. Especially for higher target concentrations the statement is valid. At low target concentrations the signal seems to drop below the lower limit of detection. Nevertheless we can distinguish between samples with 10 nM and 1 nM target concentration. The sensitive results achieved in the previous experiment (Tab. 3.5: CM5 chip: >50 RU at 50 nM antis. Match) could not be repeated.

General Discussion

Plain Au sites have a high affinity for biomolecules. Uncovered Au sites lead to drift by attracting biomolecules during the measurement. The MCU post-treatment might cover such "unprotected" sites and therefore be less prone to drift. Recycled chips might be not fully cleaned and therefore have less plain Au sites compared to commercially bought plain Au chips. Therefore recycled chips do show less drift than bare Au chips.

Reason for the high chip to chip variabilities could be varying qualities in probes and buffers for functionalization and hybridization. Thiolated sense strands for immobilization tend to form S-S double bonds which would lead to poor functionality. Furthermore the buffer components in TEAA are all volatile. To ensure the best functionalization results freshly prepared buffers are required and thiolated probes have to be protected with inert gas after extracting the DTT. The major reason for the chip to chip variability is for sure the fact that the cleaning process during recycling is not absolute. Results from XPS (shown in Sect. 3.1.1) lead to the conclusion that the sensor surface is not completely free of remains. The percentage and composition of remains will be highly different from chip to chip and therefore alter the immobilization density and quality. The antisense probe concentration was checked by NanoDrop and normalized for all experiments.

Instrumental sensitivity is for SPR often not a crucial factor. A monolayer of water which is in terms of biology one of the smallest detectable molecules, already leads to a sufficient resonance peak shift corresponding to approx. 310 pg/mm^2. What limits the assay's sensitivity is the affinity. The most common surface functionalization method is a self-assembled monolayer by thiolated probes. This fits perfectly in our strategy to build an analogue assay for CLA and SPR technology. High functionalization densities offer many binding partners, but have poor affinity due to steric hindrance as discussed before. Although an optimized immobilization protocol was used, we expect further improvements by focusing on immobilization strategies.
Compared to previous label-free DNA hybridization assay experiments we are in range (10 nM Nelson *et al.* [17]; 1 μM Peterson *et al.* [32]; 500 nM Lao *et al.* [18].

3.3.9 Summarized dose response curve

A dose response curve was plotted summarizing all SPR measurements (Fig. 3.27). For points with more than on measurement the average value was taken and error bars are shown. Included in those values are different assay preparations such as different chip types, buffers and reaction times.
The curve does not represent a perfect kinetic study. At lower concentrations the reactions did not reach saturation.

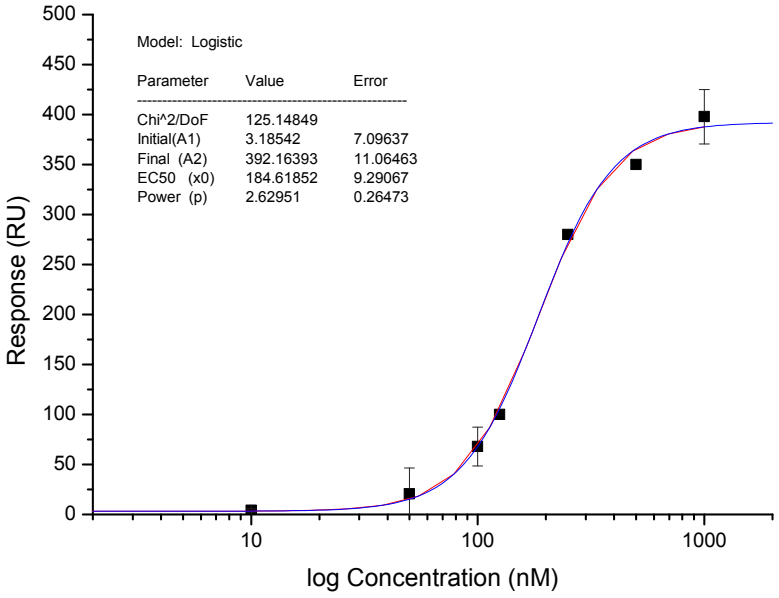

Figure 3.27: Dose-response curve for summarized SPR data: A logistic model was applied and a sigmoidal fit plotted. Error bars include chip to chip variabilities and intra chip results. Lower limit of detection, respectively sensor response threshold level is not shown. For the summarized experiments a very poor dynamic range is observed and the field of operation, respectively sensitivity is in the 10 to 1'000 nM range.

Generally it is not necessary to wait for saturation during SPR experiments. Kinetics can be calculated from association and dissociation. Therefore a k_d can be determined although the reaction did not reach saturation yet. For very low concentrations association cannot be calculated due to the fact that only a linear slope can be observed. For correct prediction at least a flattening of the curve must be visible. We have not done kinetic studies with our data.

3.3.10 Overlay of dose response curve for SPR and CLA

Comparing sensitivity and specificity from CLA and SPR data did not lead to a satisfying result for better understanding the two technologies. Main reason therefore is the fact that we were not able to detect similar concentrations by SPR as with CLA.
In Figure 3.28 we plotted an overlay of the dose response curve from the CLA experiment Sect. 3.4.6 (green curve) and a combined overview of all performed SPR experiments leading to a dose response curve for the SPR platform (blue curve) (equal to Fig. 3.27). By comparing the two curves side by side we see differences in the two types of assay. The result leads to a better understanding in terms of sensor response such as dynamic range and sensitivity.
For each concentration the corresponding response was plotted (cantilever deflection in [nm] for CLA and shift of refractive index in [RU] for SPR). A sigmoidal fit (logistic model) was applied to the existing data points. For the CLA, data points in the upper region are missing and therefore the fit is not very accurate. For CLA the data was recorded in a study with cell lysate background; sample volume 600 μL, injection speed 150 μL/min, incubation for10 min at 10 μL/min (about one chamber volume per minute). This leads to a possible time for hybridization of $\sim$12 min (2 min are lag time until the probe reaches the chamber). For SPR the data was recorded in PBS without background; sample volume 50 μL, respectively 25 μL; flow speed 5 μL/min (the camber volume in the Biacore 2000 device is estimated to be 0.5 μL). This leads to a hybridization time of 10 min, respectively 5 min.

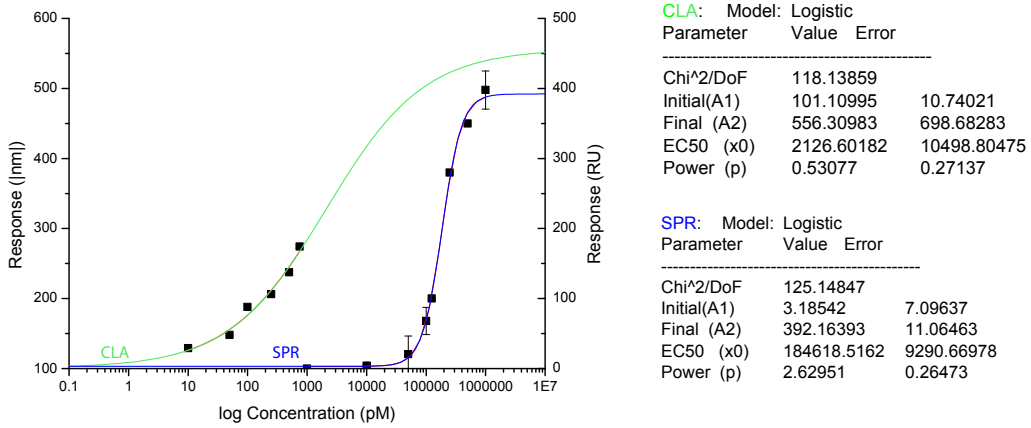

Figure 3.28: Overlay of Figure 3.38 and Figure 3.27 to compare the SPR and CLA dose response: Dynamic range, sensitivity and field of operation are different for SPR and CLA.

Although it is not a perfect comparison due to the missing CLA data and the varying SPR conditions, a trend is visible and comparability with the literature given. The SPR conditions are identical with Peterson *et al.* [32]:

- Same immobilization procedure (>10 h DNA immobilization, 1 h MCU).
- Analogue immobilization buffer. KH_2PO_4 was tested and compared to PBS with no special benefit.
- Capture probe density of 2.8×10^{12} molecules/cm^2 = 2.8×10^{10} molecules/mm^2 = 306 pg/mm^2 would lead to 300 RU signal which correlates perfectly with the measured 270 RU during the immobilization experiment on the Biacore device (Mw oligo: 6'581.8 g/mol, Avogadro constant: 6.022×10^{23} mol^{-1}).

Expected value for improved immobilization outside the instrument is 11×10^{12} molecules/cm^2 = 11×10^{10} molecules/mm^2 = 1'202 pg/mm^2 equals 1'200 RU. Saturated hybridization with 100 % efficiency would lead to an additional 1'200 RU. With the improved immobilization outside the device we achieved 400 RU. This would be 30 % efficiency. Not taken into account is the reduction of immobilization density by the MCU leading to less than 1'200 RU signal. This would lead to about 50 % efficiency which is close to the results from Peterlinz *et al.* [20].

A possible explanation for the observed deflection of the CLA at target concentrations beyond the SPR assay's lower limit of detection is a nonlinear response of the CLA. A nonlinear response can lead to a detectable signal at very low concentrations of hybridized probes on the sensor surface. A high dynamic range and increased sensitivity at lower concentrations compared to SPR would be the logic consequence. Consequently, CLA should have a lack in sensitivity at higher concentrations compared to SPR with its linear response to surface concentration of bound molecules.

3.4 Biological Application

Our goal was the label-free detection of noncoding RNAs. After showing the cantilever array instrument's feasibility to be a tool for such short oligo detection (see Sect. 3.2) we started a series of experiments towards the detection of miRNA in biological relevant probes. Table 3.7 shows the summarized results which will be explained in details in this chapter.
We started with the *in vitro* detection of synthetic samples to check the feasibility of sensing a specific strand out of a pool of totRNA (Sect. 3.4.2). Further we tested the detection of synthetic oligos in a cell lysate background (HepG2, Hep3B, ME15 and HuH7) (Sect. 3.4.3). Compared to the totRNA *in vitro* experiments cell lysates contain proteins, lipids and other cellular fragments making the background much more complex. As target for the experiments we chose a possible siRNA target construct (F7-1) and a miRNA of biological interest (miR-122). The first cell lysate experiments were done with synthetic target spiked in. Finally we analyzed biological samples with naturally occurring targets (Sect. 3.4.4, 3.4.5), concluded on their target concentration by referring to a dose-response curve (Sect. 3.4.6) and tested the detection of miRNAs directly in rat plasma (Sect. 3.4.7).
For diagnostics or as test in non-clinical safety several work-flows are conceivable. Either the total RNA including all micro RNA is purified and only the RNA is analyzed, or full cell lysate or plasma is used directly. Direct detection is preferred as explained in the introduction (Sect. 1.1).
The measurements present a new approach for label-free direct miRNA biomarker detection.

3.4.1 totRNA fragmentation

We used total RNA as artificial background for several hybridization studies. Either for improved competition to the short ncRNA targets or in case of sequence detection on mRNA, the totRNA has to be fragmented. Besides fragmentation to increase competition, fragmentation could be a method to improve sequence detection of specific targets on long mRNA strands.

We fragmented totRNA according to an established protocol for cRNA fragmentation for Affymetrix GeneChips (see Appendix A.1). Fragmentation time was varied from 10 min to 60 min to find the best fragmentation conditions to yield strands of similar length to ncRNAs. The resulting fractions were analyzed by standard methods to check for quality and size (Fig. 3.29). Complete Bioanalyzer data can be found in the appendix (Appendix B.4.2).

Table 3.8 shows the results from the NanoDrop check before fragmentation and for each fraction after fragmentation and precipitation.

Experiment	**Deflection**	**Figure**	**Negative control**	**Regeneration**	**Denaturation**	**Sample normalization**
100 pM proof of concept	230 nm	3.2	30 nm (mismatch)	no	yes	-
1 nM in 10 nM totRNA	150 nm	3.30	0 nm (totRNA)	Urea	yes	-
500 pM in 10 nM totRNA	75 nm	not shown	0 nm (totRNA)	Urea	yes	-
500 pM spike in HepG2 1:1 diluted	80 nm	3.31 (a)	50 nm (HepG2)	Urea	yes	-
500 pM spike in HepG2	80 nm	3.31 (b)	-	Urea	yes	-
F7 in Hep3B	150 nm	not shown	-	-	yes	-
F7 in Hep3B 1:1 diluted	60 nm	3.32	0 nm (HepG2)	Urea	no	yes
F7 in Hep3B	260 nm	3.34	80 nm (HepG2)	NaOH	yes	yes
miR-122 in HuH7	300 nm	3.36	100 nm (ME15)	NaOH	yes	no
miR-122 in HuH7 1:1	120 nm	not shown	60 nm (ME15)	Urea	yes	yes
repeated miR-122 in HuH7	2x 170 nm	3.37	-	Urea	yes	yes
miR-122 in rat plasma	200 nm	not shown	0 nm (untreated)	Urea	yes	no

Table 3.7: Summarized results from biological experiments: Not shown in the table are the results from the dose response curve experiments (Fig. 3.38 where we analyzed spike-in miR-122 (10 pM to 750 pM) in ME15 cell lysate.
Experiment: target detected in; Deflection: absolute differential deflection; Figure: referenced Fig.; Negative control: deflection and type of used negative control; Regeneration: regeneration agent; Denaturation: sample denaturation prior to hybridization; Sample normalization: normalization of samples on their total protein

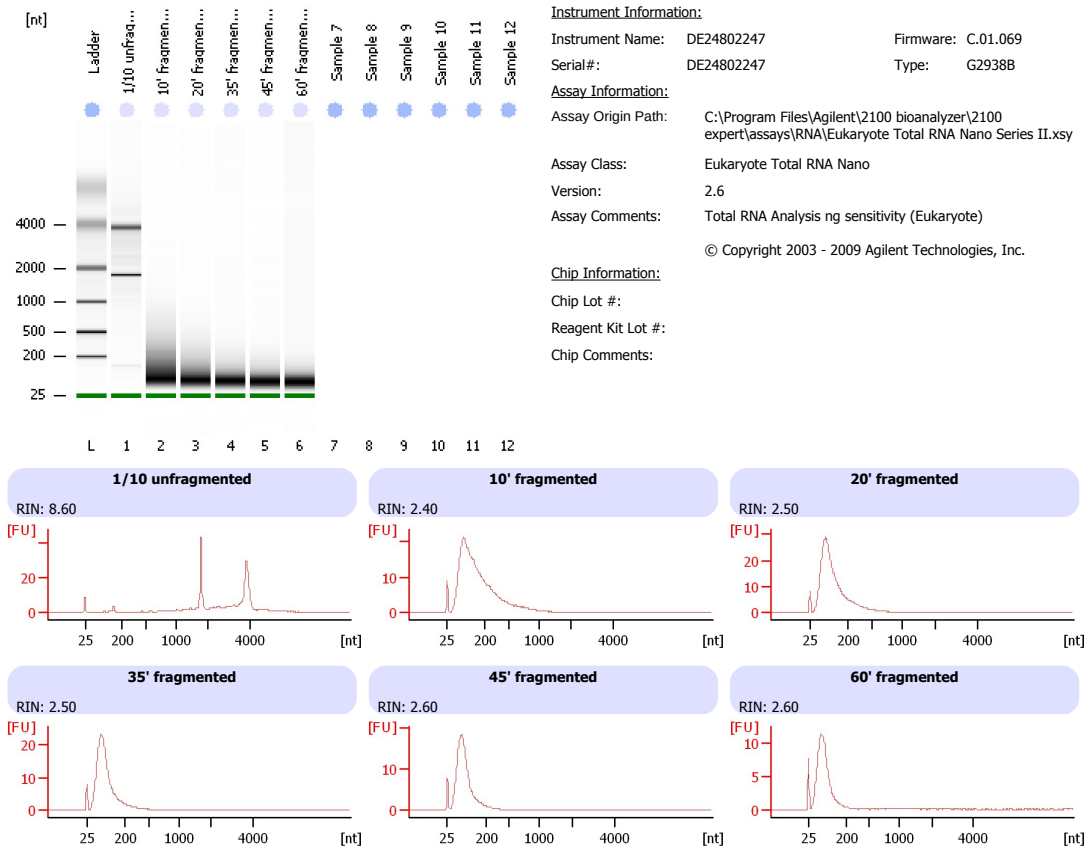

Figure 3.29: Overview of results from Bioanalyzer run: Data displayed for fragmented fractions 10 min to 60 min and an unfragmented control 1:10 from stock. Visible shift from 1'400 nt and 4'000 nt probably from the 18S and 28S rRNA towards lower fragmented length around 90 nt. The longer the fragmentation time was chosen, the more defined is the peak towards 90 nt. For times longer than 35 min the differences are minimal.

	Stock	**10 min**	**20 min**	**35 min**	**45 min**	**60 min**
Concentration (ng/μL)	500.4	611.5	885.1	889.8	776.2	780.3
A260	12.511	15.288	22.128	22.246	19.405	19.509
A280	6.340	7.718	10.824	10.899	9.680	9.830
260/280	1.97	1.98	2.04	2.04	2.00	1.98
260/230	2.21	2.25	2.21	2.20	2.21	2.20

Table 3.8: NanoDrop results for original and fragmented totRNA.

3.4.2 F7-1 detection in totRNA background

With the proof of concept experiment Sect. 3.2.1 we have shown the detection of a 100 pM antisense strand and the differentiation between a perfect match and mismatch sequence. As next step we tried to prove the detection of the same target strand in background. Figure 3.30 shows the detection of 1 nM F7-1 target in 10 nM totRNA background that consists of 346 μg fragmented 90 nt long human reference RNA. The cantilever chip was functionalized as before with four CL target capture and four CL non-matching reference sequence (see Fig. 2.3). The injection protocol was the same as described in Sect. 3.2.1 and the experiment shown in Fig. 3.2. Sample volume was decreased to 600 μL. For a real biological sample this is still way too much, but it was a first attempt to decrease the sample volume and our intention was not the optimization of the instrument towards microfluidics. Injection flow speed was increased to 150 μL/min. This value was recommended by M. Hegner due to experiences from former experiments to achieve an optimal fluid exchange in the flow chamber.

The graph (Fig. 3.30) shows the overlay of two consecutive injections: the first injection was a negative control with only totRNA and the second injection the totRNA sample with spike-in target. Between the two injections the chip was regenerated with 4 M urea. Urea denatures double stranded nucleic acids. Previous experiments without regeneration step but otherwise identical conditions did not lead to a successful detection of a target.

With the resulting net deflection of ~ -150 nm we could show that the detection of a short single strand oligo target (1 nM) is possible even in a background of totRNA (10 nM). Total RNA in a concentration of 10 nM does not lead to any differential deflection, but binds in an unspecific way such that a regeneration for subsequent specific hybridization is necessary.
Normalization as described in Ref. [45] did not had a significant effect on the result.

The experiment was repeated with a decreased spike-in target concentration of 500 pM. The net deflection resulted in ~ -75 nm proving the detection of a short single strand oligo target (500 pM) is possible in a background of totRNA (10 nM).

We did not analyze further concentrations for the detection of a short oligo target strand in totRNA background. A concentration series target versus background was one of R. Mishra's goals in a parallel study.

Mistakes by wrongly chosen sequences or due to failed chemistry during immobilization can lead to badly functionalized cantilevers and false positive results. Therefore we decided to inject prior to each measurement a negative

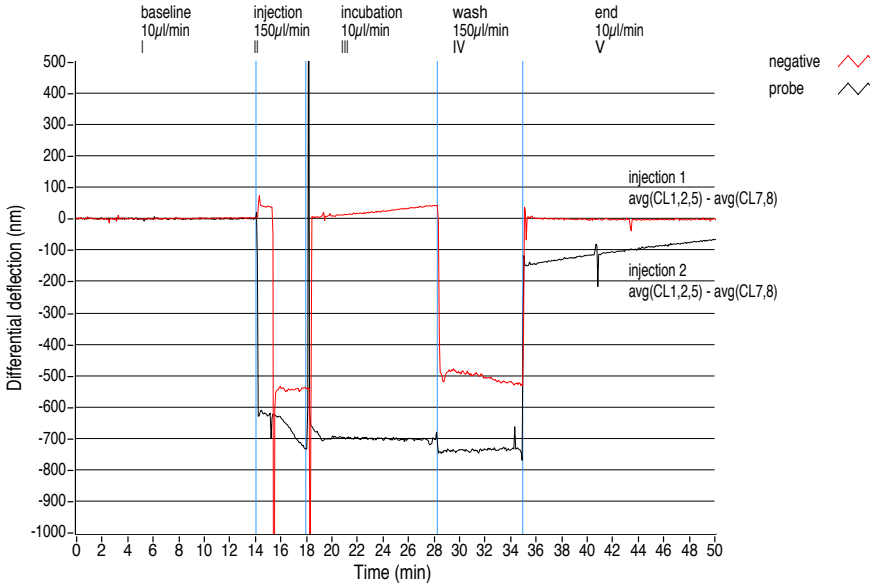

Figure 3.30: Overlay of two consecutive experiments to show the detection of a 1 nM antisense strand in a background of 10 nM fragmented totRNA: The graphic shows the significant difference between the injection of a 10 nM fragmented totRNA sample with 1 nM antisense target strand spiked in (black curve) and the injection of only the totRNA (red curve). Injecting the probe sample induces approx. −150 nm differential deflection, where the injection of only a sample with unspecific totRNA leads to no differential signal. Phase (I) shows the recorded baseline at 10 μL/min buffer flow. (II) 600 μL sample injection at 150 μL/min. (III) incubation phase at 10 μL/min. (IV) flushing with buffer 150 μL/min. (V) resulting differential deflection after injection cycle is completed (10 μL/min buffer flow). Curves correspond to the differential deflection signal of positive minus reference CL. The two injections were performed in series on the same cantilever array chip. A baseline correction, normalization, averaging and differential signal calculation (probe: CL1,2,5 minus reference: CL7,8) were done according to the literature [45].

control, although the CLA assay by itself is already a referenced system. False positive results from badly functionalized CLs either by wrong sequences or due to failed chemistry can be excluded.

3.4.3 Spike-in F7-1 detection in HepG2 cell lysate

Compared to totRNA cell lysates contain besides unspecific nucleic acids a significant amount of proteins, lipids and tissue fragments. Therefore measurements to analyze cell or tissue lysates are much more complex. As close model towards the detection of naturally occurring oligo targets we have chosen a HepG2 cell line as background for the following set of experiments. HepG2 is by nature negative for the F7 target. For detection we spiked in the F7-1 ssDNA. As negative control either the pure or diluted cell lysate in 1x lysis buffer (dilution with hybridization buffer) was used.

Figure 3.31 shows the detection of: (a) 500 pM spike-in target in 1:1 diluted HepG2 cell lysate and (b) 500 pM spike-in target in undiluted HepG2 cell lysate. Functionalization was done according to pattern Fig. 2.3. In (a) we injected first the negative control followed by a regeneration step with urea and the second injection with target probe. In (b) we skipped the negative control and only injected the target sample. All samples were denatured before injection for improved subsequent hybridization.
A typical injection pattern can be observed which is slightly different from previous experiments with pure samples or totRNA background. After recoding a stable baseline (phase (I)), we injected the sample (phase (II)). The increased flow speed of 150 μL/min induced an impact on the CLs. Following a short lag phase the sample entered the chamber and induced various forces led to a typical signal pattern with a peak towards the minimum before the signal equilibrates. Switching the flow speed for the incubation phase to 10 μL/min leads to a relaxation of the CLs and a deflection in the opposed direction than increasing the flow speed. Much more fluctuations can be observed during the incubation phase (III) with cell lysates compared to less complex probes. This is mainly due to the change in refractive index of the not fully clear solution plus the higher sample viscosity inducing more flow forces. Furthermore the PSD sum signal decreases rapidly due to the opacity, which makes a feasible kinetic readout difficult. With undiluted cell lysates it is almost impossible to interpret the data during the injection cycle. Nevertheless an endpoint measurement is feasible, because remaining probe was removed during the wash step (phase (IV)) by flushing the chamber with buffer. The increased flow speed in phase (IV) induced again strong deflection and a short lag phase can be observed, before a stable signal was recorded. Finally the automated injection cycle switched back to standby conditions (10 μL/min), and the resulting deflection values were monitored (phase (V)). Typical for all cell lysate injections is the short relaxation after the wash step. Therefore we

waited before the signal started to drift and took as final resulting values the local minimum for all cell lysate experiments.

The two graphs prove the detection of 500 pM spike-in F7 target strand either in 1:1 diluted HepG2 cell lysate or undiluted HepG2 cell lysate. Probe injection patterns (black curves) are similar for diluted (a) and undiluted (b) cell lysate experiments.

An additional injection of 100 nM pure F7-1 probe sample did not induce any further deflection (not shown in graph) indicating a saturation of probe on the CLs or blocking by unspecific bindings.

By directly injecting the probe solution without a previous negative control injection (Fig. 3.31 (b) compared to (a)) we were not able to observe higher deflections. This means the regeneration works well for this set of experiments. Negative controls are useful to check the functionality of the array and for absolute statements. With the cell lysate samples even the negative control induces a differential deflection. This might be on one hand due to higher effects of unspecific bindings. Even more likely is the possibility that negative samples do not contain absolutely zero target. Depending on the affinity and sensitivity of our assay we might catch up a signal even by very low remaining concentrations.

3.4.4 F7 detection in Hep3B cell lysate

The detection of RNA transcripts in biological samples is essential for microbiological applications. In the following section we detected full-length F7 mRNA in a biological sample to prove the feasibility of the CLA system for this application. A Hep3B cell line expresses mRNA with the F7 sequence and was selected as probe. A HepG2 cell lysate was used as negative control.

To validate the system we first tried to detect F7 RNA in Hep3B cell lysate in 1x lysis buffer (graph not shown). Functionalization was done according to pattern Fig. 2.3. As negative control we could refer on HepG2 injections from previous experiments. As in cell lysate experiments before, we can observe the typical injection pattern such as lag phase, peaks and minimums, and the relaxation after wash step. Due to the sample properties expected fluctuations during the incubation phase were induced.
The sample was denatured before injection by tempering up to 80 °C. The formation of some visible particles was observed due to the denaturing of all proteins. Those particles form a pellet during a short spin on a mini centrifuge according to protocol. Some particles remained in the liquid phase after spinning.
The injection led to a signal of ~ -150nm average differential deflection with almost no drift. The resulting signal is high compared to the previous spike-in

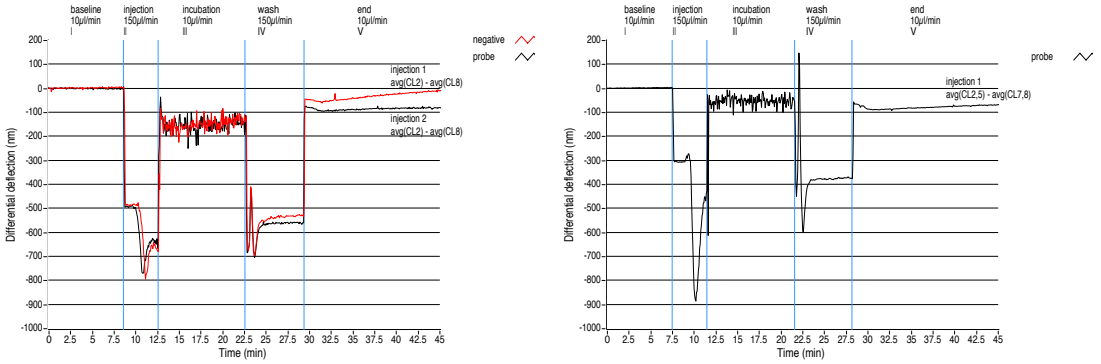

(a) 500 pM detection in 1:1 HepG2 cell lysate (b) 500 pM detection in undiluted HepG2 cell lysate

Figure 3.31: Two consecutive experiments to prove the detection of a 500 pM spike-in antisense strand in cell lysate: (a) The graph shows the significant difference between the injection of a HepG2 cell lysate containing a spike-in target (black curve) and the injection of the cell lysate negative for the target (red curve). Injecting the positive sample induces approx. −100 nm differential deflection whereas the injection of only the cell lysate leads to approx. −50 nm differential deflection signal. Phase (I) shows the recorded baseline at 10 µL/min buffer flow. (II) 600 µL sample injection at 150 µL/min. (III) incubation phase at 10 µL/min. (IV) flushing with buffer 150 µL/min. (V) resulting differential deflection after injection cycle is completed (10 µL/min buffer flow). (a) Both injections were performed in series on the same cantilever array chip with a 1:1 diluted cell lysate. A baseline correction, normalization, averaging and differential signal calculation (probe: CL2 minus reference: CL8) were done according to the literature [45]. (b) An experiment with positive probe was repeated for a undiluted 100 % cell lysate. No negative control was repeated in (b) due to its similarity to (a). Post-processing in (b) was performed with differential signal calculation (probe: CL2,5 minus reference: CL7,8) and otherwise same conditions as in (a).

experiments. This leads to the conclusion that the concentration of F7 transcripts in the Hep3B cell lysate is quite high which could be expected from the Lit. Ravon *et al.* (Ref. [48]). Therefore the detection of F7 RNA in Hep3B cell lysate looks promising (sufficient amount of target for the detection by CLA technology). The experiment should be repeated with negative control.

The detection of F7 in Hep3B cell lysate was repeated including negative control. Figure 3.32 shows the analysis of Hep3B cell lysate in 1x lysis buffer 1:1 diluted with PBS. Due to high signal intensities in the previous validation experiment we decided to dilute the sample to reduce the amount of denatured proteins and fluctuations due to the sample properties (viscosity and opacity). As negative control we used the HepG2 cell lysate. Both samples were normalized on their total protein concentration. The negative control was injected first and in between the two injections a regeneration step with urea was performed. Exceptionally we did not denature the samples to check the binding affinity under those conditions.
Injecting the probe sample induced approx. −60 nm differential deflection whereas the negative HepG2 sample led to almost no differential signal. Values for the final result were taken after the short relaxation right after the wash step. Although signals intensities are less than before, mainly due to the diluted probe and no denaturing, the detection of F7 in Hep3B cell lysate is possible and verified by the negative control.
The shown experiment proves the detection in diluted samples works as well as in undiluted cell lysates. We can distinguish between positive and negative probe (shown Fig. 3.33). The ±1 SD areas (blue) for the differential signal of positive and negative probe do not overlap. Therefore Statistical relevance is given.

Finally we repeated the previous experiment with undiluted cell lysate, with denaturing and negative control to have a full set of target detection in undiluted cell lysate with negative control. Figure 3.34 shows the analysis of undiluted Hep3B cell lysate in 1x lysis buffer. As negative control we injected primarily a HepG2 cell lysate with normalized protein concentration for both samples. Between the two sample injections we regenerated the cantilever chip with 0.5 M NaOH. A different chip regeneration agent was chosen with the idea to optimize the regeneration. With an optimized regeneration higher signal intensities were expected for the second injection. NaOH is a commonly known denaturing agent for nucleic acids used in Southern and Northern blot techniques.
Injecting the Hep3B sample induced approx. −260 nm differential deflection whereas the injection of the negative control (HepG2) led to approx. −80 nm differential signal (values taken right after relaxation in end phase and before the signal started to drift). A strong drift can be observed during the end phase (V) of the second injection possibly due to the NaOH chip regeneration (see Appendix B.4.1).

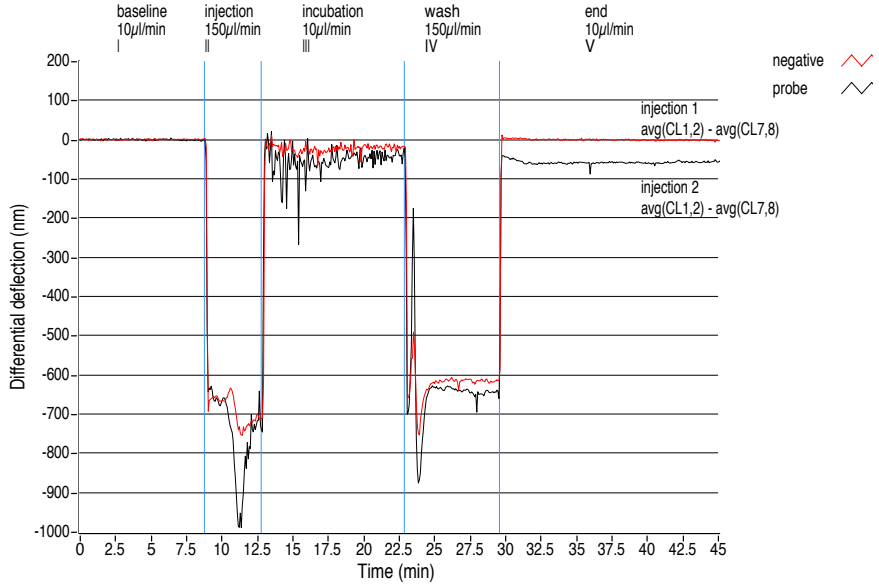

Figure 3.32: Overlay of two consecutive experiments to prove the detection of F7 in diluted Hep3B cell lysate: The graph shows the significant difference between the injection of Hep3B positive for F7 cell lysate (black curve) and the injection of HepG2 negative for F7 cell lysate (red curve). Both cell lysates were normalized on their total protein concentration and diluted 1:1 with PBS buffer. Injecting the Hep3B sample induced approx. -50 nm differential deflection whereas the injection of the negative control (HepG2) led to no differential signal. Phase (I) shows the recorded baseline at 10 μL/min buffer flow. (II) 600 μL sample injection at 150 μL/min. (III) incubation phase at 10 μL/min. (IV) flushing with buffer 150 μL/min. (V) resulting differential deflection after injection cycle is completed (10 μL/min buffer flow). The two injections were performed in series on the same cantilever array chip. A baseline correction, normalization, averaging and differential signal calculation (probe: CL1,2 minus reference: CL7,8) were done according to the literature [45].

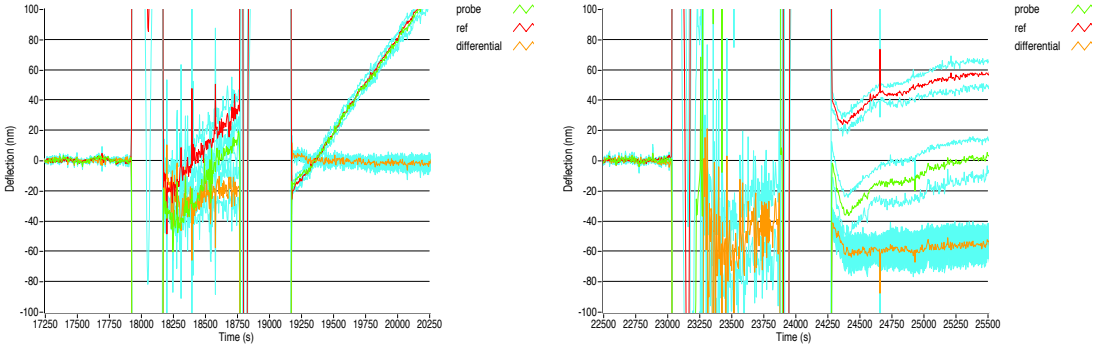

(a) (b)

Figure 3.33: ±1 SD areas for the analysis of Hep3B cell lysate 1:1 diluted: Raw data for averaged and baseline corrected deflections of probe (green) and reference (red) cantilever as well as differential deflection (orange). In blue the ±1 SD is given for each data line. Combining the two graphs (a) and (b) would lead to the conclusion that the differential deflections of (a) and (b) do not interfere with each other (no overlap of ±1 SD areas (areas of interest highlighted in blue)). Therefore the we can differentiate between probe and negative control.

As before we observed the formation of many particles during denaturing and the formation of a pellet during a short spin on a mini centrifuge (common step by protocol) due to the denatured proteins.

We can distinguish between positive and negative probe (Fig 3.35).
Undiluted cell lysates lead to higher deflections but do also induce a signal during negative control injections. The reason therefore we discussed before and might be due to the fact that negative control samples are not absolutely free of target.

Several attempts such as repeated injections (to test the reproducibility), skip of negative control (to test variations between injection 1 and 2) and different regeneration methods were shown to prove accuracy and consistency during a full experiment. A Peltier peak test was performed to monitor the functionality of the cantilever array as stated in Materials and Methods Sect. 2.5.3. Results are shown in Appendix B.4.3, Fig. B.4 and prove that the mechanical properties of a cantilever array do not change during multiple injections with regeneration.

3.4.5 miR-122 detection in ME15 and HuH7 cell lysate

Up to this point we measured mRNA transcripts which could be used for off-target analysis of siRNAs analogue to the Ref. [48]. Now we focus on the the

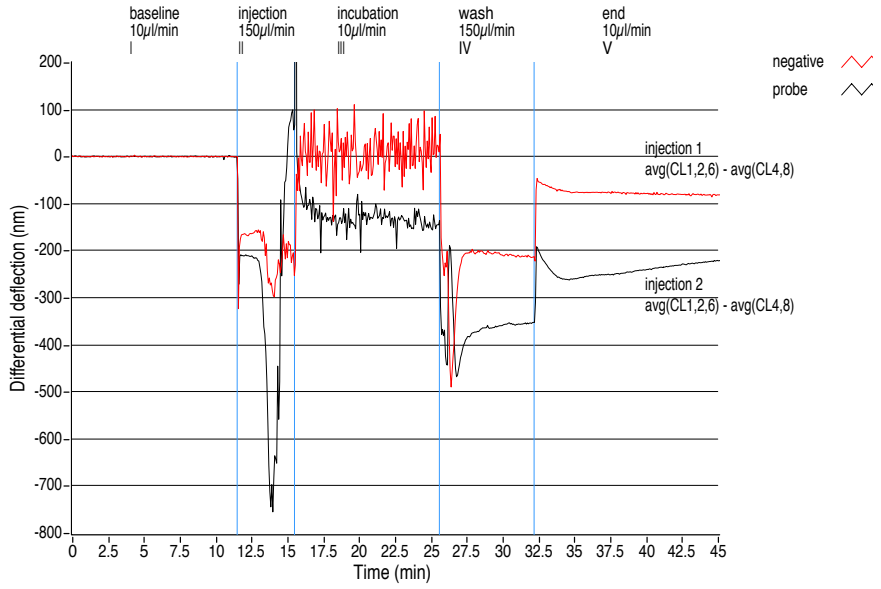

Figure 3.34: Detection of F7 mRNA in a Hep3B cell lysate: The graph shows the significant difference between the injection of Hep3B positive for F7 cell lysate (black curve) and the injection of HepG2 negative for F7 cell lysate (red curve). Both cell lysates were normalized on their total protein concentration. Injecting the Hep3B sample induced approx. −260 nm differential deflection whereas the injection of the negative control (HepG2) led to approx. −80 nm differential deflection signal. Phase (I) shows the recorded baseline at 10 μL/min buffer flow. (II) 600 μL sample injection at 150 μL/min. (III) incubation phase at 10 μL/min. (IV) flushing with buffer 150 μL/min. (V) resulting differential deflection after injection cycle is completed (10 μL/min buffer flow). The two injections were performed in series on the same cantilever array chip. A baseline correction, normalization, averaging and differential signal calculation (probe: CL1,2,6 minus reference: CL4,8) were done according to the literature [45].

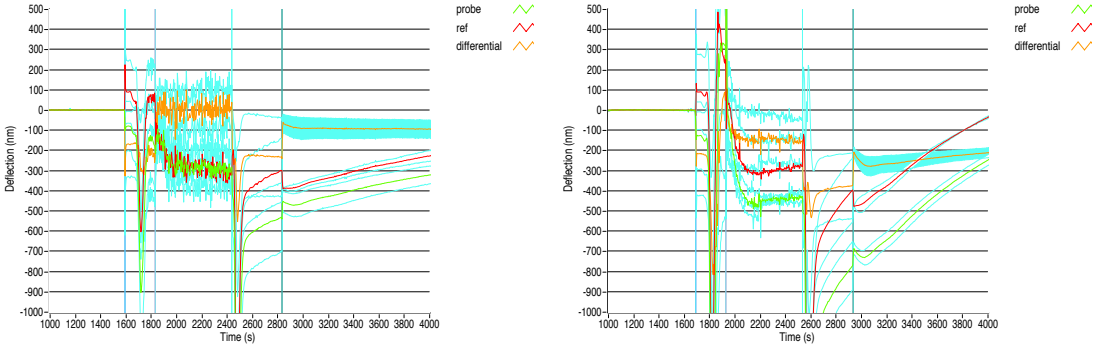

Figure 3.35: ±1 SD areas for the analysis of Hep3B cell lysate: Raw data for averaged and baseline corrected deflections of probe (green) and reference (red) cantilever as well as differential deflection (orange). In blue the ±1 SD is given for each data line. Combining the two graphs (a) and (b) would lead to the conclusion that the differential deflections of (a) and (b) do not interfere with each other (no overlap of ±1 SD areas (areas of interest highlighted in blue)). Therefore the we can differentiate between probe and reference and the experiment gains in statistical correctness.

detection of miRNAs as biomarkers of special interest. Therefore the presented assay has a high relevance for biological applications. Problematic could be the fact that miRNA is typically double strand. This would impair the binding to our immobilized capture single strand.
In the following set of experiments we prove the feasibility to detect naturally occurring miRNA targets with our label free direct binding assay based on nanomechanical cantilever arrays.

Figure 3.36 shows the detection of miR-122 in HuH7 and ME15 cell lysate in 1x lysis buffer. Both samples were denatured prior to injection. ME15, known as negative control for miR-122 (Ref. [47]), was injected prior to the HuH7 sample. In between the CLA chip was regenerated with with NaOH. No sample dilution or normalization on total protein was done.
Injecting the HuH7 sample induced approx. −300 nm differential deflection whereas the injection of the negative control (ME15) led to approx. −100 nm differential signal (values taken at the local minimum in the end phase (V) after relaxation and before the signal starts to drift). The detection of miR-122 in HuH7 cell lysate is possible. Differences between positive and negative sample injection are visible even without optimized cantilever selection (not shown in graph).
During the injection particles stuck to CL4, CL6 and CL7, although denatured

proteins were partially removed during a spin centrifuge step. Particles sticking to CLs lead to the loss or a drop of the PSD sum signal. The effect is caused either due to large deflections or by scattering the laser light at such particles. Particles sticking to CLs result in high fluctuations in the deflection signal. An increased buffer flow rate can sometimes wash away sticking particles and solve the problem.
The results from the Peltier peak test to monitor the functionality of the cantilever array are shown in Appendix B.4.3, Fig. B.5.

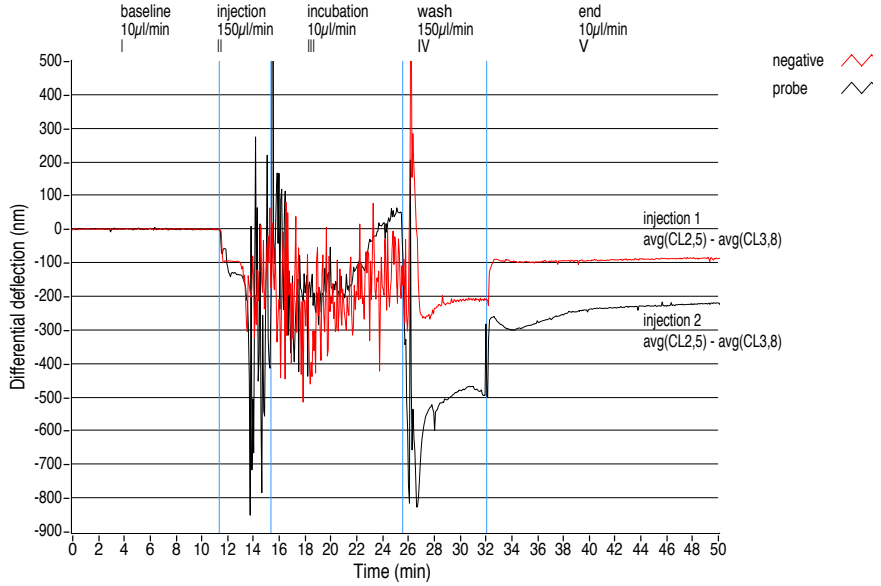

Figure 3.36: Overlay of two consecutive experiments to prove the detection of miR-122 in HuH7 cell lysate: The graph shows the significant difference between the injection of HuH7 positive for miR-122 cell lysate (black curve) and the injection ME15 negative for miR-122 cell lysate (red curve). Injecting the HuH7 sample induces −300 nm differential deflection whereas the injection of the negative control (ME15) leads to −100 nm differential deflection signal. Phase (I) shows the recorded baseline at 10 μL/min buffer flow. (II) 600 μL sample injection at 150 μL/min. (III) incubation phase at 10 μL/min. (IV) flushing with buffer 150 μL/min. (V) resulting differential deflection after injection cycle is completed (10 μL/min buffer flow). Curves correspond to the differential deflection signal of positive minus reference CL. The two injections were performed in series on the same cantilever array chip. A baseline correction, normalization, averaging and differential signal calculation (probe: CL2,5 minus reference: CL3,8) were done according to the literature [45].

As experienced before (Sect. 3.4.4), strong fluctuations were induced by in-

jecting NaOH for chip regeneration (see Appendix B.4.1). An adapted injection cycle protocol with shorter incubation phase and longer wash phase was more successful than the old protocol that was used before. The resulting differential deflections are very high and look promising (high signal amplitudes).

To exclude unknown effects due to the NaOH chip regeneration and the skipped sample normalization on total protein, we repeated the previous experiment as shown in Fig. 3.36 with different conditions: sample normalization on their total protein concentration; samples diluted 1:1 with PBS; chip regeneration with urea. The repeated experiment led to the following result: Injecting the HuH7 sample induced approx. −120 nm differential deflection whereas the injection of the negative control (ME15) led to approx. −60 nm differential deflection signal. The recorded PSD sum signal was much more stable than with undiluted lysates and NaOH chip regeneration. We experienced no problems due to sticking particles which might be due to the sample dilution. In exchange the resulting differential deflections were less in amplitude.

Finally we proved the consistency for a repeated injection with regeneration in between for the presented type of miRNA detection. This was shown by a repeated injection of positive probe in Fig. 3.37.
Figure 3.37 shows the detection of miR-122 in HuH7 cell lysate in 1x lysis buffer. The negative control was skipped and the HuH7 probe was directly injected during the first run. We repeated the injection after chip regeneration with urea. Samples were not diluted. Samples were denatured for improved subsequent hybridization. Both injections induced approx. −170 nm differential deflection. Injection 1 and 2 do have almost identical injection patterns which proves the consistency of our assay.
CL8 was excluded for further proceedings due to the loss of the PSD sum signal of CL8 during injection 1 caused by a particle from denatured protein.

3.4.6 miR-122 dose response curve

Most of the performed experiments were of qualitative significance and for most biomolecular applications a qualitative result is sufficient. Referring from the CLA signal to a concentration of target molecules is difficult because multiple factors influence the CL bending. Most commonly referenced systems map the result to a dose response curve. For the detection of miR-122 in HuH7 cell lysate we recorded a dose response curve with spike-in target in ME15 cell lysate as reference (Fig. 3.38). Several spike-in concentrations were measured in the control cell lysate ME15. As shown in Fig. 3.38 the dose response dependency can be fitted with a logistic model as expected for such sensor systems. A sigmoidal fit through the measured values has an R^2 value of 0.98559 which proves the logistic

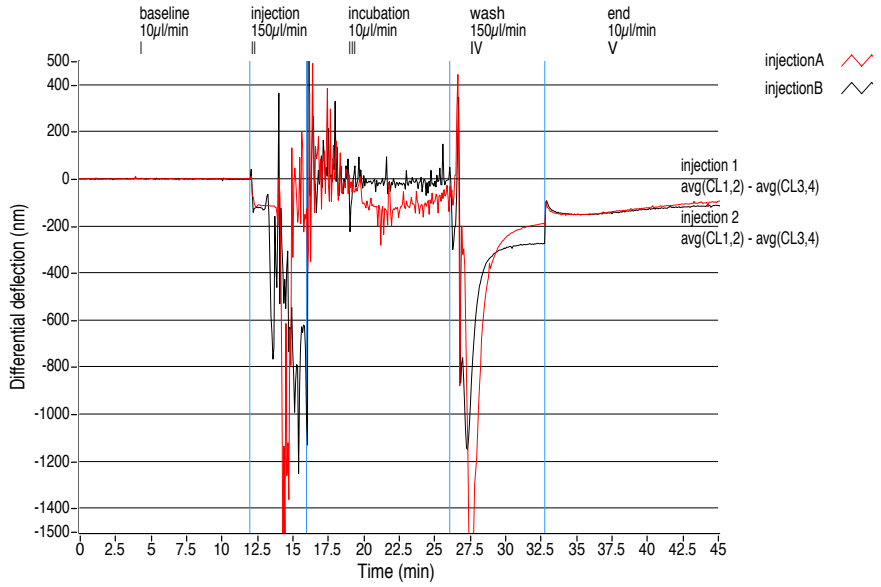

Figure 3.37: Overlay of two consecutive experiments to prove the detection of miR-122 in HuH7 cell lysate and to check the consistence of repeated injections with urea regeneration in between: The graph shows the correlation of an injection of HuH7 cell lysate which is positive for miR-122 (black curve) and an analogue repeated injection (red curve). Injection 1 and 2 induce both approx. $-150\,\mathrm{nm}$ differential deflection. Furthermore the injection patterns are almost identical. Phase (I) shows the recorded baseline at $10\,\mu\mathrm{L/min}$ buffer flow. (II) $600\,\mu\mathrm{L}$ sample injection at $150\,\mu\mathrm{L/min}$. (III) incubation phase at $10\,\mu\mathrm{L/min}$. (IV) flushing with buffer $150\,\mu\mathrm{L/min}$. (V) resulting differential deflection after injection cycle is completed ($10\,\mu\mathrm{L/min}$ buffer flow). Curves correspond to the differential deflection signal of positive minus reference CL. The two injections were performed in series on the same cantilever array chip. A baseline correction, normalization, averaging and differential signal calculation (probe: CL1,2 minus reference: CL3,4) were done according to the literature [45].

behavior of our system. Resulting deflections from unknown measurement with same conditions can now be mapped on the curve and a quantitative result can be calculated.

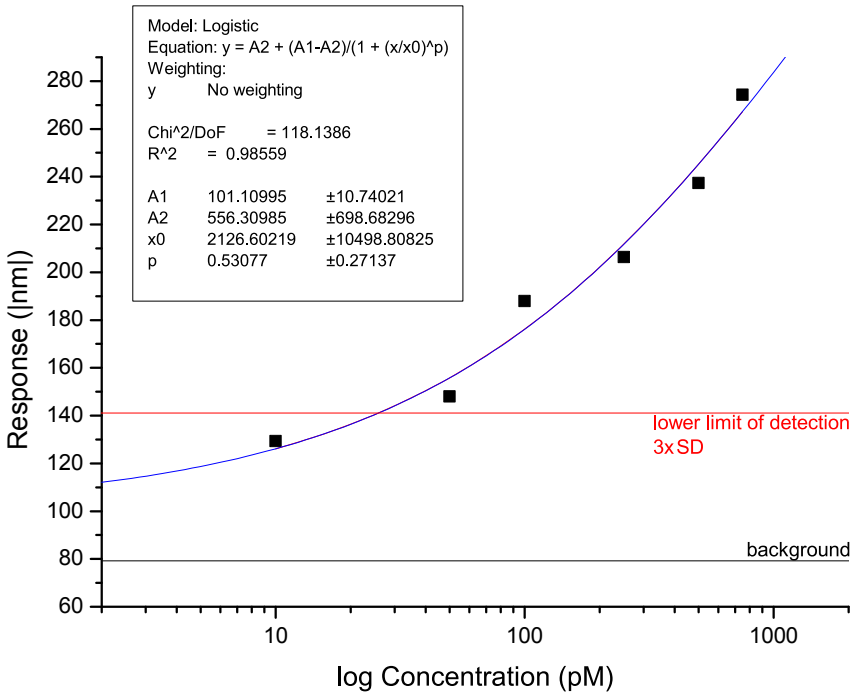

Figure 3.38: Dose response curve for miR-122 detection in ME15 cell lysate: The final differential deflection for several spike-in concentrations of miR-122 in ME15 cell lysate was recorded and plotted against the corresponding concentration. A logistic model was applied and a sigmoidal fit drawn. With the received curve we can basically map the resulted response in an experiment to its concentration. The lower limit of detection based on 3× SD above the background is just an estimation. Enough values for correct statistics are missing.

Unfortunately all measured points are in the region below the EC50. Therefore the accuracy for slope and end-point is not given.
For the dose response curve we took the deflection amplitude values at the exact same time spot for all measurements after the wash step (minute 34.6). The chosen spot in the end phase was set right after relaxation and before the cantilever bending starts to drift. The time-stamp equals the local minimum which was already used before as explained in Sect. 3.4.5. In earlier experiments we normally took an average over all points in the end-phase. This would also lead to a feasible result for the cell lysate experiments

Usually, respectively in earlier experiments we took an average over all points in the end-phase. This should also lead to a feasible result for the cell lysate experiments but was not applied.

Even though we have proven the possibility of receiving a quantitative result, the cantilever system is favored for qualitative statements. Mapping a signal to a dose response curve is a common method to quantify results. In our case the problem is that the cantilever deflection has several origins (as explained in Sect. 1.3) and is not fully understood yet. This makes a quantitative statement very difficult. For each system an own dose response reference curve has to be recorded under similar conditions (pH, salt concentration, background matrix).

3.4.7 miR-122 detection in plasma

miRNAs have a high poteintial as biomarkers to determine the health status of subjects or single organs (see Sect. 1.5). Therefore there direct detection is of high interest. miR-122 is specifically expressed and highly abundant in the human liver [44] and conserved between vertebrate species [43]. Acetaminophen in high doses induces liver toxicity in rats. In an experiment control versus treated we could show the fast and reliable detection of miR-122 in rat plasma which is a biomarker for liver toxicity. The significant difference of miR-122 level in the control and treated samples could be shown resulting in $\sim$200 nm absolute differential deflection between treated and control injection.
100 μL EDTA-Plasma probes were obtained from an untreated control rat and from an Acetaminophen treated one after 24 h. Both samples were diluted with 600 μL PBS buffer. Dilution was done to end up with enough sample for the injection according to previous protocols matching the cell lysate experiments. Prior to injection both samples were denatured for 5 min at 80 °C followed by 5 min incubation on ice. The CLA chip was functionalized according to pattern Fig. 2.3 with the same set of thiolated ssDNA (miR-122 sense: identical for rat and human [43]).

To get further experience the experiment will be repeated and other expertise with plasma or serum will be gained. Furthermore an experiment with absolute negative control should be performed. Here we recommend to spike the positive sample after denaturation with complementary ssDNA to block all binding sites. The resulting differential deflection should be zero. This would exclude that other factors which might be changed in the treated sample are the origin of the observed deflection. This is a common problem in all assays for microbiological screens. In most of the cases not only the biomarker of interest is affected by a treatment but also many other factors which might interfere with the assay result. A good assay is specific enough to only respond to changes of the biomarker of interest.
An experiment with a different dilution is the next step to confirm the dose-

response dependency.
An unspecific signal from the protein composition which might also be different for control and treated is not expected because the changes are in the minor percentage in respect of the total protein concentration.

3.5 General Discussion

We experienced high chip to chip variabilities during most of the cell lysate experiments. A major reason is expected to be the sample preparation. Samples were denatured for improved subsequent hybridizations. The increased temperature followed by quick cooling down (5 min at 80 °C followed by 5 min incubation on ice) leads to a "melting" of DNA/RNA double strands and denatures proteins as well. This leads to the additional benefit that DNase or RNase function will be stopped. Main reason for the denaturing is the chance to increase the amount of target in single strand form, which is necessary for the direct binding assay.
Spinning down proteins after denaturing might have a positive effect such as a simple sample preparation. By spinning down the proteins and removing the formed pellet we partially purify our sample and get rid of disturbing cellular parts. Although the mini spin centrifuge is not able to spin down DNA/RNA, denatured proteins might catch sterically or by charge the DNA/RNA and pull it down during centrifugation.
Depending on the spin duration the effect will be more or less distinctive and leads to the chip to chip variabilities.

Chapter 4

Conclusion

We successfully set up a direct binding assay for the label-free detection of non-coding RNAs by a nanomechanical sensing system based on cantilever arrays. Sensitivity in the lower pM regime and specificity towards single basepair mismatch were shown. In several steps towards the detection of miRNA biomarkers in biological relevant probes we finally achieved the detection of specific miRNA out of cell lysate and plasma. The specific detection of a short oligonucleotide strand at 100 pM concentration in physiological buffer conditions demonstrated proof of concept of a newly built setup. By the detection of short single stranded oligos in totRNA background and the detection of spike-in target in cell lysates the fundamental potential of our system was shown. An ultimate goal was achieved by the detection of F7 mRNA transcripts out of cell lysate positive for the target and the detection of naturally occurring miR-122 miRNA in cell lysate as well as plasma as described at the beginning. Qualitative results were supported by a broad comparison with negative control for each sample. Furthermore we set up a first attempt for quantitative analysis by referring to a dose response curve for the specific application of miR-122 detection in HuH7 cell lysate.

Assay development was supported by SPR. In a series of experiments we could show the feasibility of chip regeneration by urea as well as concentration and specificity studies.

In a broad series of buffer validation tests in several hybridization applications, such as SPR measurements and DNA microarray experiments (results not shown), we came to the conclusion that the formerly used (e. g. by M. Hegner and Ref. [13]) 0.1× SSC buffer is not the most favored hybridization buffer for our application. With PBS (+) we achieved the highest hybridization signals similar to commercially distributed and highly sophisticated buffers supplied by Affymetrix (Affymetrix Inc.) or Illumina (Illumina Inc.) hybridization buffers.

4.1 CLA Instrumentation[5]

Equilibration time and drift were significantly reduced by the fast temperature control system and continuous flow measurement. After installing the cantilever chip it takes about 1.5 h until the system is ready to measure. The major time consuming step is the cantilever functionalization although the protocol was simplified by using pre-gold coated arrays and UV/O_3 activation. Sample changes (opening the box for less than 5 min) can easily be done during experiments. The time it needs to restabilize the temperature is less than 30 min and the chamber temperature is not even affected. With CO_2 sparging, pressure compensation and Halar tubing the formation of gas bubbles and their time consuming removal was avoided. Further investigations into the effect of the continuous flow on the cantilevers were carried out and are negligible, respectively fully reversible during a full injection cycle. The gain in drift reduction (approx. 10 nm/min) compared to the flow induced bending ∼7 nm) leads to the assumption that a measurement under continuous flow is an improvement. State of the art electronic components and investigations into signal stability led to a stable and reliable device (fluctuations <5 nm for functionalized cantilever in liquid with a typical recording timescale of 0.25 Hz). Device control, measurement and data analysis by LabVIEW led to a fast and straightforward workflow. The specific detection of a short oligonucleotide strand at 100 pM concentration in physiological buffer conditions demonstrated proof of concept of this setup.

Sample volume could be reduced to 600 μL without losing sensitivity. An automated injection cycle with the following parameter was established and led to the possibility to overlay the injection of a negative control and sample of interest: (i) injection of 600 μL probe at 150 μL/min; (ii) incubation of analyte on sensor for 10 min; (iii) wash step with 1'000 μL buffer at 150 μL/min. Baseline and end phase were recorded at 10 μL/min constant flow to avoid diffusion effects.

4.2 Surface Plasmon Resonance Technology

Biacore SPR as a "gold standard" for label-free detection has many advantages compared to the CLA technology. The linear response between adsorbed mass and signal amplitude as well as the quantitative result are two main features. Furthermore the Biacore system has a very elaborate liquid handling system and microfluidic network keeping the sample volume very low. Signal handling respectively drift handling is highly implemented leading to a very user friendly device. The handy and simple chip format is an additional advantage of the SPR.

[5]Partially published in Peter Noy *et al.*,"Instrument for Label-Free Detection of Noncoding RNAs", Journal of Sensors, vol. 2012, 2012.[27]

To differentiate between match and mismatch configurations, thus specificity, we focus on the CLA platform on the signal strength, compared to the SPR platform where the signal amplitude does not change in the same percentage. In SPR, the kinetics, respectively dissociation leads to the necessary information about specificity. Not perfectly matching strands dissociate much faster than perfect match configurations. Dissociation time is dependent on the amount of mismatch base-pairings. A mismatch strand with 3 mismatch sites dissociates faster than a configuration with 2 mismatch sites. Slowest dissociation is observed with a perfect match configuration as shown in Fig. 3.24. Dissociation is configuration dependent and also dependent on the mismatch position (no further investigations were made into that topic). Distinguishing for specificity by SPR is feasible due to its capability to observe kinetics. Kinetic studies belong to the SPR technology's major benefits and are usually one of the Biacore's main fields of applications. Negative controls are required because interpretations are only feasible in referenced measurements where an analyte is compared with a negative control.
The reason for the discrepancy between CLA and SPR has its origin in the way how the transducer generates a signal. Where on the SPR an additional mass leads to the same change of index of refraction (as long as the distance to the sensor surface is equal for specific and unspecific bound material), we expect that the change of surface stress is higher for specifically bound material as compared to unspecifically bound material (higher sterical forces, more changes in charge density and better shielding of the sensor surface against the surrounding liquid). The evanescent wave in SPR has an exponential decay and penetrates about 200 nm into the media. All molecules present in the evanescent field contribute to the response of the SPR sensor. In contrast to SPR, the CLA is less sensitive to changes in unspecific surface load as long as the additional load does not lead to additional surface stress in the boundary layer between the surface of the cantilever and the liquid environment.
As final conclusion, we concur that it is advantageous to use different kinds of transducers observing different kinds of physical properties to gain a better understanding for detection of biomolecules especially with label-free techniques.

On the SPR platform regeneration by HCl is not feasible. Regeneration of the surface is not 100 %. The endpoint after regeneration does not equal the baseline. Furthermore a degeneration of the assay (signal amplitude decreases for each repeated cycle) is assumed.
Regeneration by 4 M urea works well and is consistent over 88 hybridization cycles.

A quantitative measurement is possible and is the SPR's big advantage compared to other techniques as mentioned before. The binding curve is concentration dependent in a certain dynamic range.

In our experiments the sensitivity of the SPR assay was by a factor 1'000 less than the analogue CLA assay. Although SPR is an elaborate technique for biomolecular interaction analysis its sensitivity for the mentioned application seems to be limited and not feasible for a biological study. Furthermore the dynamic range is limited and insufficient (approx. one order of magnitude).
Labeled SPR assays increasing the mass can achieve higher sensitivities such as shown in Ref. [49] but do have all the drawbacks of labeling as discussed before.

4.3 Biological Application

In a first attempt we have successfully proven the detection of 500 pM F7-1 single strand RNA (ssRNA) in a background of 10 nM totRNA. In terms of specificity the negative control did not induce any differential cantilever deflection at all, which led to an optimal differentiation between probe and negative control.
For higher competition fragmented totRNA can be used. The "Bauer Core Standard Protocol" (Appendix A.1) with 35 min fragmentation time leads to a feasible fragment length of approx. 90 nt.
Urea regeneration in between the two injection steps of negative control and sample is necessary for the successful detection of specific targets in background. This leads to the conclusion that totRNA and cellular fragments bind unspecifically to the CLA and impairs a specific binding of target ssRNA in the subsequent probe injection. This is different compared experiments without background where the injection of a mismatch and subsequent injection of a match strand did not require regeneration in between for successful analysis. The unspecific adsorption of totRNA on the sensor surface is equal for probe and reference cantilever. This is proven by the resulting zero differential deflection during negative control injection. totRNA binds with higher affinity than a pure mismatch sample.

The detection of spiked-in short ssRNA in diluted and undiluted cell lysate is possible proven by the detection of 500 pM spike-in F7 target in HepG2 cell lysate and down to 10 pM detection of miR-122 target in ME15 cell lysate.
With undiluted cell lysates it is not possible to interpret the signal behavior during injections due to strong fluctuations in the deflection signal and drop of sum signal due to the viscosity, inhomogeneity and opacity of the sample. End point measurements are feasible and the sum signal fully regenerates after flushing the chamber with buffer.
Urea regeneration works fine for cell lysate measurements proven by the fact that a direct injection of 500 pM target leads to the same differential deflection as the injection of sample after negative control analysis with regeneration in between.
Compared to previous experiments the injections of negative sample cell lysates do induce a differential deflection. One explanation is the fact that certain targets are not absolutely zero for our negative control samples. This leads to the conclusion

that our system is highly sensitive and good references plus the comparison of sample to a negative control are necessary.

The detection of naturally occurring F7 mRNA transcripts in Hep3B cell lysate(1:1 diluted and undiluted) is possible. Signal amplitudes from naturally occurring concentrations are in the range or even above the results from previous measurements with 500 pM spike-in target.
We can clearly distinguish between positive and negative probe supporting the statistical correctness of our experiments. This was shown by the non-overlap of ± 1 SD areas for the differential signal of analyte and negative control.

The detection of the miRNA miR-122 in HuH7 cell lysate was achieved. ME15 thereby is a feasible negative control. Therefore the CLA platform is a sensitive and reliable tool for direct miRNA detection in cell lysates.

Due to the complex maturation process of miRNA the ratio between ssRNA and dsRNA is unknown. Single stranded miRNAs are required for sufficient hybridization to our direct binding assay. The detection is possible either due to the competition of the high amount of capture ssDNA on the sensor surface or by a sufficient amount of naturally occurring ssRNA. Denaturing the samples prior to the hybridization supports the amount of free ssRNA target strands.
The effect of eventually bound Ago proteins respectively RISC on the target strands is unknown. Bound proteins could either support the cantilever's surface stress development or lower the binding affinity; plus sample denaturation might unfold bound proteins.
Further advantage of denaturing the samples (5 min up to 80 °C) is the inhibition of RNase activity.

The denaturing process leads to the formation of visible particles due to denatured proteins. During a short spin in a mini spin centrifuge those particles from partially a pellet. A few particles stay in liquid. Cellular fragments of bigger size can stick to the CLs and induce a false signal. Large deflections or drop of sum signal due to scattering the laser light might occur. By flushing the chamber with high flow speeds (150–250 μL/min) and/or urea sticking particles can eventually be washed away.
By working with diluted cell lysates (1:1 with PBS buffer) the obstruction of CLs due to denatured protein particles can be minimized.
A partially purified sample by spinning down the denatured proteins is not favored. The possibility to drag down oligonucleotides during the spinning process exists and has to be avoided. Therefore we prefer to work with possibly higher protein contaminated samples but in return for sure not losing any target and to work with fine suspensions which tend to stick less to the CL than whole protein colloids which form during centrifugation.

Repeated Peltier tests to track the functionality of the CLA array are crucial. Denatured protein in the high dense cell lysates tend to stick to the cantilevers. By comparing the Peltier tests before and after each injection malfunctioning cantilevers can be excluded and wrong signal interpretation avoided. Consistent Peltier tests prove that the mechanical properties of a cantilever array do not change during multiple injections.

NaOH regeneration is not feasible. Although high signal intensities during the second injection step were recorded, NaOH regeneration induces drift and long equilibration times are required. The effect of the strong pH change might be the source for the observed effects and might have additional impacts such as degradation on the chip and biolayer. Furthermore SPR experiments support the vague effects during NaOH regeneration inducing strong drifts and unstable baseline re-achievements. The regeneration with urea is more controllable.
Compared to the shown SPR experiments with more than 25 hybridization/regeneration cycles, the regeneration procedure on the CLA is not fully satisfying. Two hybridizations on the same chip work fine and data is shown to prove the consistency of the assay for two full injection cycles with urea regeneration in between.

4.4 Surface analysis and CLA rear-side passivation[6]

Some problems were encountered with sample handling due to the delicate nature of the cantilevers. Those were partially solved by the manufacturing of a sample holder where the cantilevers were fixed for batch processing and analysis.

In general we did not achieve a successful and complete trial with rear-side passivated CLAs. There are still some steps in the process which would require further optimization, and the inclusion of replicates would give a clearer picture of the results obtained. In general when coating the CLA, the problematic step seems to be the drying. Changing the functionalization protocol might solve the problem. Alternative protocols are described in the literature [50, 51]. The functionalization by a UV-linker might be extremely robust and a well-established technique for SuSoS, but does not seem to be optimal for our microdevices. Furthermore we do not require a very enduring coating. The passivation only has to retain for

[6]Results achieved in collaboration with SuSoS (SuSoS AG, Switzerland) as part of the purchase order for surface analysis and modification. Text partially free translated from untitled, unpublished protocol and results of SuSoS, unpublished 2011.

one experiment, because we are still working with disposable chips. Plus, the passivation "only" has to retain under physiological conditions.

During a wider coating development process several cantilevers should be investigated to determine whether the coating process is successful. Results should show the effect of the coating on the Au and Si sides of the cantilever after treatment on passivated cantilever devices which are nevertheless promising.
The Si side of the cantilevers should be coated with PVP in order to render the surface resistant against unspecific binding. The gold surface should be protected, to provide a clean, reactive gold surface.

In a discussion with the surface specialists from SuSoS the following knowledge was gained: An EtOH wash step after Plasma or OV/O_3 cleaning would be recommended to either get rid of oxide layers in case of Plasma cleaning or to get rid of oxidized thiols which did not went in a volatile state during the UV/O_3 treatment.
The similarity of pre Au coated arrays and fresh Au coated ones was confirmed by SuSoS. Both methods are equivalent as long as there is an adhesion layer on it and the Au is cleaned by UV/O_3 or Plasma. To store the chips a pure Ar atmosphere is not even necessary according to SuSoS.

4.5 Final Conclusion

CLA is a feasible technology for the label-free detection of noncoding RNAs. Although the quantitative informative value is only possible by references, CLA is fully capable of a qualitative analysis of biological probes. SPR has its limitations in sensitivity and dynamic range, but is useful for quantitative comparisons and establishing the CLA technology.
Assay development in terms of capture probe density for highest signals is different for CLA and SPR as expected from previous studies from the literature. Besides sensitivity the way specificity is expressed differs for CLA and SPR. SPR is a feasible tool to observe kinetics whereas the CLA has its limitations in observing effects during reaction.
Although the detection of microRNA in several kinds of biological probes is feasible, experiments are still highly elaborate (especially compared to Biacore experiments). Rendering the cantilever rear-side against unspecific bindings by a non-fouling layer might simplify the complex interpretation of cantilever deflection sources. An advanced CLA chip handling and improved microfluidics will help to overcome the steps towards commercial application. Pre-gold coated arrays and improved device control, measurement and data analysis were steps in the right direction towards industrial application.

In terms of biology, ncRNAs are highly interesting biomarkers and a promising therapeutic approach. Although miRNAs are present as double strand in many of the maturation steps, the detection of mature miRNA is possible by direct binding assays of single strands. Thermal denaturing improves subsequent hybridization.

The author recommends the CLA technology as described for the detection of ncRNAs.

Chapter 5

Outlook

5.1 Pharmaceutical Industry

Biomarker detection and system biology belong to the main pillars of innovative pharma research. Biomarkers are the key tools to characterize mechanisms and pathways processes. System biology is the understanding of the complexity of biological processes. New tools for personalized healthcare will be essential and early predictions are one of the most important factors to keep costs at a minimum. Personalized healthcare is one of the most important strategies for today's drug development.
Where old paradigms in for example cancer therapy focused on toxicity, non-selectivity and chemotherapy drugs, there have been fundamental changes in the field of oncology during the past two decades. One important change has been the increased focus on understanding tumors at the molecular level, which has major implications for both diagnostics and therapeutics. It has been known for quite some time that cancer is not a single disease; rather, it is a family of diseases, many of which are mortal. As technology advances, so does our understanding of the true diversity of cancer. Years ago, cancer was diagnosed and treated primarily based on where the physician found it. This approach was not particularly successful. Our appreciation of the true diversity of cancer has, over time, extended to the microscopic level, to the molecular level, and, most recently, to the genetic level. Collectively, appreciation for the true diversity of cancer is producing a shift from the old paradigm of toxic, non-selective cytotoxic drugs selected primarily on the anatomic site of the tumor, to a new paradigm of truly integrated diagnostics and targeted therapeutics, where selection of particular therapies is based on the molecular and genetic characteristics of the tumor [CRED, F. Hoffmann-La Roche Ltd].

In pharmaceutical industry a whole new world opened with the discovery of the RNA interference effect by siRNAs. siRNA has the therapeutic potential as a

new potent and selective drug class. siRNAs directly act on the origin of many biological mechanisms solving a miss functions on a molecular level leading to what we recognize as diseases (as illustrated in Fig. 5.1).

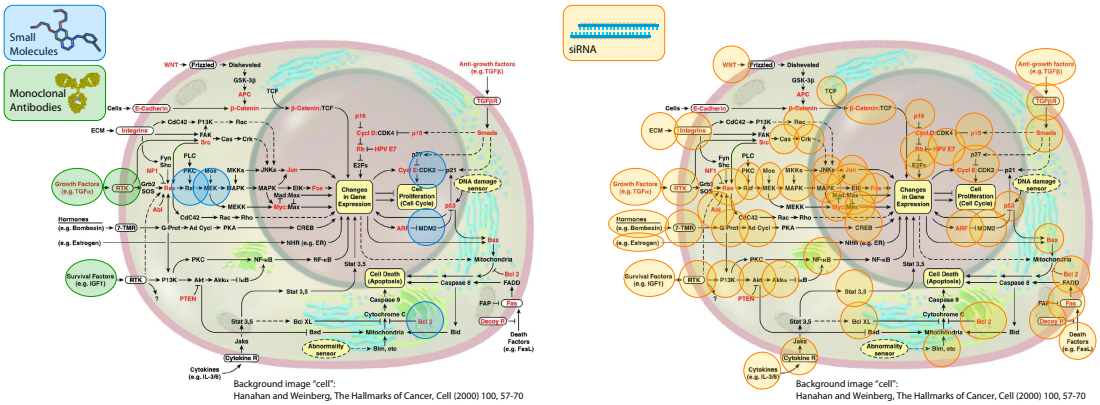

(a) Antibodies and small molecules limited to "druggable" targets.

(b) Potential use of the RNAi platform.

Figure 5.1: (a) Current approaches for cancer treatment by monoclonal antibodies and small molecules. "Druggable" targets are highly limited. (b) Possible approaches for cancer treatment by RNAi. Almost any cellular process could be regulated. The most suitable targets could be picked. [free translated from Dr. Alfred Mertens, siRNA Therapeutics: reality or dream (oral presentation), 2009]

Other drug classes are Small Molecules such as chemical compounds for treatment and therapeutic proteins including proteins such as antibodies and other biological compounds for treatment.

5.1.1 The siRNA Problematic

2010, F. Hoffmann-La Roche Ltd. discontinued their whole siRNA research section. The main hurdle to overcome is the delivery which could not be satisfyingly solved until today (see Sect. 1.5).
Nevertheless we have to keep in mind that we are still in a very young and early stage of research. If we compare where we stand with RNAi compared to today's high-end drugs such as Monoclonal Antibody (Mab) as shown in Fig. 5.2, there is still time for further research and a final product is not be expected in the next few years.

siRNA and miRNA do have for sure a huge potential for pharmaceutical industry and both would perfectly fit in the tendency towards personalized healthcare and could solve many assignments. Either for the detection as biomarkers

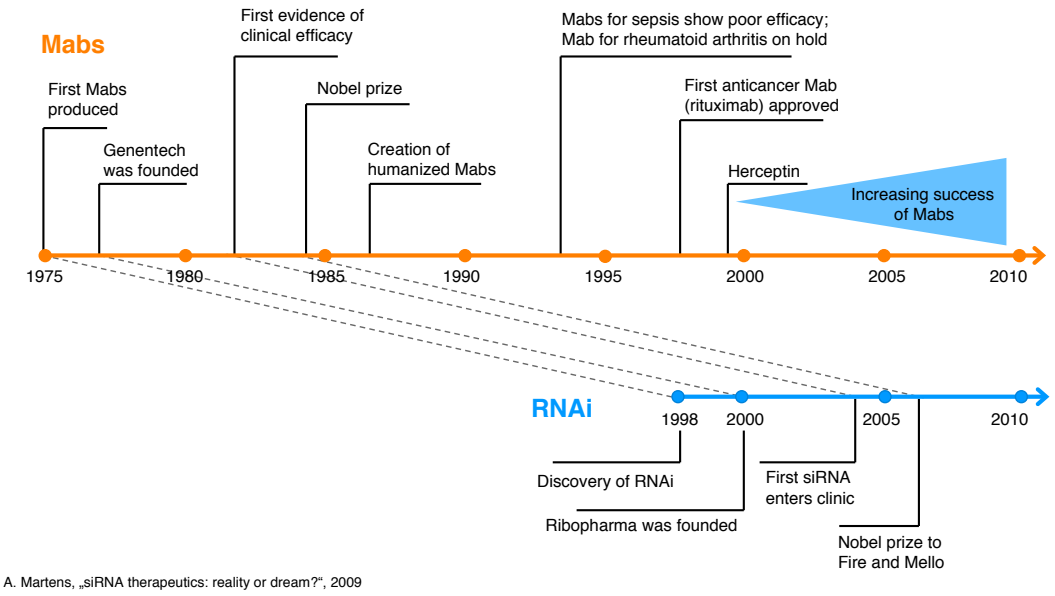

Figure 5.2: Discovery time-line of Mabs and RNAi: The figure shows the time-line between production of first monoclonal antibodies and their successful application in the drug market. In comparison an analogue time-line for RNAi is shown. It is clearly visible that RNAi research is still in its early decade and time is needed for further R&D before successful products will enter the market.

in diagnostics or in clinical and non-clinical studies during RNAi based drug development a high need exists for the detection of ncRNAs.

5.2 CLA Instrumentation

An advanced CLA chip handling and improved microfluidics will improve the CLA instrument towards industrial application.

Although the required sample volume of 600 μl for the actual protocol can be drastically reduced and sample dilution is possible as shown in the experiment detecting miRNA in rat plasma (Sect. 3.4.7) the volume is too high for a commercial biological application. Figure 5.3 shows a possible microfluidic injection method for small probe volumes.

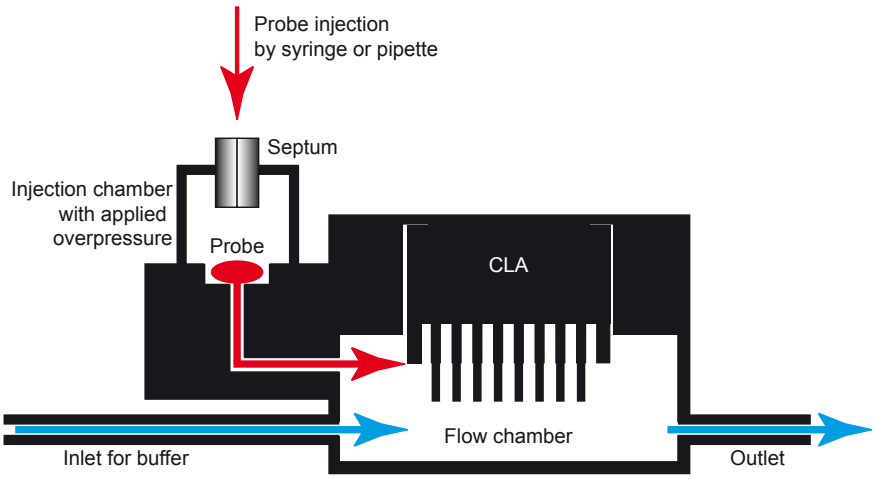

Figure 5.3: Schematic drawing of possible miniaturized sample handling: A direct injection of probe into the chamber would drastically reduce the amount of sample needed. Furthermore adsorption onto the tubing walls would completely be avoided.

A bandpass filter (635 nm) in front of the PSD suppresses ambient light and might enable measurements with an open box.

Implementing a beam splitter in the optical path between chamber and PSD would enable a constant observation with the camera. The actual mirror with tilt

function could be kept fix leading to an additional improvement to the instrument. The distance between CLA and PSD would be more defined and drift by slight mirror movements avoided. Furthermore the camera position could be chosen more flexible.

In case we have to measure much smaller signals (PSD voltages), respectively voltages, we could implement a lock-in amplifier (e. g. HF2LI, Zurich Instruments, Switzerland). With an implemented lock-in the laser-light would be modulated and we would be able to measure a very precise readout even with the PSD exposed to ambient light (e. g. with open box). This was never realized because measured voltages were in an detectable range and readout with an open box was never required.

In the introduction we claimed the CLA static mode technique to be mass independent. This relatively unique property of the nanomechanical sensor plays a fundamental role for the specific detection of target strands as explained in this thesis. The following experiment could be set up for further evidence: The pure oligo with target sequence could be compared to longer oligos with the target sequence at the 5' end plus a scrambled tail. On Biacore this should lead to an increased response for longer oligos because more mass binds to the surface. On the CLA we would only expect a slight signal increase due to steric hindrance. Furthermore, investigations into the effect of matching sequence location on longer target strands could be carried out. The effect of binding a target sequence somewhere in the middle of a long oligo compared to a matching sequence at the 5' or 3' end is an open question and not of importance for short ncRNA detection but might be interesting for genomic applications.

5.3 Biological Application

The undiluted cell lysate probes do not contain any PBS buffer or only a few micro liters. By adding Mg^{2+} to the cell lysate probes we might be able to improve the hybridization efficiency.

In case a negative control sample is missing, the positive sample could be taken and an excess of sense match added. This would block all target strands and only a few ones could bind to the assay due to competition.

To avoid dragging down the DNA/RNA during centrifugation, we could increase the salt concentration which favors the DNA/RNA to stay in solution. Protease could help to homogenize the cell lysate samples, which might reduce the viscosity and particles.

As ultimate assay the DNA/RNA detection could be combined with protein de-

Name (Ref. [43])	rno-miR-16 MIMAT0000785
Sequence	UAG CAG CAC GUA AAU AUU GGC G
Reverse complement 5' → 3'	CGC CAA TAT TTA CGT GCT GCT A
Name (Ref. [43])	rno-miR-192 MIMAT0000867
Sequence	CUG ACC UAU GAA UUG ACA GCC
Reverse complement 5' → 3'	GGC TGT CAA TTC ATA GGT CAG

Table 5.1: Table of miRNA sequences for further experiments.

tection on CLA. Few of the cantilevers could be used for the detection on genomic level and other for the e. g. corresponding proteins. Ideally such detection would be performed in a combined mode CLA instrument. The dynamic mode provides an interesting tool for protein research characterizing the intrinsic mechanics of biological receptors like ligand binding and conformational changes.

5.3.1 microRNA detection in rat plasma

The detection of miRNA biomarkers in plasma is an actual hot topic in pharmaceutical industry. Due to the promising results from the miR-122 detection in rat plasma for liver toxicity screening we will further investigate in that particular direction. Planned is the detection of miR-192, another Acetaminophen inducible microRNA and miR-16, a constitutive, not-regulated microRNA present at relatively high levels (see Tab. 5.1). Furthermore the experiments will be repeated to gain more information about reliability of the CLA assay.

5.4 SPR

In terms of signal response comparison of SPR versus CLA the following question raised: How many bound molecules (stated as mass/weight) are required to induce a cantilever deflection? Would this mass be theoretically visible on the Biacore? The answer to this question would give further clarity to the assays' efficacies. An idea would be to determine the actual amount of bound oligos on the CL. This would be possible by labeled probes or in dynamic mode (if sensitivity of dynamic mode is high enough). Due to the fact that the readout of labeled probes bound to a surface is much more difficult (higher error) than in solution, the bound probes could be stripped (by melting) from the surface and analyzed in solution.

To understand the basics behind the differences between SPR and CLA results and gain more fundamental information about the CLA response, further

investigations have to be carried out.
We expect the reason for the different assay properties in a non-linear behavior of the CL response, which has to be proven for example by comparing the slope of the early non-linear region of binding curves which do not go into saturation. An example for such recorded curves is given in Qavi *et al.* Fig. 3 a) Ref. [52].

Follow up experiments with concentration series of simple oligo hybridization on the SPR system led to further discussions and conclusions:

- The more repeated hybridization cycles were performed the more stable (less drift) the signal gets.
- Saturation was reached at 100 nM injected concentration (150 μl, 5 μl/min). Endpoint even though saturation was reached slightly less ($\sim$30 %) than after injecting a 1'000 nM sample.
- Below 50 nM concentration the significance gets vague (this does not refer to the experiments with focus on low concentrations where significant values down to 10 nM were achieved).
- Although the Biacore system is very robust and precise instrument errors such as liquid handling malfunctions occurred.
- We still observe a refractive index change during the injection of probes although the running and sample buffer were identical. A percentage of H_2O in the samples from the stock would lead to a negative signal. We observe a positive signal increase not correlating to the amount (per mill) of H_2O in the samples. A stabilizing agent in the DNA samples could be the reason and has to be discussed with the supplier (Microsynth).
- The influence of conformational changes of the biolayer during hybridization is unknown but might be existing. Tendencies towards negative signals during low concentration injection are an indication. This would lead to a cancellation of signal due to conformational change and mass adsorption. Contra this hypothesis is the size and distance of the biolayer. It is less than 10 nm and very close to the sensor surface and therefore in the strong regime of the evanescence field. Due to the fact that a surface propagating wave only has a TM mode only an influence on the polarisability of the TM mode would lead to a strong influence.
- The influence of bi-valent ions (magnesium and calcium) on the surface bound molecules is not well understood. They could interfere with the assay (changes of kinetics, respectively surface properties or act competitive). A HEPES buffer with NaCl could be an alternative to test the influence of bi-valent ions. For biological applications bi-valent ions cannot be excluded because most natural probes (cell lysates, serum) contain calcium.

Chapter 6

Acknowledgment

First of all I'd like to thank my supervisors Ulrich Certa, Christof Fattinger, Gregor Dernick, Martin Hegner and Ernst Meyer for enabling the project and guidance trough my work. Special thanks go to Martin and Ulli for initiating the project as well as Martin and Ernst for appraising this thesis.

I'd like to thank Martin Hegner's group at the Trinity College in Dublin for guidance in setting up and testing the instrument and for providing valuable data for reference measurements. I acknowledge Christof Fattinger and his team at F. Hoffmann-La Roche and Ernst Meyer, University of Basel, for their ideas, the construction and help for improvement of the instrumentation, Gregor Dernick, F. Hoffmann-La Roche, for his support in assay development, and Ulrich Certa and group at F. Hoffmann-La Roche, for support with the biological background.

I'm grateful for financial support from F. Hoffmann-La Roche Ltd. and like to thank Michael Hennig representatively as employer.

Great acknowledgments go to my coworkers:

Remo Hochstrasser, Roger Steiner, Dieter Voegelin and Jörg Völkle for instrumentation and support.

Michelle Gut for support with protein analysis, introduction to several lab techniques and bio "brain support".

Patrick Iaiza for support in liquid handling, DNA/RNA manipulation as well as introduction to everyday occurrences at Roche.

Cyrill Mangold for support with ordering supplies and introduction to everyday occurrences at Roche.
Stefan Obermüller for spotting the microarrays, many fruitful discussions and introduction to everyday occurrences at Roche.

Cristina Bertinetti-Lapatki for the introduction to miRNA and working on the miRNA detection in rat plasma project.

Laura Burleigh for proofreading several publications.

Susanne Fischer for the introduction into cell culturing, providing several probes and giving support with siRNA questions.

Nicholas Flint for helping with the Bioanalyzer and proofreading several publications.

Monika Haiker for support with the Bioanalyzer and Nimblegen consumables.

Tobias Heckel for many fruitful discussions about being a PhD.

Erich Küng for support with the RNA isolation and purification and asking many exciting math riddle keeping my brain in a good shape.

Morgane Ravon for cell culturing, support with cell culturing as well as providing reference data and probes.

Walter Huber, Josiane Kohler and Andrea Wiget for introduction and support with the Biacore SPR plus many discussions about the technology and results.

Karlheinz Baumann (Abeta project), Thomas Kremer (DCX project) and Sylwia Huber (CCR5 project) for collaboration with microfluidic immunoassay (MIA) projects.

Many thanks as well to all external collaboration partners:

Rohit Mishra (Trinity College Dublin) for the reference measurements and being my PhD buddy.

Wilfried Grange for providing the original NOSE LabVIEW software and introducing me into it.

Samuele Tosatti and the SuSoS team for the great collaboration for surface analysis and surface modification.

Michel Despont at IBM for providing the cantilever arrays and the gold coating.

Janos Vörös at the ETH for many fruitful discussions about biosensors and how to bring the comparison of SPR and CLA to a successful end.

Great thanks to Regina Mehlin (DT, F. Hoffmann-La Roche) and Germaine Weaver (IfP, University of Basel) for the administrative support.

Special thanks to Rachel Scott and Fredy Siegrist, my antessors, for being a good example to me and all the good times we had and hopefully will have in the future.

Gregor, Stefan, Cyrill, Michelle and Patrick, many thanks for the good times I experienced during my time in your group. Besides questions about assay development, biological topics and administrative stuff I enjoyed all the talks about delights and sorrows we shared.

Ulli and all members of the GCP team thanks for the fantastically dolfed gatherings.

Thanks to Andreas Wallnöfer to giving me confidence to start a PhD thesis.

Last but no least I'd like to give a big "thank you" to all the people behind my PhD life supporting me in good and bad times and without whom I would never achieved this:

Kasper, Lölli and Meret making my University time.

Jael, Lisa, Lolita, Philipp, Robi and Roland for being the "life" in "work-life balance" and your awesomeness.

And of course all the people I did not mentioned personally but playing an important role in my life.

Finally my greatest gratitude goes to my parents Antonia and Lambertus for providing the "good genes" as well as an outstanding education and offering the generous possibility to study and my sister, Birgit for everything a sister should be.

The most exciting phrase to hear in science, the one that heralds new discoveries, is not 'Eureka!' but 'That's funny'.

Isaac Asimov

Appendix A

Appendix: Material, Methods and Instrumentation

A.1 Assay development

Agilent Technologies

STRATAGENE
An Agilent Technologies Division

Lot 0006062237

Made in USA

Catalog Number	**740000**
Product Name	**Universal Human Reference RNA**
Quantity	Reference RNA, 2 tubes × 200 µg/tube RNase-free water, 1.5 ml
Certified By	Dana Faver
Quality Controlled By	Tricia Molina
Shipping Conditions	Shipped on dry ice.
Storage Conditions	Store the Universal Human Reference RNA at -80°C. Store the RNase-free water at -20°C.
Description	Stratagene Universal Human Reference RNA is composed of total RNA from 10 human cell lines. The reference RNA is designed to be used as a reference for microarray gene-profiling experiments. Since RNA species differ in abundance between cell lines, an ideal reference sample should represent these different RNAs. Equal quantities of DNase-treated total RNA from each cell line were pooled to make the Universal Human Reference RNA. This Universal Reference RNA is suitable for microarray experiments. We also supply a QPCR Human Reference Total RNA, suitable for QRT-PCR, which has undergone further DNase treatment. **Cell Line Derivations** Adenocarcinoma, mammary gland Hepatoblastoma, liver Adenocarcinoma, cervix Embryonal carcinoma, testis Glioblastoma, brain Melanoma Liposarcoma Histiocytic lymphoma; macrophage; histocyte Lymphoblastic leukemia; T lymphoblast Plasmacytoma; myeloma; B lymphocyte
Test Conditions	The quality of the Universal Human Reference RNA is assessed by observing distinct 28S and 18S ribosomal bands on a 1% MOPS agarose gel under denaturing conditions. The purity of the RNA is assessed by spectrophotometry (A260/A280≥1.8). The RNA is then shown to be free of contaminating RNases by incubation in a suitable buffer at 37°C followed by gel analysis against known RNAse-free controls. The RNA is further tested functionally by synthesizing labeled cDNA, which is then hybridized to a microarray to examine gene representation and coverage.
Additional Materials Required	RNase-free 70% Ethanol
Instructions for Use	Universal Human Reference RNA is provided in a solution of 70% ethanol and 0.1 M sodium acetate. Prepare the Reference RNA for use as follows: 1. Centrifuge the tube at 12,000 × g for 15 minutes at 4°C. 2. Carefully remove the supernatant. 3. Wash the pellet in 70% ethanol. 4. Centrifuge the tube at 12,000 × g for 15 minutes at 4°C. 5. Carefully remove the supernatant and air-dry the pellet at room temperature for 30 minutes to remove retained ethanol. 6. Resuspend the pellet in RNase-free water to the desired concentration. Proceed with the preparation of labeled cDNA and interrogate the arrays according to the manufacturer's instructions.
Limited Product Warranty	This warranty limits our liability to replacement of this product. No other warranties of any kind, express or implied, including, without limitation, implied warranties of merchantability or fitness for a particular purpose, are provided by Stratagene. Stratagene shall have no liability for any direct, indirect, consequential, or incidental damages arising out of the use, the results of use, or the inability to use this product.

For in vitro use only. This certificate is a declaration of analysis at the time of manufacture.

Stratagene Products

In Vitro Use Only

Stratagene US & Canada
Order: 800-424-5444 x3
Technical Service: 800-894-1304 x2

Stratagene Europe
For Orders and Technical Assistance, please visit www.stratagene.com/contacts

Stratagene Japan K.K.
Order: 0120-477-111
Technical Service: 0120-477-111

http://sysbio.harvard.edu/csb/resources/downloads/Bauer_Core_GeneChip_Fragmentation_Protocol.doc

Bauer Core Standard Protocol		
Title: Fragmentation of cRNA for Affymetrix GeneChips		
Pages: 2	Revision:	Date: August 26, 2003
Author(s): Jennifer A. Couget	Reviewers: Shufen Meng	
Contact: affyinfo@cgr.harvard.edu	Comment:	

1. Purpose
This protocol describes the fragmentation procedure of cRNA for Target Cocktail Hybridization of Affymetrix GeneChips.

2. Materials
5X Fragmentation Buffer (stored at room temperature)
DEPC-water
Labeled cRNA
0.65 ml RNase-free tubes to prevent evaporation

3. Instrumentation
To maintain proper fragmentation temperature, using a Thermal Cycler is recommended, but not required.

4. Reagent preparation
5X Fragmentation Buffer may be bought as part of the Affymetrix GeneChip Clean-up Module (Affymetrix, p/n 900371)

5X Fragmentation Buffer

200mM Tris-acetate, pH 8.1, 500 mM KOAc, 150 mM MgOAc

1M Tris acetate pH 8.1	*4 ml*
MgOAc	*0.64 g*
KOAc	*0.98 g*
DEPC-water	*to 20 ml*

Mix thoroughly and filter through a 0.2 µm vacuum filter. Aliquot and store at room temperature.

5. Procedure

5.1 *It is usually best to perform the fragmentation on the same day as hybridization whenever possible to minimize freeze-thawing effects on cRNA.*

5.2 *Quantify cRNA concentration and A_{260}/A_{280} ratio. cRNA must be at a minimum concentration of 0.6 µg/µl. If it is not, concentrate under vacuum without heat. A_{260}/A_{280} ratio should be between 1.9 and 2.1.*

5.3 *Use 2 µl of 5X Fragmentation Buffer for every 8 µl of cRNA plus water together (ratio is 2:8). In addition, the cRNA final concentration in the fragmentation reaction must be no less than 0.5 µg/µl.*

5.4 *We recommend fragmenting 20 µg of cRNA in a 40-µl fragmentation reaction.*

5.5 *For example, cRNA with a concentration of 1 µg/µl:*

cRNA (1 µg/µl)	*20 µl*	*Final concentration 0.5µg/µl*
DEPC-water	*12 µl*	
5X Fragmentation Buffer	*8 µl*	*Final concentration 1X*
Total Volume	*40 µl*	

5X Fragmentation Buffer 8 µl: cRNA plus water 32µl
ratio is 2:8

5.6 *Incubate at 94 ℃ for 35 minutes. Cool to 4℃ and place on ice.*

5.7 *Check quality of cRNA by Agilent Bioanalyzer using mRNA Smear Nano Assay.*

5.8 *Run 100 ng of unfragmented cRNA side-by-side with 1 µl fragmented undiluted cRNA directly from fragmentation reaction.*

5.9 *Assay should reveal long unfragmented cRNAs, majority greater than 400 bp and fragmented cRNAs ideally between 35 and 200 bp.*

5.10 *Use all remaining fragmented cRNA in target hybridization cocktail immediately.*

5.11 *Store fragmented cRNA at –20 ℃ short-term for immediate future hybridization.*

5.12 *Store unfragmented cRNA and extra fragmentation reactions at -80 ℃ long-term.*

A.2 CLA Instrumentation

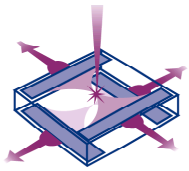

SiTek® ELECTRO OPTICS

Data sheet
1L10-10-A_SU15

Active area: 10,0 x 10,0 mm²
Chip area: 12,2 x 12,0 mm²

Characteristics	Min.	Typ.	Max.	Unit
Position non-linearity		0,2	0,5	% (±)
Detector resistance	3,7	4,0	4,8	kΩ
Leakage current		100	800	nA
Noise current		3,0	4,0	pA/√Hz
Responsivity		0,68		A/W
Capacitance		80	100	pF
Rise time (10%-90%)		60	110	ns
Bias voltage (reverse)	5	15	30	V
Thermal drift		20	100	ppm/°C
Saturation density	100			kW/m²
Maximum ratings				
Reverse voltage			30	V
Operating temperature			70	°C
Storage temperature			100	°C

Test conditions: Room temperature 23 °C, bias voltage 15V, light source wavelength 940 nm. Position non-linearity and thermal drift are valid within 80 % of the detector length.

Package: Ceramic package, 25,0 x 21,0 mm², with solderable pins and protective window.

Registration no.	Part no.	Written by:	Date.
S1-0204-D_A	S1-0204	Anders Lundgren	2002-10-22

NEMESYS® DOSING UNIT

High Precision Syringe Pump

Features

The dosing module is a pulsation-free dosing unit for high-precision dosing of fluid streams in the range of microlitres and nanolitres. Connect up to 12 of these modules to a BASE-module.

Mechanical Data

Weight ..... 1,3 kg
Dimensions (L x W x H) ..... 310 x 47 x 56 mm

Electrical Data

Power Supply Voltage ..... 24 VDC
Dosing Unit Current typical at 24 VDC ..... 0,3 A
Dosing Unit Current peak at 24 VDC ..... 0,6 A

Environment

Operating Temperature ..... 0°C to 45°C
Storage Temperature ..... -40°C to 75°C
Operating Humidity ..... 20% to 80%, non-condens.
Storage Humidity ..... 20% to 80%, non-condens.

Interfaces

CAN ..... max. 1 Mbit / s
RS-232 ..... max. 115200 bit/s

Configuration

Gear ..... 14,1 (optional 1 / 23,7 / 29,2)
Syringes outer diameter ..... 6 to 30 mm
Syringes stroke ..... 62 mm

Valve

Body material ..... PEEK
Seal material ..... FFPM (EPDM, FPM)
Temperature media ..... 10 to +40°C
Viscosity ..... max. 20 mm^2/s
Internal Volume ..... < 13 µl
Orifice ..... DN 0.6 mm or 1,35 mm
Port connection ..... Flange, UNF 1/4"-28

Dosing Performance

Gear	1,0	14,1*	23,7	29,2
Pusher Velocity min (nm/s)	383,333	**27,259**	16,190	13,146
Pusher Velocity max (mm/s)	89,000	**6,329**	3,759	3,052
Pusher Force max. (N)	40	**390**	660	815
Syringe 0,5 µl / 60 mm stroke				
Flow Rate min (pl/min)	191,667	**13,630**	8,095	6,573
Flow Rate max (µl/min)	44,500	**3,164**	1,879	1,526
Dosing Vol. min (pl) = 1 step	4,100	**0,289**	0,172	0,140
Syringe 100 µl / 60 mm stroke				
Flow Rate min (nl/min)	38,333	**2,726**	1,619	1,315
Flow Rate max (ml/min)	8,900	**0,633**	0,376	0,305
Dosing Vol. min (pl) = 1 step	8,138	**0,579**	0,344	0,279
Syringe 2,5 ml / 60 mm stroke				
Flow Rate min (µl/min)	0,958	**0,068**	0,040	0,033
Flow Rate max (ml/min)	222,500	**15,822**	9,397	7,630
Dosing Vol. min (pl) = 1 step	203,450	**14,468**	8,593	6,977
Syringe 25 ml / 60 mm stroke				
Flow Rate min (µl/min)	9,583	**0,681**	0,405	0,329
Flow Rate max (ml/min)	2225,000	**158,222**	93,973	76,303
Flow Rate min (µl/min)	9,583	**0,681**	0,405	0,329

*standard configuration

Valve options

Orifice	Working Pressure (max)	Materials
DN 0.60 mm*	**3 bar**	**FFPM** / EPDM / FPM
DN 1.35 mm	1 bar	FFPM / EPDM / FPM

*standard configuration

Mechanical Drawing

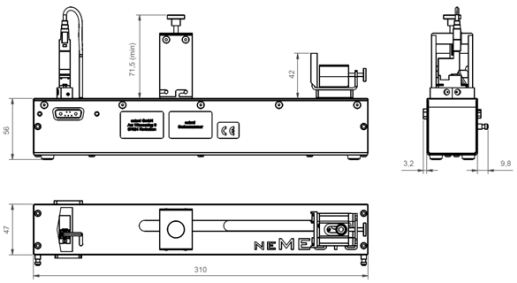

04.12.2009

cetoni GmbH
Am Wiesenring 6
07554 Korbussen
Germany

Phone: +49 36602 338 0
Fax: +49 36602 338 11
Email: info@cetoni.de
www.cetoni.de

AI Absolute Accuracy Table

Nominal Range		Residual Gain Error (ppm of Reading)	Gain Tempco (ppm/°C)	Reference Tempco	Residual Offset Error (ppm of Range)	Offset Tempco (ppm of Range/°C)	INLError (ppm of Range)	Random Noise, σ (μVrms)	Absolute Accuracy at Full Scale[1] (μV)	Sensitivity[2] (μV)
Positive Full Scale	Negative Full Scale									
10	–10	75	25	5	20	57	76	244	3,100	97.6
5	–5	85	25	5	20	60	76	122	1,620	48.8
1	–1	95	25	5	25	79	76	30	360	12.0
0.2	–0.2	135	25	5	80	175	76	13	112	5.2

AbsoluteAccuracy = Reading · (GainError) + Range · (OffsetError) + NoiseUncertainty

GainError = ResidualAIGainError + GainTempco · (TempChangeFromLastInternalCal) + ReferenceTempco · (TempChangeFromLastExternalCal)

OffsetError = ResidualAIOffsetError + OffsetTempco · (TempChangeFromLastInternalCal) + INL_Error

$$NoiseUncertainty = \frac{RandomNoise \cdot 3}{\sqrt{100}}$$ For a coverage factor of 3 σ and averaging 100 points.

[1] Absolute accuracy at full scale on the analog input channels is determined using the following assumptions:

TempChangeFromLastExternalCal = 10 °C

TempChangeFromLastInternalCal = 1 °C

number_of_readings = 100

CoverageFactor = 3 σ

For example, on the 10 V range, the absolute accuracy at full scale is as follows:

GainError = 75 ppm + 25 ppm · 1 + 5 ppm · 10 GainError = 150 ppm

OffsetError = 20 ppm + 57 ppm · 1 + 76 ppm OffsetError = 153 ppm

$$NoiseUncertainty = \frac{244\ \mu V \cdot 3}{\sqrt{100}}$$ NoiseUncertainty = 73 μV

AbsoluteAccuracy = 10 V · (GainError) + 10 V · (OffsetError) + NoiseUncertainty AbsoluteAccuracy = 3,100 μV

[2] Sensitivity is the smallest voltage change that can be detected. It is a function of noise.

Accuracies listed are valid for up to one year from the device external calibration.

A.2.1 LabVIEW connections

Signal Name	Signal Type	NI-Channel	NI-Connector	Rack Connector	Rack Wire
PSD SUM+	AI	0	68	15ab	W2 gn
PSD DIFF+	AI	1	33	17ab	W2 bn
Temp. U-Ref.	AI	2	65	19ab	W1 ws
Temp. Room	AI	3	30	20ab	W1 bn
Temp. Box	AI	4	28	21ab	W1 gn
Temp. Chamber	AI	5	60	22ab	W1 gb
BNC In	AI	6	25	-	W3 bn
PSD SUM-	AI	8	34	16ab	W2 gb
PSD DIFF-	AI	9	66	18ab	W2 ws
PSD GND	AI GND	-	67	-	W2 shield
Temp. GND	AI GND	-	59	-	W1 bu
BNC In GND	AI GND	-	27	-	W3 ws
Laser Sel. A0	DI	P0.0	52	27/28ab	W3 ws
Laser Sel. A1	DI	P0.1	17	29/30ab	W3 bn
Laser Sel. A2	DI	P0.2	49	31/32ab	W3 gn
Laser Enable	DI	P0.3	47	25/26ab	W3 gb
Chamber Peltier Enable	DI	P0.4	19	23/24ab	W4 ws
Laser GND	D GND	-	15	-	W3 ra
Chamber Peltier GND	D GND	-	18	-	W4 bn

Table A.1: CLA instrument's electronic signal connections.

Appendix B

Appendix: Results

B.1 Assay development

Experiment on January 05, 2010

Objective Compare the mixing efficiency of shaker MixMate from Eppendorf with the BioShake iQ from Quantifoil Instruments in 96 and 384 well plates

material
MixMate shaker form Eppendorf (mixing radius 1.5 mm)
BioShake iQ from Quantifoil Instruments (mixing radius 1 mm)
Eppendorf 96/500ul deepwell plate Prot LoBind PCR clean, #0030 504.119
Eppendorf 384/200 µl deepwell plate DNA LoBind, #0030 523.130
Costar 384 PS clear plate, flat bottom # 3702
Bromophenol blue solution in 10% glycerol / water.
1 X PBS solution

protocol The different volumes of PBS are first pipetted in the wells, for each volume 5 wells are used. Then 10 µl of BPB soln are pipetted very carefully in the bottom of the well, so as the colored layer is well separated from the PBS solution.

The plate is inserted and shacked.
The rating is done visually after the given time.

Plate 96 deepwell 500ul Eppendorf, #0030 504.119

IQ Instruments BioShake iQ at 1000 rpm

Dilution (ml)		Time (min)									
Buffer	Dye sol	0.5	1	2	3	4	5		1*		
50	10	2	2	2	2	2	2		2		
100	10	2	2	2	2	2	2		2		
200	10	2	2	2	2	2	2		2		
300	10	1	1	2	2	2	2		2		
400	10	1	1	1	2	2	2		2		

Eppendorf MixMate at 1000 rpm

Dilution (ml)		Time (min)									
Buffer	Dye sol	0.5	1	2	3	4	5		1*		
50	10	2	2	2	2	2	2		2		
100	10	2	2	2	2	2	2		2		
200	10	2	2	2	2	2	2		2		
300	10	2	2	2	2	2	2		2		
400	10	2	2	2	2	2	2		2		

* at 1400 rpm with new sample

SCORING

0 not mixed **1** not complete **2** mixed

Plate 384 well flat bottom Costar # 3702

IQ Instruments BioShake iQ at 2000 rpm

Dilution (ml)		Time (min)									
Buffer	Dye sol	1	2	3	4	5	10	15	16*	20*	21**
20	10	1	2	2	2	2	2	2	2	2	2
40	10	0	0	1	1	1	1	1	2	2	2
60	10	0	0	0	0	1	1	1	2	2	2
80	10	0	0	0	0	0	0	0	1	1	2

Eppendorf MixMate at 2000 rpm

Dilution (ml)		Time (min)									
Buffer	Dye sol	1	2	3	4	5	10	15	16*	20*	21**
20	10	2	2	2	2	2	2	2	2	2	2
40	10	2	2	2	2	2	2	2	2	2	2
60	10	1	2	2	2	2	2	2	2	2	2
80	10	1	1	1	1	1	2	2	2	2	2

* at 2200 rpm (+ 1 min increments)
** at 2400 rpm (+ 1 min increments)

SCORING

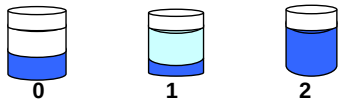

0 not mixed **1** not complete **2** mixed

Plate 384 deepwell 200ul Eppendorf, #0030 523.130

IQ Instruments BioShake iQ at 2000 rpm

Dilution (ml)		Time (min)									
Buffer	Dye sol	1	2	3	4	5	10	15	16*	20*	21**
25	10	2	2	2	2	2	2	2	2	2	2
50	10	1	1	1	1	1	1	2	2	2	2
100	10	0	0	0	0	1	1	1	1	1	2
150	10	0	0	0	0	0	1	1	1	1	1

finally managed to complete mix
at 2600 rpm for 1 min

Eppendorf MixMate at 2000 rpm

Dilution (ml)		Time (min)									
Buffer	Dye sol	1	2	3	4	5	10	15	16*	20*	21**
25	10	2	2	2	2	2	2	2	2	2	2
50	10	2	2	2	2	2	2	2	2	2	2
100	10	1	1	1	1	1	1	2	2	2	2
150	10	0	0	0	0	1	1	1	1	1	2

* at 2200 rpm (+ 1 min increments)
** at 2400 rpm (+ 1 min increments)

SCORING

0 not mixed **1** not complete **2** mixed

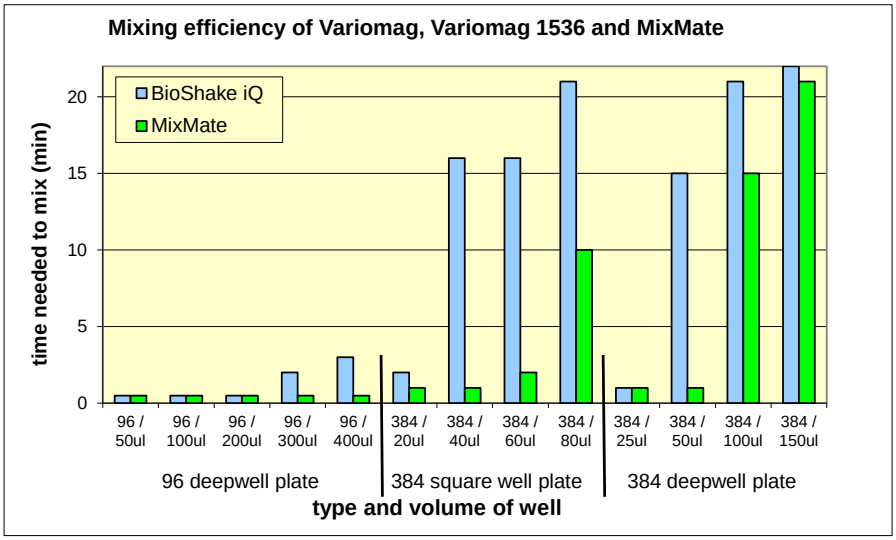
Mixing efficiency of Variomag, Variomag 1536 and MixMate
BioShake iQ
MixMate
time needed to mix (min)
0
5
10
15
20
96 / 50ul
96 / 100ul
96 / 200ul
96 / 300ul
96 / 400ul
384 / 20ul
384 / 40ul
384 / 60ul
384 / 80ul
384 / 25ul
384 / 50ul
384 / 100ul
384 / 150ul
96 deepwell plate
384 square well plate
384 deepwell plate
type and volume of well

SuSoS

Results

Table 1: 'As received' cantilever, normalized At.-% of all components

Ref No.	Description	C-C	C=O	CON	O 1s A	O 1s B	O 1s C	Si 2p A	Si 2p B	N 1s	F 1s	Au 4f	P 2p
1	Tube 10 As Rec Si Side Array 5 Position 1	20.8	3.2	1.2	6.7	63.2	0.0	0.9	0.8	2.3	0.0	1.0	0.0
2	Tube 10 As Rec Si Side Array 5 Position 2	20.8	2.5	1.5	6.6	64.7	0.0	0.9	0.9	1.1	0.0	1.1	0.0
3	Tube 9 As Rec Si Side Array 5 Position 1	21.3	1.7	0.7	5.6	66.8	0.0	0.9	0.9	0.4	0.0	1.7	0.0
4	Tube 9 As Rec Si Side Array 5 Position 2	21.1	2.4	0.6	5.9	64.8	0.0	0.9	0.8	1.4	0.0	2.1	0.0
5	Tube 9 As Rec Si Side Array 5 Position 3	22.3	2.9	1.9	6.6	61.4	0.0	0.8	0.8	1.1	0.0	2.2	0.0
6	Tube 10 As Rec Si Side Array 4	20.8	3.4	1.7	5.9	64.8	0.0	1.0	0.8	0.7	0.0	0.9	0.0
7	Tube 9 As Rec Si Side Array 3 Position 1	21.5	2.5	1.3	5.1	63.7	0.1	1.0	0.8	2.5	0.0	1.6	0.0
8	Tube 10 As Rec Si Side Array 3	28.3	3.8	3.3	6.5	52.2	0.0	0.7	0.6	2.3	0.0	2.2	0.0
9	Tube 9 As Rec Si Side Array 4 Position 1	20.6	2.8	2.1	4.7	66.9	0.0	0.9	0.8	0.1	0.0	0.9	0.0

Table 2: Example PVP coated cantilevers (ref. 10-13) and treated coated cantilevers received from Roche, normalized At.-% of all components.

Ref No.	Chip	Description	C-C	C=O	CON	O 1s A	O 1s B	O 1s C	Si 2p A	Si 2p B	N 1s	F 1s	Au 4f	P 2p
10		Tube 10 Only thiol Coated Au Side Array 1 Position 1	45.3	6.0	3.2	9.3	18.2	0.6	0.1	0.0	3.9	0.1	13.3	0.0
11		Tube 10 PVP Coated Au Side Array 4 Position 1	33.0	7.0	3.9	17.8	28.3	4.8	0.0	0.0	2.7	1.6	0.8	0.0
12		Tube 10 PVP Coated Si Side Array 4 Position 1	35.0	20.6	10.8	19.8	5.2	0.4	0.0	0.0	8.2	0.0	0.0	0.0
13	B17	Tube 11 PVP UVO Oligo Si Side Array 3	34.4	10.9	4.8	13.6	27.8	0.0	0.1	0.1	4.3	1.4	0.1	2.4
14	I14	Tube 11 No PVP UVO Oligo Si Side Array 4	21.5	4.4	1.3	4.8	61.3	0.0	0.9	0.8	1.4	0.2	0.8	2.6
15	B18	Tube 11 No PVP UVO Au Side Array 1	29.1	5.8	3.5	1.5	15.7	1.5	0.1	0.1	2.3	0.0	37.4	2.9
16	C11	Tube 11 PVP UVO Au Side Array 2	31.3	2.1	2.3	7.3	31.1	7.0	0.0	0.1	2.5	3.4	12.9	0.0
17	B17	Tube 11 PVP UVO Oligo Au Side Array 3	27.3	11.7	4.1	5.9	25.4	8.1	0.1	0.0	5.7	2.3	7.6	1.7
18	I14	Tube 11 No PVP UVO Oligo Au Side Array 4	34.0	8.8	4.8	2.0	14.6	0.3	0.2	0.1	3.2	0.0	32.0	0.0

SuSoS

Table 3: Treated uncoated cantilevers received and SPR chips from Roche, normalized At.-% of all components.

Ref No.	Chip	Description	C-C	C=O	CON	O 1s A	O 1s B	O 1s C	Si 2p A	Si 2p B	N 1s	F 1s	Au 4f	P 2p
19	SPRPN052	SPR Chip 1	40.7	6.4	2.2	0.4	7.7	0.0	0.1	0.0	0.8	0.0	40.6	1.1
20	SPRPN044	SPR Chip 2	20.3	4.5	1.1	3.8	8.7	0.5	0.2	0.1	0.8	0.6	58.6	1.0
21	SPRPN042	SPR Chip 3	37.8	8.5	2.6	0.5	7.3	0.0	0.1	0.0	0.8	0.0	41.8	0.4
22	SPRPM043	SPR Chip 4	21.7	9.9	4.2	4.4	10.1	0.0	0.3	0.0	6.2	0.1	41.7	1.4
23	CLAPN039	Tube 4 Au Side	25.6	10.7	4.6	1.2	16.2	0.0	0.2	0.0	5.9	0.0	35.6	0.0

B.2 CLA Instrumentation

B.2.1 Fluidics

Fluid	H_2O 20 °C	H_2O 20 °C
Flow rate	0.001 l/min $\equiv$ 1'000 μL/min	0.001 l/min $\equiv$ 1'000 μL/min
Density	998.206 kg/m^3	998.206 kg/m^3
Dynamic viscosity	1001.61×10^6 kg/ms	$1'001.61 \times 10^6$ kg/ms
Tubing shape	circular tube	circular tube
Tubing dimensions	d: 0.03 in, l: 1 m	d: 0.0015 in, l: 1 m
Flow speed	0.04 m/s	0.15 m/s
Reynolds number	28	56
Flow	laminar	laminar
Tubing roughness	0 mm	0 mm
Tubing friction coefficient	2.31	1.15
Zeta value	3026.21	3026.21
Pressure loss	20.17 mbar	322.78 mbar

Table B.1: Calculation of pressure loss over tube distance for tubing diameter of 0.03 in which corresponds to the actual tubing dimension and 0.015 in. A flow speed of $\sim$150 μL/min has been approved by M. Hegner to be a feasible value for proper liquid exchange in the chamber.

Halar	**PEEK**	**Teflon**
$25 \frac{cc}{100\,in^2} \cdot 24\,h \cdot \frac{atm}{mil}$ @ 24 °C	$14 \frac{cc}{100\,in^2} \cdot 24\,h \cdot \frac{atm}{mil}$ @ 24 °C	$800 \frac{cc}{100\,in^2} \cdot 24\,h \cdot \frac{atm}{mil}$ @ 24 °C

Table B.2: Gas permeability values for Halar, PEEK and Teflon tubing from Upchurch Scientific, respectively Ercatech.

B.2.2 Optical Fibers

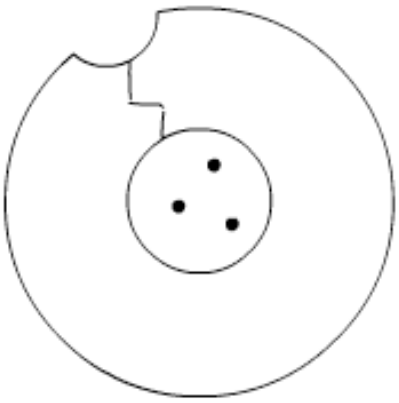

Figure B.1: A cross-section of a bad cleavage site with dirt on the core and some cracks in the cladding. Such a fiber can not be used for proper light guiding. Damages can be detected by observing the light projection and investigating the fiber-ends with some optical magnification tools like a binocular.

27.04.2010 Pigtail laser projection on wall

Mounted lasers in optical setup to check the array linearity and laser spot quality.

A

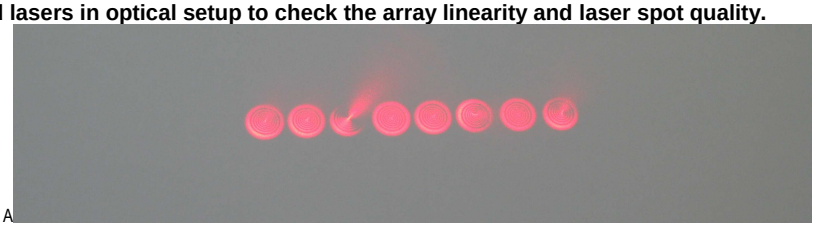

Date	Image	Laser	Lens I	Lens I Orientation	Lens II	Lens II Orientation
27.04.2010	IMG_0408.JPG	8x	Planoconvex f50	Laser -> |)		

B

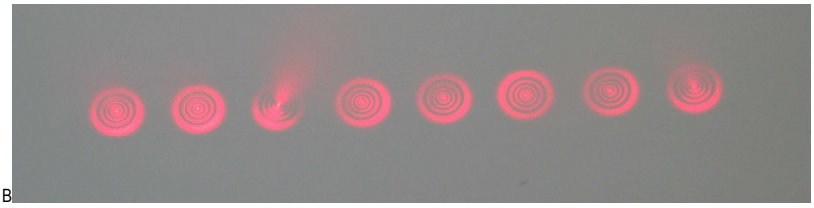

Date	Image	Laser	Lens I	Lens I Orientation	Lens II	Lens II Orientation
27.04.2010	IMG_0409.JPG	8x	Bestform f25 MellesGriot	Laser -> (|		

C

Date	Image	Laser	Lens I	Lens I Orientation	Lens II	Lens II Orientation
27.04.2010	IMG_0410.JPG	8x	Bestform f25 MellesGriot	Laser -> (|	Plano-conv. f50	Laser -> |)

D

Date	Image	Laser	Lens I	Lens I Orientation	Lens II	Lens II Orientation
27.04.2010	IMG_0411.JPG	8x	Bestform f25 MellesGriot	Laser -> |)	Plano-conv. f50	Laser -> |)

E

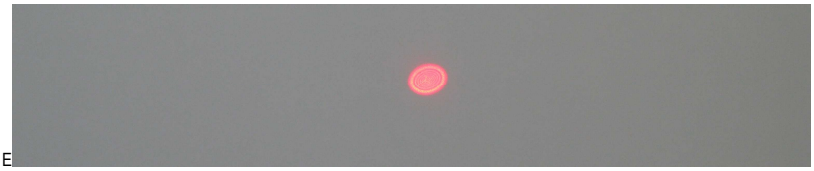

Date	Image	Laser	Lens I	Lens I Orientation	Lens II	Lens II Orientation
27.04.2010	IMG_0412.JPG	FC	Planoconvex f50	Laser -> |)		

- No major differences between lenses and setups. (B) leads to best result and will therefore be used in the final setup.
- Laser spot quality is not sufficient for application. Fibers have to be stripped and cleaved newly.

B.2.3 Beam waist calculation

The spot size can be calculated theoretically from the beam waist and wavelength of the laser light as explained in Fig. B.2 and equations B.1, B.2.

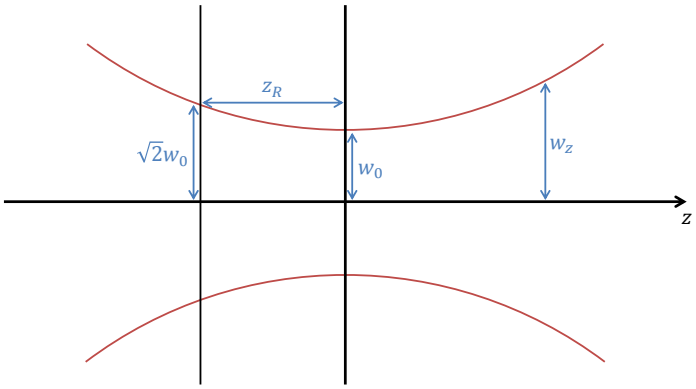

Figure B.2: Schematic drawing of laser light beam shape with w_0: beam waist, w_z: spotsize at z.

Beam waist calculation:

$$w(z) = w_0 \times \sqrt{1 + \left(\frac{z}{z_R}\right)^2} \tag{B.1}$$

$$z_R = \frac{\pi \times {w_0}^2}{\lambda} \tag{B.2}$$

B.3 Surface Plasmon Resonance Technology

SPR is the gold standard for quantification of surface occupancy by biological interactions. Goal was to gain an additional knowledge for the CLA technology as well as referencing the CLA in terms of sensitivity and specificity.
To get an impression how the SPR signal is acquired, we recorded the reflection versus incidence angle (Fig. B.3) on a very basic and fully accessible experimental device (Francis Mueller, F. Hoffmann-La Roche, Ltd., Switzerland) with Kretschmann configuration. As sample we had chosen a Au metallic layer (44 nm) towards ambient air. Starting at a small angle, a slight increase in reflection can be observed until the critical angle of the total reflection Θ_{crit} is reached. In an optimal case, where the Au layer has perfect dimensions, the resonance angle Θ_{SP} can be zero [16]. The reflection increases again after leaving the resonance conditions at higher angles.

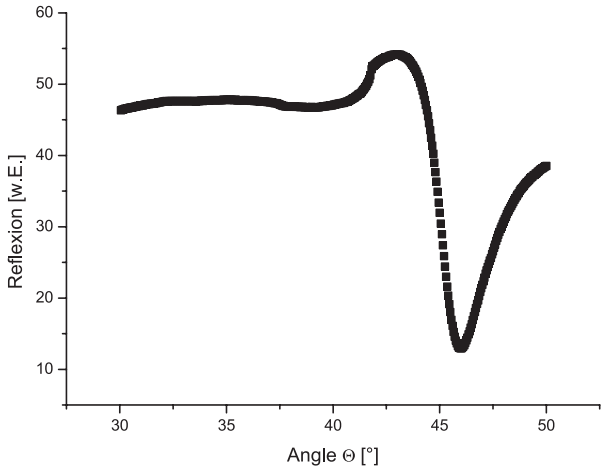

Figure B.3: Recorded signal of reflection versus incidence angle measured with a basic SPR device on a 44 nm Au metallic layer towards air.

B.4 Biological Application

B.4.1 NaOH chip regeneration

We observed a very unstable sum and averaged differential signal after injecting NaOH. The strong pH from the NaOH (pH 14) might be too harsh for the cantilever. Many unknown effects might occur on the chip and biolayer and it might be possible that the chamber is not fully washed with the chosen settings or equilibration times were not reached.
NaOH regeneration is not favored which was additionally proven in Biacore experiments (results not shown). Very high fluctuations and suspicious effects (loss of signal and long equilibration times) were induced. Urea for chip regeneration was therefore favored although the signals intensities were promisingly high and above all expectations with NaOH (see Fig. 3.34). A shorter incubation phase plus prolonged or repeated wash phase during NaOH regeneration might solve the problem.

B.4.2 Bioanalyzer Data

2100 expert_Eukaryote Total RNA Nano_DE24802247_2010-09-01_09-24-18.xad Page 1 of 11

Assay Class: Eukaryote Total RNA Nano
Data Path: C:\...Eukaryote Total RNA Nano_DE24802247_2010-09-01_09-24-18.xad

Created: 01.09.2010 09:24:18
Modified: 01.09.2010 09:40:03

Electrophoresis File Run Summary

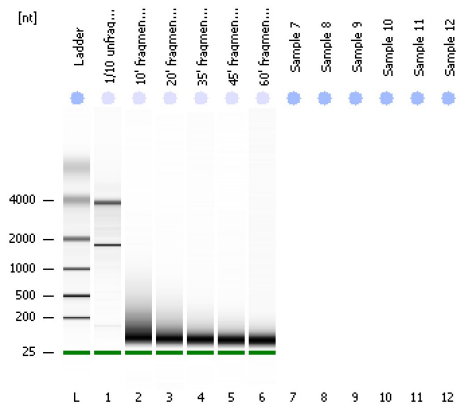

Instrument Information:
Instrument Name: DE24802247 Firmware: C.01.069
Serial#: DE24802247 Type: G2938B

Assay Information:
Assay Origin Path: C:\Program Files\Agilent\2100 bioanalyzer\2100 expert\assays\RNA\Eukaryote Total RNA Nano Series II.xsy
Assay Class: Eukaryote Total RNA Nano
Version: 2.6
Assay Comments: Total RNA Analysis ng sensitivity (Eukaryote)

© Copyright 2003 - 2009 Agilent Technologies, Inc.

Chip Information:
Chip Lot #:
Reagent Kit Lot #:
Chip Comments:

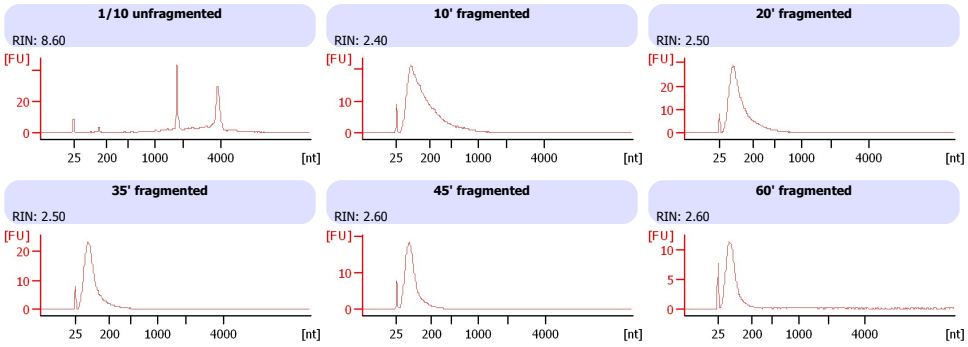

 © Copyright 2003 - 2009 Agilent Technologies, Inc. Printed: 01.09.2010 09:42:04

2100 expert_Eukaryote Total RNA Nano_DE24802247_2010-09-01_09-24-18.xad Page 2 of 11

Assay Class: Eukaryote Total RNA Nano Created: 01.09.2010 09:24:18
Data Path: C:\...Eukaryote Total RNA Nano_DE24802247_2010-09-01_09-24-18.xad Modified: 01.09.2010 09:40:03

Electrophoresis File Run Summary (Chip Summary)

Sample Name	Sample Comment	Status	Result Label	Result Color
1/10 unfragmented		✔	RIN: 8.60	
10' fragmented		✔	RIN: 2.40	
20' fragmented		✔	RIN: 2.50	
35' fragmented		✔	RIN: 2.50	
45' fragmented		✔	RIN: 2.60	
60' fragmented		✔	RIN: 2.60	
Sample 7				
Sample 8				
Sample 9				
Sample 10				
Sample 11				
Sample 12				

Chip Lot # **Reagent Kit Lot #**

Chip Comments :

2100 Expert (B.02.07.SI532) © Copyright 2003 - 2009 Agilent Technologies, Inc. Printed: 01.09.2010 09:42:04

Assay Class:	Eukaryote Total RNA Nano	Created:	01.09.2010 09:24:18
Data Path:	C:\...Eukaryote Total RNA Nano_DE24802247_2010-09-01_09-24-18.xad	Modified:	01.09.2010 09:40:03

Electrophoresis Assay Details

General Analysis Settings

Number of Available Sample and Ladder Wells (Max.) : 13
Minimum Visible Range [s] : 17
Maximum Visible Range [s] : 70
Start Analysis Time Range [s] : 19
End Analysis Time Range [s] : 69
Ladder Concentration [ng/µl] : 150
Lower Marker Concentration [ng/µl] : 0
Upper Marker Concentration [ng/µl] : 0
Used Lower Marker for Quantitation
Standard Curve Fit is Logarithmic
Show Data Aligned to Lower Marker

Integrator Settings

Integration Start Time [s] : 19
Integration End Time [s] : 69
Slope Threshold : 0.6
Height Threshold [FU] : 0.5
Area Threshold : 0.2
Width Threshold [s] : 0.5
Baseline Plateau [s] : 6

Filter Settings

Filter Width [s] : 0.5
Polynomial Order : 4

Ladder

Ladder Peak	Size
1	25
2	200
3	500
4	1000
5	2000
6	4000

 © Copyright 2003 - 2009 Agilent Technologies, Inc.

2100 expert_Eukaryote Total RNA Nano_DE24802247_2010-09-01_09-24-18.xad Page 4 of 11

Assay Class: Eukaryote Total RNA Nano
Data Path: C:\...Eukaryote Total RNA Nano_DE24802247_2010-09-01_09-24-18.xad

Created: 01.09.2010 09:24:18
Modified: 01.09.2010 09:40:03

Electropherogram Summary

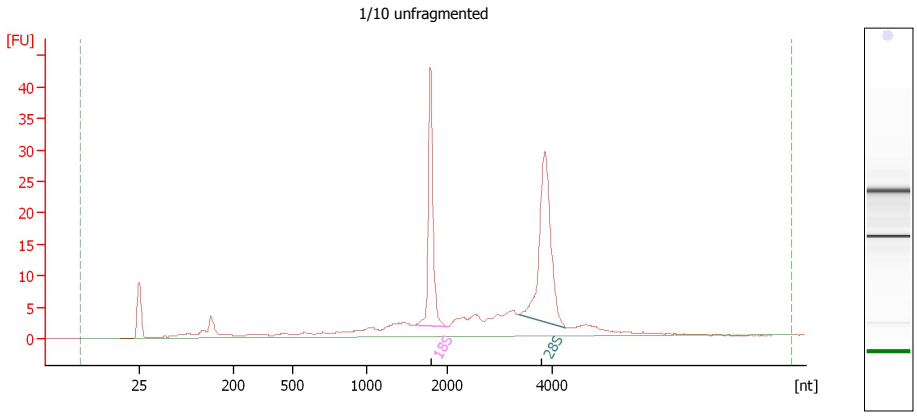

Overall Results for sample 1 : 1/10 unfragmented

RNA Area:	199.6	RNA Integrity Number (RIN):	8.6 (B.02.07)
RNA Concentration:	151 ng/µl	Result Flagging Color:	
rRNA Ratio [28s / 18s]:	1.3	Result Flagging Label:	RIN: 8.60

Fragment table for sample 1 : 1/10 unfragmented

Name	Start Size [nt]	End Size [nt]	Area	% of total Area
18S	1'583	2'018	37.0	18.5
28S	3'372	4'247	47.8	24.0

2100 Expert (B.02.07.SI532) © Copyright 2003 - 2009 Agilent Technologies, Inc. Printed: 01.09.2010 09:42:04

2100 expert_Eukaryote Total RNA Nano_DE24802247_2010-09-01_09-24-18.xad Page 5 of 11

Assay Class: Eukaryote Total RNA Nano Created: 01.09.2010 09:24:18
Data Path: C:\...Eukaryote Total RNA Nano_DE24802247_2010-09-01_09-24-18.xad Modified: 01.09.2010 09:40:03

Electropherogram Summary Continued ...

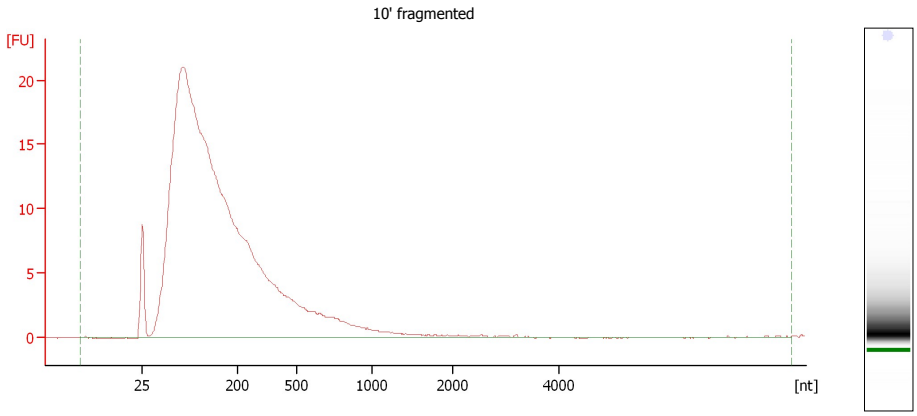

Overall Results for sample 2 : 10' fragmented

RNA Area:	360.8	RNA Integrity Number (RIN):	2.4 (B.02.07)
RNA Concentration:	272 ng/µl	Result Flagging Color:	
rRNA Ratio [28s / 18s]:	0.0	Result Flagging Label:	RIN: 2.40

2100 Expert (B.02.07.SI532) © Copyright 2003 - 2009 Agilent Technologies, Inc. Printed: 01.09.2010 09:42:04

2100 expert_Eukaryote Total RNA Nano_DE24802247_2010-09-01_09-24-18.xad Page 6 of 11

Assay Class: Eukaryote Total RNA Nano
Data Path: C:\...Eukaryote Total RNA Nano_DE24802247_2010-09-01_09-24-18.xad

Created: 01.09.2010 09:24:18
Modified: 01.09.2010 09:40:03

Electropherogram Summary Continued ...

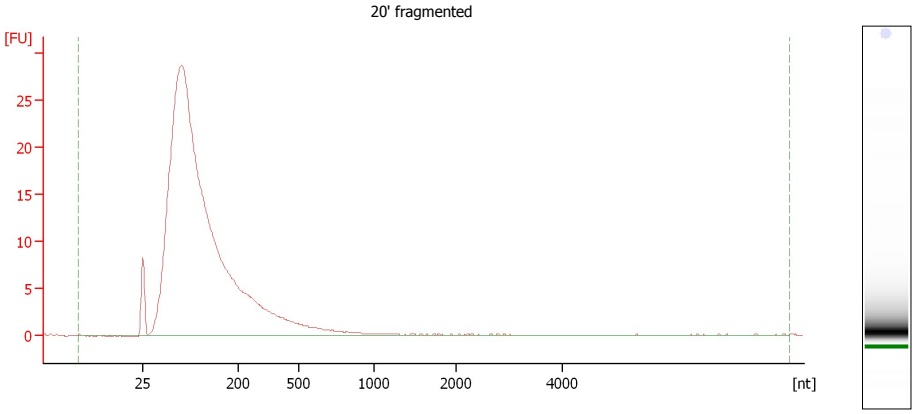

Overall Results for sample 3 : 20' fragmented

RNA Area:	344.9	RNA Integrity Number (RIN):	2.5 (B.02.07)
RNA Concentration:	260 ng/µl	Result Flagging Color:	
rRNA Ratio [28s / 18s]:	0.0	Result Flagging Label:	RIN: 2.50

2100 Expert (B.02.07.SI532) © Copyright 2003 - 2009 Agilent Technologies, Inc. Printed: 01.09.2010 09:42:04

2100 expert_Eukaryote Total RNA Nano_DE24802247_2010-09-01_09-24-18.xad Page 7 of 11

Assay Class: Eukaryote Total RNA Nano Created: 01.09.2010 09:24:18
Data Path: C:\...Eukaryote Total RNA Nano_DE24802247_2010-09-01_09-24-18.xad Modified: 01.09.2010 09:40:03

Electropherogram Summary Continued ...

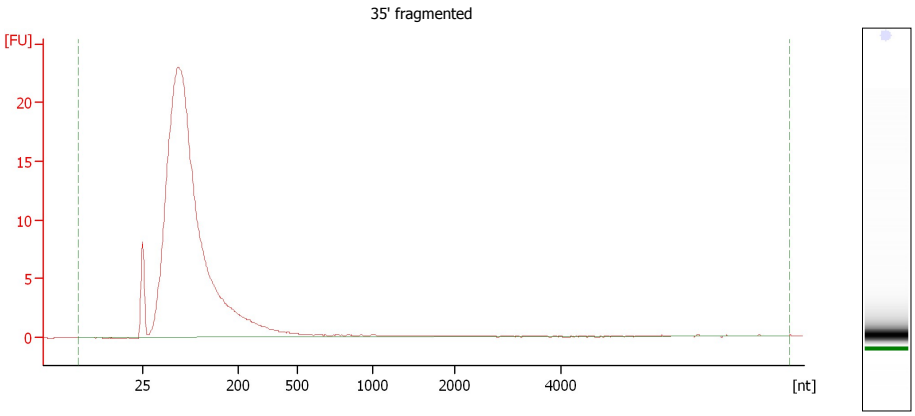

Overall Results for sample 4 : 35' fragmented

RNA Area:	229.1	RNA Integrity Number (RIN):	2.5 (B.02.07)
RNA Concentration:	173 ng/µl	Result Flagging Color:	
rRNA Ratio [28s / 18s]:	0.0	Result Flagging Label:	RIN: 2.50

2100 Expert (B.02.07.SI532) © Copyright 2003 - 2009 Agilent Technologies, Inc. Printed: 01.09.2010 09:42:04

2100 expert_Eukaryote Total RNA Nano_DE24802247_2010-09-01_09-24-18.xad Page 8 of 11

Assay Class: Eukaryote Total RNA Nano
Data Path: C:\...Eukaryote Total RNA Nano_DE24802247_2010-09-01_09-24-18.xad

Created: 01.09.2010 09:24:18
Modified: 01.09.2010 09:40:03

Electropherogram Summary Continued ...

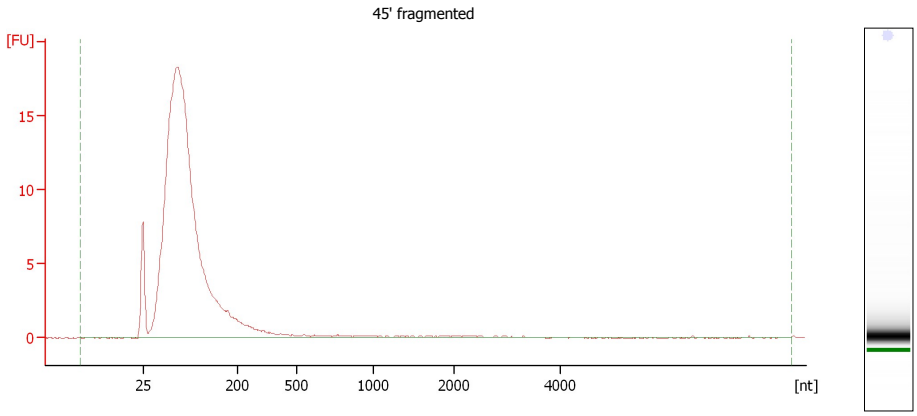

Overall Results for sample 5 : 45' fragmented

RNA Area:	170.2	RNA Integrity Number (RIN):	2.6 (B.02.07)
RNA Concentration:	128 ng/µl	Result Flagging Color:	
rRNA Ratio [28s / 18s]:	0.0	Result Flagging Label:	RIN: 2.60

2100 Expert (B.02.07.SI532) © Copyright 2003 - 2009 Agilent Technologies, Inc. Printed: 01.09.2010 09:42:04

Assay Class: Eukaryote Total RNA Nano
Data Path: C:\...Eukaryote Total RNA Nano_DE24802247_2010-09-01_09-24-18.xad

Created: 01.09.2010 09:24:18
Modified: 01.09.2010 09:40:03

Electropherogram Summary Continued ...

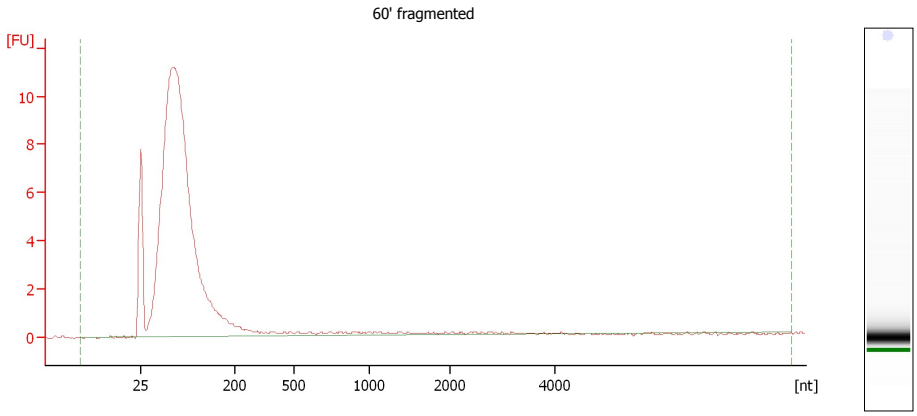

Overall Results for sample 6 : 60' fragmented

RNA Area:	104.9	RNA Integrity Number (RIN):	2.6 (B.02.07)
RNA Concentration:	79 ng/µl	Result Flagging Color:	
rRNA Ratio [28s / 18s]:	0.0	Result Flagging Label:	RIN: 2.60

 © Copyright 2003 - 2009 Agilent Technologies, Inc.

2100 expert_Eukaryote Total RNA Nano_DE24802247_2010-09-01_09-24-18.xad Page 10 of 11

Assay Class: Eukaryote Total RNA Nano Created: 01.09.2010 09:24:18
Data Path: C:\...Eukaryote Total RNA Nano_DE24802247_2010-09-01_09-24-18.xad Modified: 01.09.2010 09:40:03

Gel Image

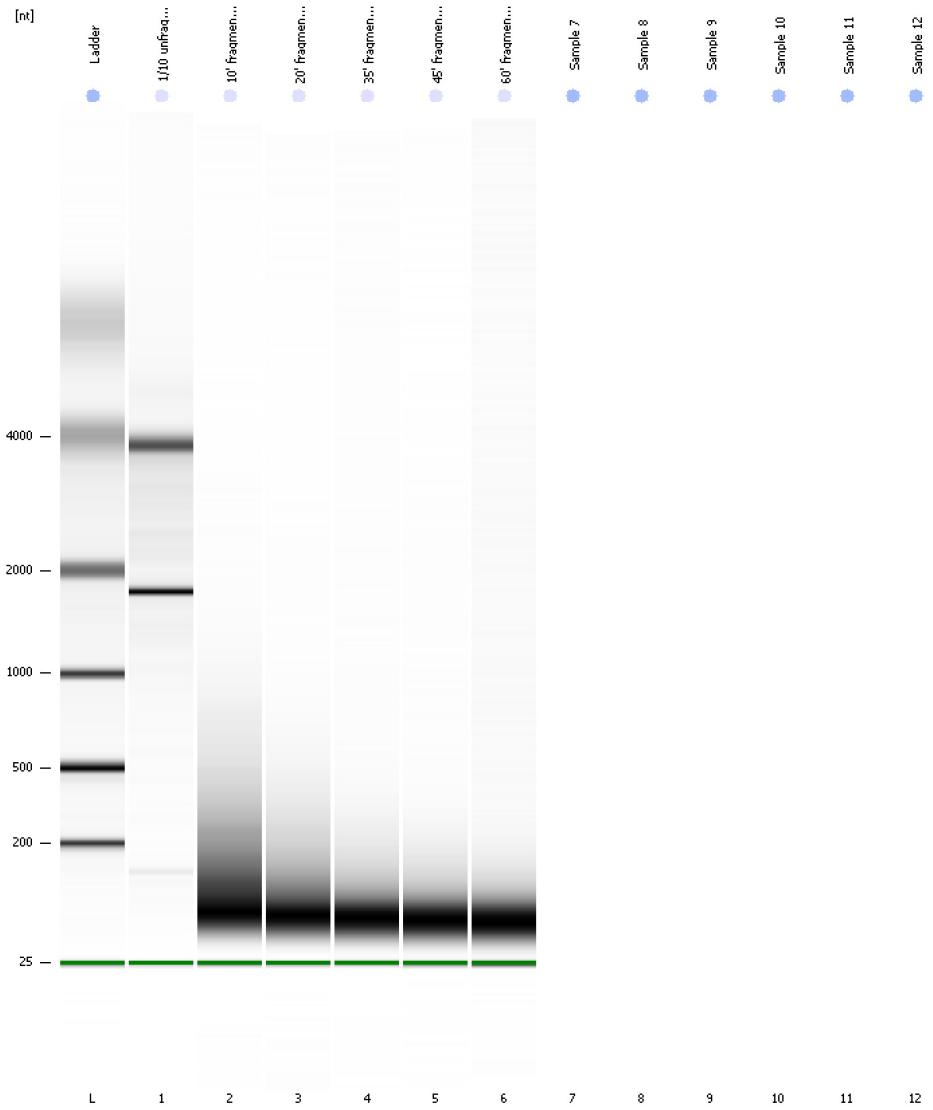

2100 Expert (B.02.07.SI532) © Copyright 2003 - 2009 Agilent Technologies, Inc. Printed: 01.09.2010 09:42:04

2100 expert_Eukaryote Total RNA Nano_DE24802247_2010-09-01_09-24-18.xad Page 11 of 11

Assay Class: Eukaryote Total RNA Nano Created: 01.09.2010 09:24:18
Data Path: C:\...Eukaryote Total RNA Nano_DE24802247_2010-09-01_09-24-18.xad Modified: 01.09.2010 09:40:03

Run Logbook

Description	Number	Source	Category	Sub Category	Time Stamp	Time Zone	User	Host
Run ended on port 1 (Number of wells acquired: 7)		Instrument	Run		01.09.2010 09:39:55	(GMT +02:00) W. Europe Standard Time	haikerm	RBAMOUSER
Run started on port 1 (File: C:\Program Files\Agilent\2100 bioanalyzer\2100 expert\Data\2010-09-01\2100 expert_Eukaryote Total RNA Nano_DE24802247_2010-09-01_09-24-18.xad)		Instrument	Run		01.09.2010 09:24:25	(GMT +02:00) W. Europe Standard Time	haikerm	RBAMOUSER
Product Number : G2938B		Instrument	Run		01.09.2010 09:24:25	(GMT +02:00) W. Europe Standard Time	haikerm	RBAMOUSER
Name :		Instrument	Run		01.09.2010 09:24:25	(GMT +02:00) W. Europe Standard Time	haikerm	RBAMOUSER
Vendor : Agilent Technologies		Instrument	Run		01.09.2010 09:24:25	(GMT +02:00) W. Europe Standard Time	haikerm	RBAMOUSER
Serial# : DE24802247		Instrument	Run		01.09.2010 09:24:25	(GMT +02:00) W. Europe Standard Time	haikerm	RBAMOUSER
Firmware : C.01.069		Instrument	Run		01.09.2010 09:24:25	(GMT +02:00) W. Europe Standard Time	haikerm	RBAMOUSER
Cartridge : Electrode		Instrument	Run		01.09.2010 09:24:24	(GMT +02:00) W. Europe Standard Time	haikerm	RBAMOUSER

2100 Expert (B.02.07.SI532) © Copyright 2003 - 2009 Agilent Technologies, Inc. Printed: 01.09.2010 09:42:04

B.4.3 Peltier Test

Data from F7 detection in Hep3B cell lysate

Two Peltier peaks (Fig. B.4) were recorded under similar experimental conditions (Detection of F7 in Hep3B cell lysate as shown in Fig. 3.34). Peltier test 1 ((a) and (c), before injection 1) and Peltier test 2 ((b) and (d), before injection 2) are almost identical proving the consistency of mechanical properties over two injections with chip regeneration in between. Furthermore the functionality of single cantilevers can be monitored (example Fig. B.4: malfunction of CL4 in (a) and (b)).

Data from miR-122 detection in ME15 and HuH7 cell lysate

A series of Peltier peaks were recorded in the experiment of miR-122 detection in ME15 and HuH7 cell lysate. Results are shown in Fig. B.5. Peltier peak 1, 2 and 3 were recorded before injection 1, before injection 2 and after injection 2. The loss and regaining of cantilever signals is clearly visible. Therefore Peltier tests are a necessary tool to keep track of the cantilever functionality.

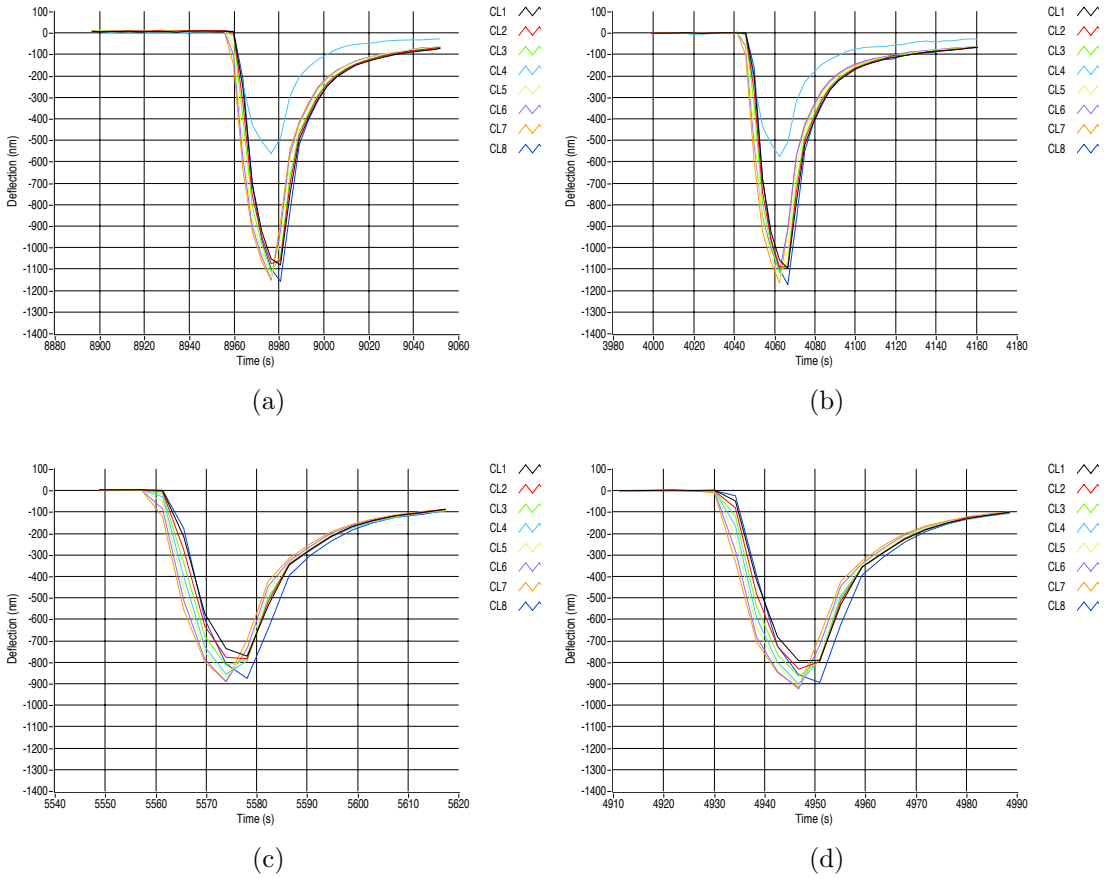

Figure B.4: Two sets of sequential Peltier peak tests: Graphs show the cantilever deflection signal for all 8 CLs induced by a heat pulse. Upper graphs (a) and (b) belong to the same experiment series and lower graphs (c) and (d) belong to the same experiment, respectively CLA chip. For each set the Peltier test was recorded before a first (negative control) and a second (analyte) injection with regeneration in between. CL4 in (a), (b) is defect visible by the odd deflection signal during the Peltier test. Otherwise the cantilever characteristics are almost identical for the initial and follow up test. Furthermore the deflection amplitudes, respectively the mechanical properties of each array is similar.

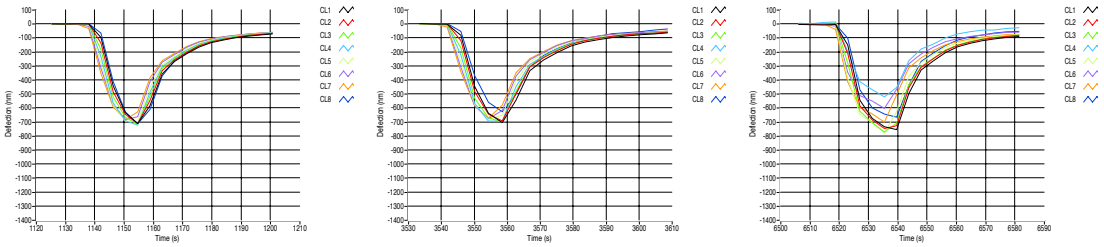

(a) (b) (c)

Figure B.5: Series of three Peltier tests performed during one experiment on the same CLA chip: Tests were recorded before a first (negative control) and second (analyte) injection with regeneration in between and after the second injection. Before the two injections ((a) and (b)) the cantilever characteristics are almost identical. After the second injection (c) at least CL4 and CL6 are different. Reason could be sticking protein particles on the CLs. In that specific experiment the odd behaving CLs were excluded for final data processing and result presentation as shown in Fig. 3.36.

Glossary

AB	Antibody.
AFM	Atomic Force Microscope.
Ago	Argonaute.
avg	Average.
BF	Brightfield Microscopy.
BW	Bandwidth.
cDNA	complementary DNA.
Chap.	Chapter.
CL	Cantilever.
CLA	Cantilever Array.
DF	Darkfield Microscopy.
diff	Differential - Differential signal, respectively probe CL minus reference CL.
DNA	Deoxyribonucleic acid.
dsRNA	double strand RNA.
DTT	Dithiothreitol.
ELISA	Enzyme-Linked Immunosorbent Assay.
ESD	Electrostatic Sensitive Device.
Fig.	Figure.
HCV	Hepatitis C.
LabVIEW	Laboratory Virtual Instrumentation Engineering Workbench; a platform and development environment for visual programming language from National Instruments.

Lit.	Literature.
Mab	Monoclonal Antibody.
MCU	11-Mercapto-1-undecanol.
miRNA	micro RNA.
mRNA	messenger RNA.
ncRNA	noncoding RNA.
NI	National Instruments.
nt	Nucleotide.
NTC	Negative Temperature Coefficient Thermistors.
PBS	Phosphate Buffered Saline.
PBS (+)	Phosphate Buffered Saline with Calcium and Magnesium.
PCR	Polymerase Chain Reaction.
PEG	Polyethylene glycol.
PMT	Photomultiplier.
PSD	Position Sensitive Detector.
PVP	Polyvinylpyrrolidone.
QCM	Quartz Crystal Microbalance.
qPCR	Real Time Quantitative Polymerase Chain Reaction.
R&D	Research & Development.
ref	Reference - Reference Cantilever.
Ref.	Reference.
RISC	RNA-Induced Silencing Complex.
RNA	Ribonucleic acid.
RNAi	RNA interference.
rRNA	ribosomal RNA.
RTq-PCR or qPCR	Real Time Quantitative Polymerase Chain Reaction.
RU	"Response Units".
SAM	Self-Assembled Monolayer.
SD	Standard Deviation.

Sect.	Section.
SEM	Scanning Electron Microscope.
siRNA	small interfering RNA.
snoRNA	small nucleolar RNA.
snRNA	small nuclear RNA.
SPR	Surface Plasmon Resonance.
SSC	Saline-Sodium Citrate.
ssDNA	single strand DNA.
ssRNA	single strand RNA.
Tab.	Table.
totRNA	total RNA.
tRNA	transfer RNA.
VCSEL	Vertical Cavity Surface Emitting Laser.
VI	Virtual Instrument - A LabVIEW program.

Bibliography

[1] Galasso, M., Sana, M. E., and Volinia, S. *Genome Med* **2**(2), 12 Jan (2010).

[2] Carthew, R. W. and Sontheimer, E. J. *Cell* **136**(4), 642–55 Feb (2009).

[3] Collins, M. L., Irvine, B., Tyner, D., Fine, E., Zayati, C., an Chang, C., Horn, T., Ahle, D., Detmer, J., Shen, L.-P., Kolberg, J., Bushnell, S., Urdea, M. S., and Ho, D. D. *Nucleic Acids Research* **25**(15), 2979–2984 (1997).

[4] Acinas, S. G., Sarma-Rupavtarm, R., Klepac-Ceraj, V., and Polz, M. F. *Applied and Environmental Microbiology* **71**(12), 8966–9 Dec (2005).

[5] Polz, M. F. and Cavanaugh, C. M. *Applied and Environmental Microbiology* **64**(10), 3724–30 Oct (1998).

[6] McKendry, R., Zhang, J., Arntz, Y., Strunz, T., Hegner, M., Lang, H. P., Baller, M. K., Certa, U., Meyer, E., Güntherodt, H.-J., and Gerber, C. *PNAS* **99**(15), 9783–8 Jul (2002).

[7] Huber, F., Backmann, N., Grange, W., Hegner, M., Gerber, C., and Lang, H. P. *J of Physics , Conference Series* **61**, 450 Mar (2007).

[8] Mertens, J., Rogero, C., Calleja, M., Ramos, D., Martín-Gago, J. A., Briones, C., and Tamayo, J. *Nature Nanotech* **3**(5), 301–7 May (2008).

[9] Arntz, Y., Seelig, J. D., Lang, H. P., Zhang, J., Hunziker, P., Ramseyer, J. P., Meyer, E., Hegner, M., and Gerber, C. *Nanotechnology* **14**(1), 86 (2003).

[10] Braun, T., Ghatkesar, M. K., Backmann, N., Grange, W., Boulanger, P., Letellier, L., Lang, H.-P., Bietsch, A., Gerber, C., and Hegner, M. *Nature Nanotech* **4**(3), 179–85 Mar (2009).

[11] Braun, T., Backmann, N., Vögtli, M., Bietsch, A., Engel, A., Lang, H.-P., Gerber, C., and Hegner, M. *Biophysical Journal* **90**(8), 2970–7 Apr (2006).

[12] Backmann, N., Zahnd, C., Huber, F., Bietsch, A., Plückthun, A., Lang, H.-P., Güntherodt, H.-J., Hegner, M., and Gerber, C. *Proceedings of the National Academy of Sciences of the United States of America* **102**(41), 14587–92 Oct (2005).

[13] Zhang, J., Lang, H. P., Huber, F., Bietsch, A., Grange, W., Certa, U., McKendry, R., Güntherodt, H.-J., Hegner, M., and Gerber, C. *Nature Nanotech* **1**(3), 214–20 Dec (2006).

[14] Lang, H. P., Berger, R., Andreoli, C., Brugger, J., Despont, M., Vettiger, P., Gerber, C., Gimzewski, J. K., Ramseyer, J. P., Meyer, E., and Güntherodt, H.-J. *Appl. Phys. Lett.* **72**, 383–385 Jan (1998). (c) 1998: American Institute of Physics.

[15] Meyer, G. and Amer, N. M. *Appl. Phys. Lett.* **57**, 2089 Nov (1990).

[16] Huber, W. and Mueller, F. *Curr Pharm Des* **12**(31), 3999–4021 Jan (2006).

[17] Nelson, B., Grimsrud, T., Liles, M., Goodman, R., and Corn, R. *Anal. Chem.* **73**(1), 1–7 Jan (2001).

[18] Lao, A. I. K., Su, X., and Aung, K. M. M. *Biosensors and Bioelectronics* **24**(6), 1717–22 Feb (2009).

[19] Li, Y.-J., Xiang, J., and Zhou, F. *Plasmonics* **2**, 79–87 Jun (2007).

[20] Peterlinz, K. A., Georgiadis, R. M., Herne, T. M., and Tarlov, M. J. *J. Am. Chem. Soc.* **119**(14), 3401–3402 Apr (1997).

[21] Löfås, S., Malmqvist, M., Rönnberg, I., Stenberg, E., Liedberg, B., and Lundström, I. *Sensors & Actuators, B* **5**(1–4), 79–84 (1991).

[22] Jung, L. S., Shumaker-Parry, J. S., Campbell, C. T., Yee, S. S., and Gelb, M. H. *J. Am. Chem. Soc.* **122**(17), 4177–4184 (2000).

[23] Khilko, S. N., Corr, M., Boyd, L. F., Lees, A., Inman, J. K., and Margulies, D. H. *J. Biol. Chem.* **268**(21), 15425–15434 (1993).

[24] Wink, T., van Zuilen, S. J., Bult, A., and van Bennekom, W. P. *Anal. Chem.* **70**(5), 827–32 Mar (1998).

[25] Stenlund, P., Frostell-Karlsson, A., and Karlsson, O. P. *Anal Biochem* **353**(2), 217–25 Jun (2006).

[26] Andersson, K., Karlsson, R., Löfås, S., Franklin, G., and Hämäläinen, M. D. *Expert Opinion on Drug Discovery* **1**(5), 439–446 (2006).

[27] Noy, P., Steiner, R., Voelkle, J., Hegner, M., and Fattinger, C. *Journal of Sensors* **2012**, 1–5 Jan (2012).

[28] Stoney, G. G. *Proceedings of the Royal Society of London. Series A* **82**, 172–175 May (1909).

[29] Miyatani, T. and Fujihira, M. *J Appl Phys* **81**(11), 7099–7115 Jan (1997).

[30] Godin, M., Tabard-Cossa, V., Miyahara, Y., Monga, T., Williams, P. J., Beaulieu, L. Y., Lennox, R. B., and Grutter, P. *Nanotechnology* **21**(7), 75501 Feb (2010).

[31] Lang, H. P., Hegner, M., Meyer, E., and Gerber, C. *Nanotechnology* **12**, R29–R36 Sep (2002).

[32] Peterson, A. W., Heaton, R. J., and Georgiadis, R. M. *Nucleic Acids Research* **29**(24), 5163–8 Dec (2001).

[33] Wang, R., Tombelli, S., Minunni, M., Spiriti, M. M., and Mascini, M. *Biosensors and Bioelectronics* **20**(5), 967–74 Nov (2004).

[34] Herne, T. M. and Tarlov, M. J. *J. Am. Chem. Soc.* **38**(119), 8916–8920 Sep (1997).

[35] Wild, D. *The immunoassay handbook*. (2005).

[36] Riccelli, P. V., Merante, F., Leung, K. T., Bortolin, S., Zastawny, R. L., Janeczko, R., and Benight, A. S. *Nucleic Acids Research* **29**(4), 996–1004 Feb (2001).

[37] Franks, W., Tosatti, S., Heer, F., Seif, P., Textor, M., and Hierlemann, A. *Biosensors and Bioelectronics* **22**(7), 1426–33 Feb (2007).

[38] Biosicherheit.de. *Biosicherheit.de* , 2 Jan (2006).

[39] Mattick, J. S. and Makunin, I. V. *Human Molecular Genetics* **15 Spec No 1**, R17–29 Apr (2006).

[40] Castanotto, D. and Rossi, J. J. *Nature* **457**(7228), 426–33 Jan (2009).

[41] Akinc, A., Zumbuehl, A., Goldberg, M., Leshchiner, E. S., Busini, V., Hossain, N., Bacallado, S. A., Nguyen, D. N., Fuller, J., Alvarez, R., Borodovsky, A., Borland, T., Constien, R., de Fougerolles, A., Dorkin, J. R., Jayaprakash, K. N., Jayaraman, M., John, M., Koteliansky, V., Manoharan, M., Nechev, L., Qin, J., Racie, T., Raitcheva, D., Rajeev, K. G., Sah, D. W. Y., Soutschek, J., Toudjarska, I., Vornlocher, H.-P., Zimmermann, T. S., Langer, R., and Anderson, D. G. *Nat Biotechnol* **26**(5), 561–9 May (2008).

[42] Callis, T. E. and Wang, D.-Z. *Trends Mol Med* **14**(6), 254–60 Jun (2008).

[43] University of Manchester. *miRBase: the microRNA database*, January (2012). http://www.mirbase.org/.

[44] Jopling, C. L., Yi, M., Lancaster, A. M., Lemon, S. M., and Sarnow, P. *Science* **309**(5740), 1577–81 Sep (2005).

[45] Braun, T., Huber, F., Ghatkesar, M. K., Backmann, N., Lang, H. P., Gerber, C., and Hegner, M. *Sensors & Actuators, B* **128**(1), 75–82 Jan (2007).

[46] Kern, W. *Handbook of Semiconductor Wafer Cleaning Technology - Science, Technology, and Applications*. May (1993).

[47] Siegrist, F., Singer, T., and Certa, U. *Biol Proced Online* **11**, 113–29 Jan (2009).

[48] Ravon, M., Berrera, M., Ebeling, M., and Certa, U. *rnabiology* **9**(1) Jan (2012).

[49] Su, X., Teh, H. F., Aung, K. M. M., Zong, Y., and Gao, Z. *Biosensors and Bioelectronics* **23**(11), 1715–20 Jun (2008).

[50] Paul, S. M. D., Falconnet, D., Pasche, S., Textor, M., Abel, A. P., Kauffmann, E., Liedtke, R., and Ehrat, M. *Anal. Chem.* **77**(18), 5831–8 Sep (2005).

[51] Marie, R., Dahlin, A. B., Tegenfeldt, J. O., and Höök, F. *Biointerphases* **2**(1), 49–55 Mar (2007).

[52] Qavi, A. J. and Bailey, R. C. *Angew Chem Int Ed Engl* **49**(27), 4608–11 Jun (2010).